3
Force Models for Molecular Geometry

H. Nakatsuji and T. Koga
Department of Hydrocarbon Chemistry
Faculty of Engineering
Kyoto University
Kyoto, Japan

Contents

3-1. INTRODUCTION

In order to explain the great variety and regularity in structural chemistry, general principles and conceptual models are of fundamental importance, since they provide a unified viewpoint for interrelating diverse chemical phenomena

(*142*, *225*). Until recently, most models for molecular geometry were constructed on energetic grounds. In this chapter our main purpose is to explain the force concept as applied to molecular geometry by fully utilizing the physical simplicity and visuality of the electrostatic Hellmann-Feynman (H-F) theorem (*101*, *133*)

$$F_A = Z_A \int r_{A1}/r_{A1}^3 \rho(r_1)\, dr_1 - Z_A \sum_{B \neq A} Z_B R_{AB}/R_{AB}^3, \qquad (3\text{-}1)$$

where F_A is the force acting on nucleus A of charge Z_A, $\rho(r_1)$ the 3-D electron density, r_{A1} and R_{AB} position vectors from nucleus A to electron 1 and nucleus B, respectively (see chapters 1 and 2).

Among earlier workers, Mulliken (*204*) and Walsh (*294*) considered molecular shapes, drawing angular correlation diagrams[1] in which the energies of simple "empirical" MOs were plotted against the valence angle of a molecule. This gave rise to the celebrated *Walsh rules*, which provided a beautiful correlation between molecular shapes and the number of valence electrons.[2] In spite of minor exceptions like highly ionic molecules, the Mulliken-Walsh MO model has had much influence on later developments in structural chemistry (*134*) and theoretical chemistry (*142*). About the same time, Sidgwick and Powell (*274*), Gillespie and Nyholm (*121*) and Gillespie (*118–120*) developed the valence-shell electron-pair repulsion (VSEPR) model for molecular shapes based on Pauli repulsions between electron pairs. The comparatively recent second-order Jahn-Teller (SOJT) theory for molecular shapes is based on second-order perturbation theory (*13*, *14*, *28*, *48*, *232*, *233*, *235*). These energetic models are reviewed briefly in Section 3-2.

More recently, the H-F theorem has been applied to molecular geometries with great success, e.g., the relation between electron density and molecular shapes of simple hydrides (*20–22*), the origin (*127*, *277*) of the internal rotation barrier in ethane (see Chapter 4), the FOJT effect (*56*, *65*, *71*), and a reinterpretation of the Walsh diagram (*66*). Subsequently, Nakatsuji and co-workers (*207–211*, *215*, *216*, *219–221*), and Deb and co-workers (*76–79*, *82*) have proposed versatile force models for molecular geometry which are very successful in explaining the variety and regularity in structural chemistry. Nakatsuji's electrostatic force (ESF) theory is applicable to both isolated and interacting molecules, including long-range forces (*167*, *215*) and chemical reactivity. These two force models will be discussed in detail in Sections 3-3 and 3-4. In Section 3-5 we study the dynamic behavior of electron density during nuclear rearrangement processes which occur in molecular geometry, molecular vibrations and chemical reactions, using both H-F and integral H-F theorems (*166*, *227*; see also Chapter 4). Next we will study a border area between molecular geometry and chemical reaction, namely, the change in the geometries of reactant molecules during a chemical reaction.

3-1-1. Comparison of the Energy and Force Viewpoints in Their Exact Limits

In the energetic viewpoint, a stable molecular geometry corresponds to the minimum in the potential surface which is calculated by

$$E = \langle \psi, H\psi \rangle$$

$$= \int \left[-\tfrac{1}{2} \Delta \rho(r_1' | r_1) \right]_{r_1' = r_1} dr_1 - \sum_A \int (Z_A / r_{A1}) \rho(r_1)\, dr_1$$

$$+ \int (1/r_{12})\, \Gamma(r_1 r_2 | r_1 r_2)\, dr_1\, dr_2 + \sum_{A<B} Z_A Z_B / R_{AB}, \qquad (3\text{-}2)$$

where ψ is the exact wavefunction, H the Born-Oppenheimer (*39*) Hamiltonian, and ρ and Γ are the first- and second-order reduced density matrices (*180*, *181*; see Chapter 8), respectively. In contrast to the force expression (3-1), the energy expression (3-2) is much more cumbersome, since (i) one simultaneously considers four energy terms which are usually competitive with one another; (ii) one requires both first- and second-order density matrices in contrast to just the electron density in (3-1); (iii) (3-1) permits a classical electrostatic interpretation *even in the exact limit*.

The H-F force has a severe drawback in that it is more sensitive than energy to inaccuracies of the (approximate) wavefunctions used. This has prevented quantification from this approach (however, see Refs. 220, 221, and 221a), except for some simple systems (*16*, *140*, *215*). Although the so-called energy gradient (see Chapter 9) is as accurate as the energy and has been employed to study potential surfaces (*103*, *115*, *169*, *188*, *196*, *248*), it does not have a simple meaning like the H-F force.

A wavefunction which satisfies the H-F theorem is called "floating" (*67*, *147*, *148*) or "stable" (*129*). When we expand the wavefunction in terms of an incomplete basis set (e.g., LCAO-MO), it becomes unstable (nonfloating) if the basis AOs are fixed on the constituent nuclei, since then electronic coordinates are not treated as free from nuclear coordinates. Floating wavefunctions have been calculated for H_2 (*273*), H_2O, NH_3, CH_3^+, and NH_3^+ (*220*, *221*). The floating spherical Gaussian orbital (FSGO) wavefunctions (*106*) also satisfy the H-F theorem. Recently, a new method of obtaining a stable wavefunction was given[3] and shown to be useful in the force theoretic approach (*221*a).

As seen in Section 3-2, since the energetic models of molecular geometry start from more or less drastic approximations to (3-2), their underlying concepts themselves are approximate. On the other hand, the force models (especially that in Sections 3-3 and 3-5) start from the exact equation (3-1) and,

although certain approximations are introduced for practical reasons, the concept itself is rigorous and preserved in both approximate and exact treatments.

3-2. ENERGETIC MODELS FOR MOLECULAR SHAPE

Although one can nowadays perform ab initio geometry calculations for molecules of moderate size, in good agreement with experiment, such calculations by themselves are usually ineffective in explaining the various trends in structural chemistry (*26*). Since "to calculate a molecule is not to understand a molecule" (*228*), the need for molecular geometry models is as great as ever. We review here briefly the more important energetic models so that we can compare them with the force models described later.

3-2-1. Walsh's Correlation Diagram

Figure 3-1 gives an example of Walsh's correlation diagrams (*294*) for AH_2 molecules. It plots the MO "binding" energies for valence electrons against the HAH angle. The MO energy variations can be easily rationalized (Fig. 3-2). Thus, in the π_u-b_1 correlation, the p_{zA} AO (MO) having a node on the AH_2 plane is not affected much by bending in the xy plane. In the π_u-a_1 (lone-pair) correlation, the p_{yA} AO at linear shape is mixed by bending with the s_A AO of lower energy and the two hydrogenic AOs can overlap in phase with the bottom lobe of p_{yA} AO (*123*) and with each other. Therefore, bending rapidly stabilizes the a_1 (lone-pair) MO. In the σ_u-b_2 correlation, bending pulls two s_H AOs

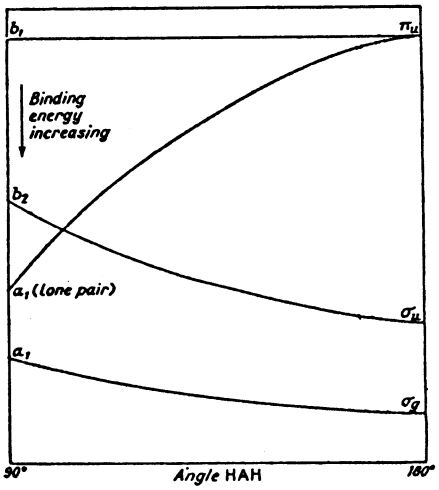

Fig. 3-1. Orbital correlation diagram for AH_2 molecules. (Reproduced from Ref. 294, courtesy the Chemical Society, London.)

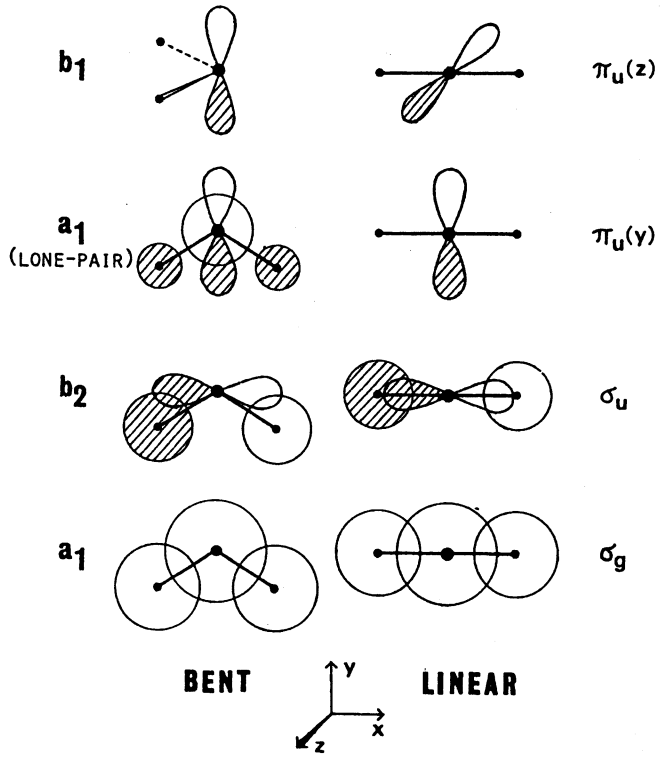

Fig. 3-2. Schematic MOs of linear and bent AH_2 molecules (see also Fig. 3-16).

out of overlap with the lobes of p_{xA} AO and destabilizes the b_2 MO as compared to the σ_u MO (*123*). The slope of the σ_g-a_1 curve in Fig. 3-1 is of the wrong sign; the a_1 MO will be lower in energy than the σ_g MO, mainly because of the overlap among two s_H and p_{yA} AO's (*4, 66, 123, 240*; Fig. 3-16).

With this correction in Fig. 3-1, the shapes of AH_2 molecules (see Table 3-3) can be explained as follows: For molecules with 4 valence electrons, the lowest two MOs are occupied and therefore the shape is linear. For molecules with 5–8 valence electrons, the steep π_u-a_1 (lone pair) leads to a bent structure. With 2 valence electrons, the *corrected* Walsh diagram rightly predicts a bent structure, e.g., LiH_2^+ and H_3^+ (*245, 249*). Further, when an electron jumps from the a_1 (lone-pair) to the b_1 MO, the HAH angle increases, e.g., in NH_2 and PH_2.

The Walsh rules (Table 3-1) generally agree well with experimental data (*134*), though interesting exceptions exist, e.g., highly ionic molecules like alkaline earth dihalides with heavy metal-light halogen combinations (Section 3-3-7d)

Table 3-1. Walsh Rules Linking the Shapes of Ground-State Molecules with the Numbers of Valence Electrons.[a]

Molecule	Shape (Number of valence electrons)
AH_2	linear (4), bent (5–8)
AH_3	planar (<6), pyramidal (7–8)
HAB	linear (<10), bent (10–14), linear (16)
AB_2, ABC	linear (<16), bent (17–20), linear or nearly linear (22)
H_2AB	planar (12), nonplanar (13–14)
AB_3	planar (<24), pyramidal (25–26)[b], planar or nearly planar (28)
HAAH	linear (10), bent but planar (12), bent and nonplanar (14)

[a]Reprinted from Ref. 294.
[b]The BAB angle will be less for 26-electron molecules than for 25-electron molecules.

and the sensitive problem of the shapes of 7-valence electron AH_3 molecules like CH_3, NH_3^+, and BH_3^- (Section 3-3-7a). The Walsh diagram predicts the former type to be linear and the latter type to be nonplanar. While molecules like SiH_3, GeH_3, and SnH_3 (*151*, *152*, *197*), having heavier central atoms, and CH_2F, CHF_2, and CF_3, having electronegative substituents (*100*), are pyramidal, the radical CH_3 is planar or almost planar, in that the potential barrier to inversion is very shallow (experimental: *12*, *59*, *91*, *98*, *99*, *134*, *195*, *285*; theoretical: *51*, *87*, *194*, *198*, *282*, *306*). BH_3^- and NH_3^+ are experimentally reported as planar (*58*, *285*, *286*). The ESF theory (Section 3-3) satisfactorily explains these trends.

In the Walsh model the total molecular energy is supposed to be expressible as the sum of "effective" MO energies. However, in spite of many attempts, the reasonings for such a summation based on more refined quantum theories are not completely satisfactory, because of electron-electron and nuclear-nuclear repulsion terms (*4*, *5*, *34–37*, *44*, *46*, *66*, *69*, *240*, *242*, *256*, *280*, *303*, *304*).

Extensions and modifications of the Walsh diagram have been suggested (*45*, *113*, *122–124*). Hayes (*131*) considered outer *d* AOs for alkaline earth dihalides (see also Ref. 126). Other workers (*266*, *287–289*) viewed the Walsh diagram in ways that are related to the VSEPR model.

3-2-2. Valence-Shell Electron-Pair Repulsion (VSEPR) Model

The VSEPR model, extensively developed by Gillespie (*118–120*), regards Pauli repulsions among bonding and nonbonding electron pairs in the valence shell of the central atom as the most important factor in determining stereochemistry. For example, when the central atom has four equivalent bonding

pairs the interpair repulsion will lead to the tetrahedral arrangement, e.g., CH_4. The main postulates concerning such electron-pair repulsions are as follows: (1) since nonbonding electron pairs occupy larger and less confined orbitals (they are influenced by one nucleus, in contrast to *two* nuclei for a bonding electron pair), they repel adjacent electron pairs more strongly than bonding electron pairs. (2) The repulsions due to bonding electron pairs decrease with increasing electronegativity of the ligand. (3) Multiple-bond orbitals repel other orbitals more strongly then single-bond orbitals, the order being triple bond > double bond > single bond.

Consider the shapes of AX_2 molecules. For molecules having no nonbonding electron pair, the repulsion between two bonding pairs makes the molecules linear (see Tables 3-3 to 3-5). Molecules with one and two nonbonding pairs are bent, with $\angle XAX < 120°$, because of rule (1) above. With three nonbonding pairs the shape becomes linear again, e.g., ICl_2^-, XeF_2, etc.

The VSEPR model is intuitive and quite successful. However, it has certain limitations (*86*). It is restricted only to ground-state molecules, neglects interaction between ligands, and is not applicable to the internal rotation problem. In fact, the model's underlying concept itself may be incorrect (see below). It is indeed interesting that the Walsh model (which does not explicitly consider electron repulsion) and the VSEPR model (which considers *only* electron-pair spin repulsion) both give similar shape predictions that agree with experiment (*27*; see also Ref. 29).

The underlying concept of the VSEPR model, namely, that Pauli repulsions between electron pairs determine molecular shapes, has been questioned (*22*, *33*). The Pauli repulsion was defined as the effect of antisymmetrization for the overlapping orbital bases including two electrons of antiparallel spins in each. In the simplest case of two orbitals, e.g., the He–He short-range interaction, antisymmetrization leads to strong repulsion (exclusion shell, see Ref. 258). However, in the more general case, the effect leads to incorrect molecular shape, contrary to rule (1) above. Second, the effect can be quite arbitrary, depending on the choice of basis orbitals. Further, if one identifies Pauli repulsion as the "Fermi hole" between parallel spins, this Fermi hole is actually quite local and does not have the expected effect on either the average interelectronic distance or repulsion energy, contrary to the familiar explanation of Hund's rule (*1*, *72*, *73*, *130*, *163*, *164*, *170*, *173*, *193*). Thus, the Pauli repulsion appears to be a misleading fiction (*33*). Nevertheless, question remains: why is the VSEPR model so successful? For a possible answer, see Section 3-3-9 and Ref. 265a.

3-2-3. Second-Order Jahn–Teller (SOJT) Theory

When a molecule is distorted by a small nuclear displacement Q_i along the ith normal symmetry coordinate, its energy is given by second-order perturbation

theory as (*13*, *14*, *48*)

$$E(Q_i) = E_0 + Q_i \langle \psi_0 | \partial H/\partial Q_i | \psi_0 \rangle + \tfrac{1}{2} Q_i^2 \langle \psi_0 | \partial^2 H/\partial Q_i^2 | \psi_0 \rangle$$

$$+ Q_i^2 \sum_{k \neq 0}^{\infty} |\langle \psi_0 | \partial H/\partial Q_i | \psi_k \rangle|^2 / E_0 - E_k), \quad (3\text{-}3)$$

where ψ_0 and ψ_k are the ground and kth excited states of the undistorted molecule ($Q_i = 0$), E_0 and E_k the corresponding energies, and H the Hamiltonian; the derivatives are taken at $Q_i = 0$. We are interested in only such Q_i's that change molecular shapes, and hence are *not* totally symmetric.

Now, while H and $\partial^2 H/\partial Q_i^2$ belong to the totally symmetric representation, $\partial H/\partial Q_i$ has the same symmetry as Q_i. Since the ground electronic states ψ_0 of most molecules are nondegenerate and totally symmetric, the integral in the term linear in Q_i in (3-3) vanishes for such molecules. This first-order term is nonvanishing only for molecules in degenerate electronic states (e.g., benzene cation and anion) and causes the well-known Jahn-Teller distortion (*92*, *153*; Section 3-4-3). The term involving $\partial^2 H/\partial Q_i^2$ in (3-3) is clearly positive and will cause destabilization, indicating that the electron density at $Q_i = 0$ operates to resist the nuclear displacement Q_i. The last term, called relaxability (*261*), is always negative and causes stabilization, representing the effect of electron reorganization induced by nuclear displacement. In this infinite sum, *which includes continuum states*, only those ψ_k for which the direct-product representation of ψ_0 and ψ_k contains the representation of Q_i will contribute to relaxability. Writing the second-order terms as $\frac{1}{2} Q_i^2 (f_{00} - f_{0k})$, where $f_{00} - f_{0k}$ is an approximate force constant for Q_i, one obtains *three* situations, assuming all first-order distortions to have already occurred: (i) $f_{00} > f_{0k}$, i.e., the original configuration is stable; (ii) $f_{00} < f_{0k}$, i.e., the original configuration changes spontaneously along the normal mode Q_i; (iii) $f_{00} \simeq f_{0k}$, i.e., the two structures are readily interconvertible, being separated by a low energy barrier.

Using simple MO theory, let us approximate the ground and excited states by the electronic configurations:

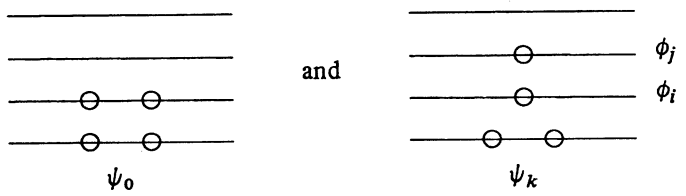

The symmetry rules for molecular structure that decide whether the original configuration will relax spontaneously along the normal mode Q_i are as fol-

lows (*28, 232–237, 261*): (1) Replace the infinite sum in f_{0k} by only the first term, corresponding to HOMO-LUMO transition, $\phi_i \rightarrow \phi_j$. The energy gap for this one-electron excitation must be less than 4 eV. (2) The direct-product representation of ϕ_i (HOMO) and ϕ_j (LUMO) must contain the representation of Q_i. (3) The transition density $\psi_0 \psi_k$, which in this approximation is proportional to $\phi_i \phi_j$, must be concentrated in the regions of nuclear displacement Q_i.

As an illustrative example, consider the stability of linear AH_2 molecules. The MO order in increasing energy is $(1\sigma_g)(1\sigma_u)(1\pi_u)(2\sigma_g)(2\sigma_u)$. For molecules having 4 valence electrons the HOMO-LUMO direct product is $\sigma_u \times \pi_u = \pi_g$, which is not the mode that converts linear into bent form; hence the linear form is stable. For molecules with 5–8 valence electrons the direct product is $\pi_u \times \sigma_g = \pi_u$, which is the converting mode. Since the $1\pi_u$-$2\sigma_g$ energy gap may not exceed 4 eV, the molecules will bend spontaneously. A 10-valence-electron molecule (e.g., NeH_2) will be linear, since $\sigma_g \times \sigma_u = \sigma_u$. However, the procedure is not applicable to the stability of the bent form, since the normal mode which converts bent into linear form is totally symmetric. The SOJT conclusions generally agree with known results, including Walsh rules (Tables 3-1 and 3-3).

Since the SOJT model is largely based on symmetry considerations, some difficulties may arise with less symmetric molecules. Also, to know the MO energy sequence is in some cases a delicate problem. The model is inapplicable to internal rotation about a single bond (*233, 234*), but can be extended to excited states (*235*).

The basic equation (3-3) of SOJT theory is quite general if Q_i is small. It can be applied to a wide range of nuclear rearrangement processes, e.g., potential interaction constants (*13*), chemical reactivity (*14, 234, 236, 237, 262*), vibrationally induced stabilization of vertically excited states (*83*), etc. We will again refer to the SOJT approach in Section 3-5-3.

3-2-4. Other Recent Models

3-2-4a. The Model Due to Takahata, Schnuelle, and Parr. Assuming certain empirical force laws for the Pauli repulsion in VSEPR model, several authors have tried to make semiquantitative predictions for molecular geometries and force constants (*40, 53, 117, 229, 266, 271, 272, 287, 289, 290*). For example, Searcy (*271, 272*) assigned empirical "electrostatic repulsion numbers" to various bonding and lone-electron pairs, and minimized the resulting effective point-charge repulsion energy with respect to bond angle. The calculated molecular shapes were in reasonable agreement with experiment.

The model proposed by Takahata, Schnuelle, and Parr contains four assumptions, the first three being related to a localized description of bonding and lone-pair electrons, while the last gives a rule for calculating stable geometries (*266*).

(1) Simple VB structures are adequate to describe the bonding. (2) Structures with closed shells on terminal atoms are preferred.[4] Between such alternative structures, the one with all atoms neutral is preferred. (3) The electrons left after procedure 2 constitute lone pairs on the central atom. The lone pairs are described by crystal-field theory, with the terminal closed-shell atoms as field-generating ligands. For example, consider AX_2 molecules in linear and bent forms,

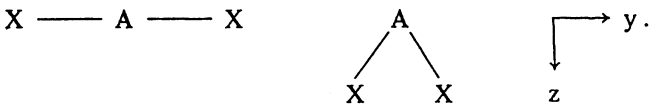

Using crystal-field theory the energy levels of central-atom AOs may be depicted as follows:

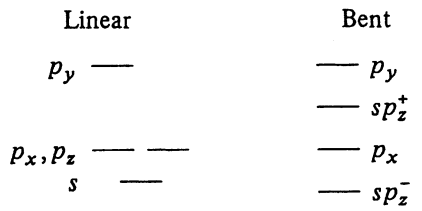

When 1 or 2 electrons are left on the central atom, they occupy the lowest sp_z^- lone-pair orbital, leading to a bent molecule. When 3 or 4 electrons are left, the sp_z^- and p_x AOs are occupied; since the latter are insensitive to the bending mode, little change will occur in the apex angle. With 5 electrons, the apex angle increases since the sp_z^+ AO is now occupied, whereas with 6 electrons the doubly occupied s, p_x, and p_z AOs make the linear configuration more stable. Such conclusions generally agree with known shapes (Tables 3-3 and 3-5). (4) Using assumptions 1-3, and by assigning integral charges on terminal atoms and on the centroid of the Slater sp lone-pair orbital, apex angles and force constants can be calculated by minimizing the classical point-charge repulsion potential, in satisfactory agreement with experimental results.

3-2-4b. Liebman's Fragmentation Model. Liebman (*176*) divides a molecule into two fragments and uses the number of valence electrons in each fragment to qualitatively predict molecular shapes. The model was also applied to excited states (*177*), inversion barriers, and singlet-triplet energy differences (*178*).

As an illustration, the shapes of ABC molecules can be predicted as follows. The triatomic molecule is divided into an atomic and a diatomic fragment. The

former is blocked if it has either a closed-shell electronic configuration or one electron less; otherwise it is porous. The diatomic fragment may belong to one of four classes: (i) σ-rich species, like 4-valence-electron BH(σ^4), 10-valence-electron CO($\sigma^6\pi^4$), and their isoelectronic analogs (*30, 31, 62, 175*). (ii) π-rich species like 8-valence-electron HF($\sigma^4\pi^4$), 14-valence-electron F_2($\sigma^6\pi^8$), and their isoelectronic analogs. (iii) H_2 and its isoelectronic analogs, alkali-metal hydrides and dimers. (iv) He_2, Ne_2, and their isoelectronic analogs.

Now divide the ABC molecule into AB^{q+} and C^{r-} such that AB^{q+} is either σ-rich or π-rich and C^{r-} is either blocked or porous; q and r are zero or integers ($\pm$). The shape of ABC molecule is given by the following rule:

	C^{r-}	
AB^{q+}	blocked	porous
σ-rich	bent	linear
π-rich	linear	bent

This rule is quite successful (see Tables 3-3 and 3-5). Thus, CO_2 can be divided into either σ-rich CO plus porous O or π-rich CO^{2+} plus blocked O^{2-} fragments; both possibilities yield a linear molecule. Note, however, that for C_3 two such fragmentations ($C_2^{2-} + C^{2+}$, $C_2 + C$) give contradictory predictions (linear and bent, respectively).

Liebman (*176*) explained the relations of this model to previous energetic models. For example, the connection with VSEPR model is as follows: σ-rich + porous → no lone pair (on central atom); σ-rich + blocked → one lone pair; π-rich + porous → two lone pairs; π-rich + blocked → three lone pairs. This indicates that the two models make identical predictions.

As mentioned before, the predictions from the models of Liebman and Takahata and co-workers generally agree with known results. However, the physical principles underlying both models and the reasons for their success seem to be unclear. Although both models may be related to the VSEPR concept, the latter itself has some problems (see Sections 3-2-2 and 3-3-9).

3-3. ELECTROSTATIC FORCE THEORY APPLIED TO MOLECULAR SHAPE

3-3-1. Introduction

In this section we describe the ESF theory of Nakatsuji and co-workers as applied to molecular shapes, although the theory is applicable to a wide range of phenomena such as molecular structures, chemical reactions, and long-range

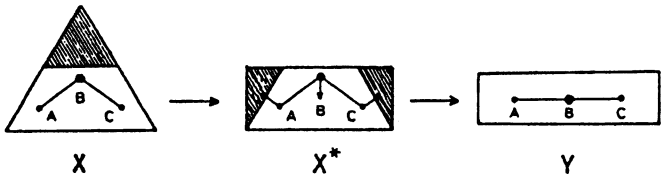

Fig. 3-3. Illustration of forces and electron clouds. (Reproduced from Ref. 207, courtesy the American Chemical Society.)

forces (see Section 7-3). We decompose the H-F force into three pictorial forces (related to chemical concepts such as bond and lone pair), and examine molecular structure in ground and excited states as a stable balance of these separate forces. This provides another explanation of Walsh rules (Table 3-1). Various effects of changes in concerned atoms and their neighboring substituents are systematized and a simple rule for molecular shape is devised. The origin of the internal rotation barrier is also clarified.

It will be instructive to start from the following imaginary example: Consider a stable bent molecule X whose nuclei A, B, C are embedded in the triangular electron cloud of Fig. 3-3. If one transfers (e.g., by electron excitation) the shaded portion of the electron cloud of X to that of X* (e.g., as in the Franck-Condon state), the nuclei A and C in X* receive attractive forces from the shaded portions of electron cloud, while the nucleus B receives a downward (recoil) force due to the break of electrostatic equilibrium in X. These forces induce nuclear movements (arrows in Fig. 3-3) until they die away in structure Y. This example illustrates how the H-F force determines molecular geometry and why the bent molecule X (ground state) becomes linear in the excited state Y.

3-3-2. Partitioning of the Hellmann-Feynman Force

In order to obtain an insight into the relation between force and electron cloud, it is convenient to expand the electron density $\rho(r_1)$ by a sufficiently large AO basis set $\{\chi_r\}$ as

$$\rho(r_1) = \sum_{r,s} P_{rs}\chi_r(r_1)\chi_s(r_1), \tag{3-4}$$

where P_{rs} is the (generalized) bond order between χ_r and χ_s. Then the H-F theorem (3-1) is rewritten as

$$F_A = Z_A\left\{\sum_{r,s} P_{rs}\langle\chi_r|f_A|\chi_s\rangle - \sum_{B(\neq A)} Z_B R_{AB}/R_{AB}^3\right\}, \tag{3-5}$$

where $f_A = r_A/r_A^3$ is the force operator per unit nuclear charge.

For simplicity, we assume that our basis $\{\chi_r\}$ has its center on respective nuclei and its angular part is expressed by the spherical harmonics. We designate the center of basis by subscript, like χ_{rA}, and classify the force integrals in (3-5) into: one-center type $\langle\chi_{rA}|f_A|\chi_{sA}\rangle$; two-center types $\langle\chi_{rA}|f_A|\chi_{sB}\rangle$ (exchange integral) and $\langle\chi_{rB}|f_A|\chi_{sB}\rangle$ (shielding integral); and three-center type $\langle\chi_{rB}|f_A|\chi_{sC}\rangle$. Within the one-center type, the diagonal one ($\chi_{rA}=\chi_{sA}$) vanishes identically from symmetry, since f_A is a vector operator. The off-diagonal integrals which survive are of types $\langle s_A|f_A|p_A\rangle$, $\langle p_A|f_A|d_A\rangle$, etc., where $s, p, d, \ldots$ are sets of $s, p, d, \ldots$ orbitals. These one-center integrals are important when the electron density in atomic region is polarized in the direction of f_A. For the two-center exchange integrals, we introduce a net-exchange-force integral defined by

$$\langle\chi_{rA}|(f_A)_0|\chi_{sB}\rangle \equiv \langle\chi_{rA}|f_A|\chi_{sB}\rangle - \tfrac{1}{2}S_{rAsB}\langle\chi_{sB}|f_A|\chi_{sB}\rangle, \qquad (3\text{-}6)$$

where S_{rAsB} is the overlap integral between χ_{rA} and χ_{sB}. The net-exchange integral represents the net attractive (or repulsive) force due to the accumulation (or depletion) of electron density in the overlap region between χ_{rA} and χ_{sB}. This is seen as follows: Like the electrons of atom B, the electrons in the overlap region also shield the nuclear charge Z_B. This effect is given by $\frac{1}{2}S_{rAsB}\langle\chi_{sB}|f_A|\chi_{sB}\rangle$, which is just the Mulliken (*205*) approximation of the first term. The net-exchange integral is obtained by subtracting this shielding effect from the exchange integral. Further, considering Ruedenberg's (*255*) interference partitioning of electron density into quasi-classical part and quantum interference part, the net-exchange integral represents just the quantum interference effect [see (3-34)].

We now partition the H-F force equation (3-5) into three parts:[5] The *atomic dipole (AD) force* coming from one-center integrals, the *exchange (EC) force* coming from net-exchange force integrals, and the rest called *extended gross charge (EGC) force*, namely,

$$F_A = F_A^{AD} + F_A^{EC} + F_A^{EGC}, \qquad (3\text{-}7)$$

where

$$F_A^{AD} = 2Z_A \sum_{r>s}^{A}\sum^{A} P_{rAsA}\langle\chi_{rA}|f_A|\chi_{sA}\rangle \qquad (3\text{-}8)$$

$$F_A^{EC} = \sum_{B(\neq A)} F_A^{EC}(AB) \qquad (3\text{-}9a)$$

$$F_A^{EC}(AB) = 2Z_A \sum_{r}^{A}\sum_{s}^{B} P_{rAsB}\langle\chi_{rA}|(f_A)_0|\chi_{sB}\rangle \qquad (3\text{-}9b)$$

$$F_A^{EGC} = \sum_{B(\neq A)} F_A^{EGC}(AB) \tag{3-10a}$$

$$F_A^{EGC}(AB) = Z_A \sum_r^B \sum_s^B P_{rBsB} \langle \chi_{rB} | f_A | \chi_{sB} \rangle$$

$$+ Z_A \sum_r^A \sum_s^B P_{rAsB} S_{rAsB} \langle \chi_{sB} | f_A | \chi_{sB} \rangle$$

$$+ Z_A \sum_{C \neq A,B} \sum_r^B \sum_s^C P_{rBsC} \langle \chi_{rB} | f_A | \chi_{sC} \rangle$$

$$- Z_A Z_B R_{AB} / R_{AB}^3. \tag{3-10b}$$

Here Σ_r^A implies summation over the AO bases of atom A. The first three terms in (3-10b) represent the shielding of the bare nuclear repulsion given by the last term.

The physical interpretations of the AD, EC, and EGC forces defined above are as follows: The AD force represents the attraction on nucleus A by the centroid (weight factor $1/r_a^3$) of the polarized atomic density (e.g., lone pair), as illustrated by

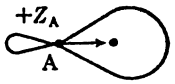

Such polarizations occur typically because of s–p and p–d AO mixing. The EC force represents the attraction (or repulsion) on nucleus A by the electron density accumulated (or depleted) in the overlap region between A and B, as illustrated by

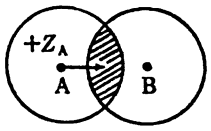

The EGC force represents the interaction between nuclei A and B, the latter shielded by the remainder of electron cloud.

Although the above definitions of AD, EC, and EGC forces are rigorous and include no integral approximation, the EGC force may be further interpreted by invoking the following integral approximations: (1) A point-charge approxi-

mation[6] for the shielding integral

$$\langle \chi_{sB} | r_A / r_A^3 | \chi_{sB} \rangle \simeq R_{AB}/R_{AB}^3, \tag{3-11}$$

and (2) the Mulliken approximation for the smaller integrals $\langle \chi_{rB} | f_A | \chi_{sC} \rangle$ (B, C $\neq$ A and r $\neq s$),

$$\langle \chi_{rB} | f_A | \chi_{sC} \rangle \simeq \tfrac{1}{2} S_{rBsC} \{ \langle \chi_{rB} | f_A | \chi_{rB} \rangle + \langle \chi_{sC} | f_A | \chi_{sC} \rangle \}. \tag{3-12}$$

Then, (3-10) is approximated as

$$F_A^{EGC}(AB) \simeq F_A^{GC}(AB), \tag{3-13a}$$

$$F_A^{GC}(AB) = Z_A \delta_B R_{AB}/R_{AB}^3, \tag{3-13b}$$

where $\delta_B = Z_B - N_B$ is the gross charge (GC) on atom B and $N_B = \Sigma_r^B \Sigma_s^{all} P_{rs} S_{rs}$ is gross atomic population (*205*). The GC force in (3-13b) represents the electrostatic interaction between Z_A and δ_B, as illustrated by

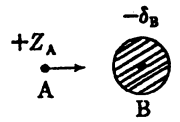

Since the shielding of nuclear charge is usually incomplete,[6a] nuclear-nuclear repulsion is more stressed in the EGC force than in the GC force. Further, since the approximations (3-11) and (3-12) might be inadequate (see also Refs. 52 and 74) we will not use them in force calculations of actual systems.

3-3-3. Construction of a Model for Molecular Shape

We first examine how the AD, EC, and EGC forces operate in a real molecule, e.g., NH_3 [Fig. 3-4(a)]. The AD force (especially important for lone-pair electrons[7]) pulls the N nucleus upwards and operates to make the molecule nonplanar.[8] But, the vector sum of three EC forces due to N—H bond electrons pulls N downwards, operating to make the molecule planar. The EGC or GC forces on N due to three H's and those between the H's are repulsive but small (see below), and the balance of all these forces make the NH_3 molecule pyramidal. However, for CH_3^+, which has no lone pair, the three EC forces make the molecule D_{3h}. Generally, molecules with no lone pair acquire maximum symmetry in which the EC forces balance (e.g., CH_4).

For molecular shape, the respective ratios of AD, EC, and EGC (or GC) forces are important. Comparing these forces on A in A—A and A—H pairs

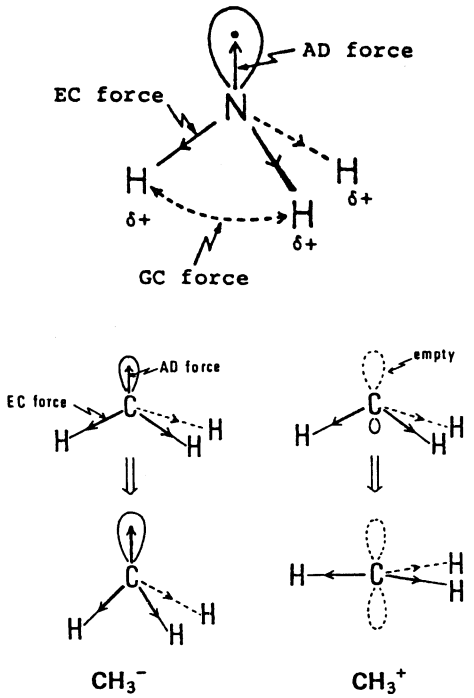

Fig. 3-4(a). Important forces acting in (i) NH_3, (ii) CH_3^-, and (iii) CH_3^+. (Reproduced from Ref. 207, courtesy the American Chemical Society.)

(A is not hydrogen), Nakatsuji (*207*) came to the following conclusions: (1) The AD/EC ratio is larger than unity and is approximately constant for atoms belonging to the same period.[9] (2) The EC force increases with increasing bond multiplicity. For a single bond, EC forces on A in A—A and A—H bonds are approximately equal. One obtains the result

$$\text{AD force} > \text{EC force (triple bond} > \text{double bond} > \text{single bond)} > \text{EGC force.} \tag{3-14}$$

This sequence is consistent with the fact that in the force operator r_{A1}/r_{A1}^3 the nearer electron 1 is to nucleus A the larger is the operator. Thus, the AD and EC forces on nucleus A will mainly determine the shapes of neutral molecules. For ions or highly unshielded atoms, the EGC force may be appreciable.[10,11]

Some examples of rule (3-14) follow: In NH_3 (Fig. 3-4) the AD (>EC) force makes the HNH angle smaller (107.8°)[12] than the tetrahedral value (109.47°). In isobutene and ethylene, ∠C—C—C (111.5°, 117.6°) is smaller than ∠C—C=C

(124.3°, 121.2°), since the EC force along C=C bond is larger than that along C—C and C—H bonds.

3-3-4. Various Influences on the AD and EC Forces

The most important reason for the great variety of molecular shapes is that the valence-electron distribution near A varies from molecule to molecule and state to state. Since the AD and EC forces are dominant factors for molecular shape, it is worthwhile to consider the effects on these forces due to changes in A and the neighboring substituent B, in order to apply the theory to a wide range of molecules. For the AD force, we consider only *s-p* mixing, since with, e.g., H_2S the *p-d* mixing was found to be small.

3-3-4a. Central-Atom Effects on AD and EC Forces. If one replaces the central atom A with heavier atoms in the same group of the periodic table, then the extent of *s-p* (or *p-d*) mixing increases if the energy difference between valence *s* and *p* AOs decreases. This energy difference may be measured by the difference in Mulliken's orbital electronegativity (Fig. 3-4(b); *137, 203, 207*). From Fig. 3-4(b) one then concludes that *within the same group, the extent of s-p mixing and hence the AD/EC ratio will increase with increasing atomic number.*[13] Further, because of the large differences between the first- and second-row elements of groups IV to VII, *there are frequent sharp decreases in valence angles for these elements.*

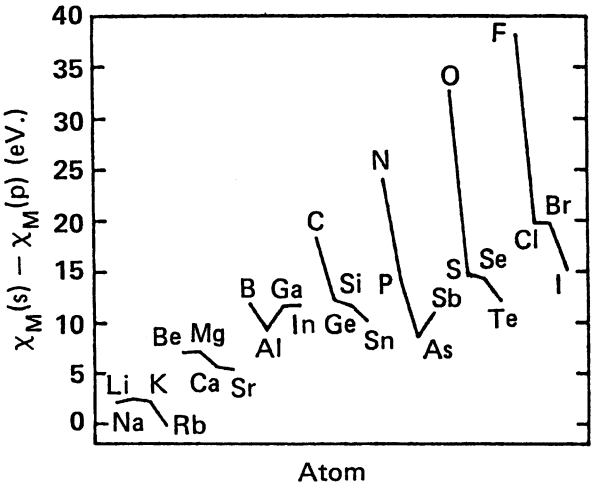

Fig. 3-4(b). Differences in the Mulliken orbital electronegativity between valence *s* and *p* AOs for the elements from the first to fourth rows in the periodic table. (Reproduced from Ref. 207, courtesy the American Chemical Society.)

Consider now the EC force. Since the inner-shell (core) radius increases with atomic number within the same group (see, e.g., Ref. 231), the bond electrons are kept away from the nucleus, and *the EC force is reduced.* Here, too, a sharp difference is found between first- and second-row elements.

The above central-atom effects on AD and EC forces are cooperative, making the molecule with a heavier central atom more bent or pyramidal; for example,

Group V: $NH_3(107.8°)$, $PH_3(93.3°)$, $AsH_3(92°)$
Group VI: $H_2O(105.2°)$, $H_2S(92.2°)$, $H_2Se(91°)$, $H_2Te(90.25°)$.

The sharp decrease in valence angle from NH_3 to PH_3 and from H_2O to H_2S is as expected. We find the same trend in Table 3-3 even for excited states.

3-3-4b. Central-Symmetry Effect on the AD Force. This is the effect of local symmetry of the electron cloud near A. For a distribution which is spherically symmetric around A, or symmetric along the x axis (e.g., when s and p_x AOs are completely filled), no AD force is generated.[14] Examples of this central-symmetry effect can be seen with FHF^-, $ClHCl^-$, $BrHBr^-$ (*95-97, 149*), $LiHLi^-$, $BeHBe^+$ (*154, 247*), $HHHe^+$, He_3^+, $LiHeH^+$ (*245*), ICl_2^-, I_3^-, $IBrCl^-$, Br_3^- (*283, 284*), XeF_2 (*250, 291*). The first eight molecules have H or He as central atom and, since the AD force does not arise due to large $1s$-$2p$ promotion energy, they are linear. The latter molecules are also linear since here the s, p_x, and p_y AOs are completely filled and no important AD force arises even if the molecules are bent from linearity. The same is true for ClF_3, BrF_3, and the planar Jahn-Teller systems LiH_3^+, HeH_3^+ (*245*). In the former two molecules (anchor shape), $\angle FClF$, $\angle FBrF < 90°$, since the in-plane AD force attracts the central atom more than do the EC forces along the bonds.

3-3-4c. Inductive Substituent Effects on AD and EC Forces. Consider the effect of substituent B in the A—B fragment. Since the AD force on A arises mainly from s-p mixing, we look for a σ-inductive effect and a π-inductive effect. For the latter, a π-donating (or attracting) substituent B increases (or decreases) the coefficient of $p_{\pi A}$ AO and the AD force on A. The less direct σ-inductive effect is just the reverse of the π-effect (*207*). The π-effect is more effective than the σ-effect, although the two are usually cooperative[15] (see below).

Consider the effect on the EC force at a fixed A—B distance. If B is more electronegative than A, B draws electron density in the A—B bond region toward itself and thus the EC force on A decreases. Hence, at fixed A—B distance, the more electronegative the substituent B, the smaller is the EC force on A.

As an example, consider the out-of-plane angles (and also the corresponding

force constants) in fluoromethyl radicals (*100*). The systematic increase, CH_3 (0°), CH_2F(<5°), CHF_2(~12.5°) CF_3(~17.8°) is explained as follows: Since F is π donating and σ attracting, it increases the AD force on C; and since F is more electronegative than H the EC force on C diminishes. The two effects cooperate to make the fluorosubstituted molecule nonplanar. The planarity of the CH_3 radical is due to a sensitive balance of AD and EC forces (see Section 3-3-6). These considerations also explain why ESR experiments reveal the series CCl_3, CCl_2F, $CClF_2$, CF_3 to be increasingly nonplanar (*60*).

3-3-4d. Overlap Effects on AD and EC Forces. Orbital overlap is quite important for both molecular structure and chemical reaction. The overlap effect usually causes larger changes in electron density than the inductive effect. For a homopolar A—B fragment, the bonding and antibonding MOs are

$$\phi_b = (\chi_{rA} + \chi_{sB})/(2 + 2S)^{1/2} \tag{3-15a}$$

$$\phi_a = (\chi_{rA} - \chi_{sB})/(2 - 2S)^{1/2}, \tag{3-15b}$$

where S is the overlap integral between AOs χ_{rA} and χ_{sB}. Equations (3-15) indicate that in the bonding interaction the electrons in each AO flow into the overlap region and, in the antibonding interaction, the electrons in the overlap region are transferred back into each atomic region because of the presence of a node.

Table 3-2 summarizes the overlap effects on AD and EC forces. $D(\chi_{rA})$ denotes the electron density in the χ_{rA} AO. Since an increase in the coefficients of s_A and p_A AOs facilitates the formation of atomic dipole, the change in $D(\chi_{rA})$ parallels that in the AD force.[16] In the bonding interaction, the AD force decreases, since $D(\chi_{rA})$ decreases from 1 to $1/(1 + S)$ and the EC force increases by $2I_{EC}/(1 + S)$. Both effects *cooperate* to make the molecule linear or planar. The antibonding overlap effect is just the reverse and facilitates bending. When both χ_{rA} and χ_{sB} are doubly occupied, the antibonding effect surpasses the bonding effect and again facilitates bending. Generalization of Table 3-2 to more than two interacting AO systems is easy. There, we have to consider the nonbonding interaction (recall the second π MO of allyl radical) where the AD and EC overlap effects are approximately zero (see Section 3-3-7c).

Clearly, the overlap effect[17] becomes appreciable when (1) the AOs χ_{rA} and χ_{sB} overlap significantly, (2) their energy levels are close, and (3) electrons in both AOs are not tightly bound.

The fact that EC force increases with bond multiplicity is a manifestation of overlap effect. Compare the shapes [Fig. 3-4(c)] of acetylene and triplet $CH_2(^3B_1)$. In linear form, the $p_{\pi C}$ AO in CH_2 does not have overlap, but that

Table 3-2. Overlap Effect on Molecular Geometry and Chemical Reaction.

Interaction	$D(p_{\pi A})$ AD force	EC force[a,b]	Corresponding phenomena		
			Molecular shape	Chemical reaction	
Bonding interaction[c]	$\frac{1}{1+S}$	$\frac{2}{1+S}I_{EC}$	linear or planar	driving force	Conservation of molecular orbital symmetry
Antibonding interaction[d]	$\frac{1}{1-S}$	$-\frac{2}{1-S}I_{EC}$	bent or pyramidal	repulsive force	
Interaction between fully occupied AOs	$\frac{2}{1-S^2}$	$-\frac{4S}{1-S^2}I_{EC}$	bent or pyramidal	repulsive force	(i) Non-least motion reaction path (ii) Exchange repulsion

[a] $I_{EC} = \langle \chi_A | (f)_0 | \chi_{sB} \rangle$. The prefactor of I_{EC} is the bond order between χ_{rA} and χ_{sB}.
[b] Plus and minus signs correspond to the attractive and repulsive forces between A and B.
[c] The values correspond to the electronic configuration $(\phi_b)^2(\phi_a)^0$.
[d] The values correspond to the electronic configuration $(\phi_b)^0(\phi_a)^2$.
SOURCE: Ref. 209. Courtesy the American Chemical Society.

in acetylene strongly overlaps with the adjacent $p_{\pi C}$ AO. Since $D(p_{\pi C})$ is 1.0 for CH_2 but ~0.75 for acetylene, the AD force on C produced by small bending is stronger in CH_2. Second, because of overlap the EC force on C is stronger in acetylene. Thus, while CH_2 is bent (*135*) acetylene is linear.

Overlap effect is also important for molecules in which the central atom p AO overlaps with lower lying vacant AOs of adjacent atoms (e.g., $p\pi$-$d\pi$ conjugation).[18] Consider the change in valence angle in the ammonia derivatives, NF_3(102.5°), NH_3(107.8°), $N(SiH_3)_3$(120°; Ref. 132). The change from NH_3 to NF_3 is due to inductive-substituent effects on AD and EC forces. The larger change from NH_3 to $N(SiH_3)_3$ is mainly due to overlap conjugation between $p_{\pi N}$ and $d_{\pi Si}$ AOs, which reduces the AD force on N and strengthens the EC force due to the multiple-bond character of the N—Si bond.[19] The less important inductive-substituent effect on the EC force also facilitates this change. Similar examples are seen in the difference in the COC angles of aliphatic (108-110°) and aromatic (120-125°) ethers (*116*), planarity (*125*) around N in $N_2(SiH_3)_4$, and in the water derivatives OF_2(103.8°), OH_2(105.2°), $O(SiH_3)_2$(144.1°; Ref. 6), $O[TiCl_2(C_5H_5)]_2$(180°; Ref. 61). The larger bond angle in OCl_2(110.8°) compared with H_2O indicates that the overlap effect is more important than the inductive effect. However, the two effects are cooperative in alkali metal derivatives of H_2O (Section 3-3-7b). When the central atoms N and O are replaced by heavier atoms such strong p_π-d_π interaction does not seem to occur (*116*).

The overlap effect on the EC force is quite important for choosing chemical reaction pathways. The attractive EC force due to bonding overlap between χ_{rA} and χ_{sB} (A and B are reaction sites) provides the driving force of the reaction (*207, 216*), but the antibonding overlap and overlap between fully occupied AOs cause repulsive forces. When this knowledge is combined with HOMO-LUMO interactions (*109–112*) one obtains the well-known Woodward-Hoffmann

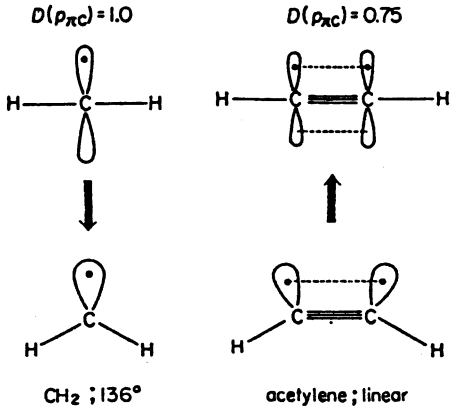

Fig. 3-4 (c). Structures of triplet carbene and acetylene as examples of overlap effect.

rule (*108*, *302*). The overlap stabilization proposed by Fukui (*107*) is an energetic expression of the overlap effect on the EC force. The repulsive EC force between fully occupied AOs expresses short-range exchange repulsion and corresponds to the so-called exclusion shell[20] (*258*, *260*). For example, the non-least motion reaction path studied by Hoffmann et al. (*143*) is determined by a combination of the attractive and repulsive EC forces.

3-3-5. Changes in Force Due to Changes in Electronic State

We will employ MO theory in dealing with changes in electronic state such as electron excitation, ionization, and attachment (recall Fig. 3-3). Let $\{\phi_i\}$ be a set of MOs with occupation numbers $\{m_i\}$. The electron density $\rho(r_1)$ is

$$\rho(r_1) = \sum_i m_i \phi_i^*(r_1)\, \phi_i(r_1) = \sum_i m_i \rho_i(r_1). \tag{3-16}$$

Denoting the ith MO contribution to the force as f_{Ai}

$$f_{Ai} \equiv \int f_A(r_1)\, \rho_i(r_1)\, dr_1, \tag{3-17}$$

we obtain the H–F theorem in the form

$$F_A = Z_A \sum_i m_i f_{Ai} - Z_A \sum_{B(\neq A)} Z_B R_{AB}/R_{AB}^3. \tag{3-18}$$

If we neglect the changes in MOs following the change in electronic state, $\alpha \rightarrow \beta$ (vertical state), the change in the force acting on A is

$$\Delta F_A^{\alpha \rightarrow \beta} = Z_A \sum_i (m_i^\beta - m_i^\alpha) f_{Ai}. \tag{3-19}$$

For example, for excitations between states with the same electronic configurations,

$$\Delta F_A^{\alpha \rightarrow \beta} = 0, \tag{3-20}$$

which implies that the differences in the geometries, force constants, etc. of the two states are quite small. Hurley (*148*) confirmed this.

For the excitation from ith to jth MO,

$$\Delta F_A^{i \rightarrow j} = Z_A (f_{Aj} - f_{Ai}); \tag{3-21}$$

for ionization from ith MO,

$$\Delta F_A^{i\to\infty} = -Z_A f_{Ai}; \tag{3-22}$$

and for electron attachment to ith MO,

$$\Delta F_A^{\infty\to i} = Z_A f_{Ai}. \tag{3-23}$$

For cations (R^+), radicals ($R\cdot$), and anions (R^-) having electronic configurations $(\phi_i)^0$, $(\phi_i)^1$, and $(\phi_i)^2$, the force at radical geometry satisfies

$$\Delta F_A(R\cdot \to R^+) = -\Delta F_A(R\cdot \to R^-), \tag{3-24}$$

implying that the force-dependent properties of $R\cdot$ should always be intermediate between those of R^+ and R^- (*207*).

Consider now the changes in the AD, EC, and EGC forces. We rewrite (3-21) as

$$\Delta F_A^{i\to j} = Z_A \int f_A(r_1)\, \Delta\rho(r_1)\, dr_1, \tag{3-25}$$

where $\Delta\rho(r_1) = \rho_j(r_1) - \rho_i(r_1)$ is the change in electron density due to excitation. The change in the atomic region changes the AD force, while that in the bond region changes the EC force. As an example, consider electronic transition from the lone-pair orbital to the Rydberg *ns* or *np* orbital in NH_3. Since the electron densities in these Rydberg orbitals are almost symmetric with respect to the N nucleus, they exert no force on N and hence the geometry in these excited states should be planar (*134*), like NH_3^+. (For more detailed studies on such geometry changes, see Refs. 38, 49, 68, 155, 214, and 241).

3-3-6. Illustrative Applications of the ESF Model and a Simple Rule for Molecular Shape

Consider the roles of AD and EC forces when the molecules CH_3^-, CH_3^+, and CH_3 are slightly bent from planar shape.[21] With CH_3^- (Fig. 3-4), an atomic dipole rapidly forms on the C atom and pulls it upwards while the vector sum of three EC forces pulls it downwards. In view of relation (3-14), the molecule continues to bend until the two opposing forces on C balance. Thus, CH_3^- is pyramidal (experimental: *47*; theoretical: *43*, *87*, *88*, *162*, *282*). For CH_3^+, the upward atomic dipole is not generated, since the corresponding orbital is empty, and the three EC forces balance each other by restoring the molecule into planar shape (D_{3h}). Similarly, isoelectronic BH_3 and BeH_3^- are planar D_{3h}

(*240*). According to (3-24), CH_3 is intermediate between CH_3^- and CH_3^+, and its shape is the result of a sensitive balance between AD, EC, and EGC forces. It is planar (*134*) like its isoelectronic analogs NH_3^+ (*58*) and BH_3^- (*286*). The qualitative arguments given here were justified by ab initio force calculations with floating wavefunctions for NH_3, CH_3^+, and NH_3^+ which satisfy the H-F theorem (*221*). Further, the out-of-plane bending force constant should be larger for CH_3^+ than for CH_3.

On the basis of such examples as those given above, we shall now formulate a simple and quite general rule that links molecular shape with $D(p_{\pi A})$, A being the central atom. As $D(p_{\pi A})$ we take the value when the molecule is set in *planar or linear* form.

The relation of $D(p_{\pi A})$ with planarity (or linearity) and bending force constant is given by the simple rule in Fig. 3-5. AXY and AXYZ molecules differ mainly in the number of EC forces, two for the former and three for the latter, e.g., CH_2 (bent) and CH_3 (planar) although $D(p_{\pi C})$ is unity for both molecules.

Three EC forces
Planar

Two EC forces
Bent

The critical values of $D(p_{\pi A})$ in Fig. 3-5, separating shaded from dark regions, are chosen from this example. The generality of this rule for AXY and AXYZ molecules arises from the fact that the inductive substituent effects on the AD and EC forces are generally cooperative, as are the overlap effects on the AD and EC forces[22] (Sections 3-3-4c, d). The quantity $D(p_{\pi A})$ is taken as an indicator common to these effects. *Figure 3-5 is quite useful in predicting molecular shapes in ground and excited states*, e.g., the vast number of planar aromatic hydrocarbons for which $D(p_{\pi C})$ is always less than unity. This is also reminiscent of Walsh rules, although $D(p_{\pi A})$ is likely to be more useful for shape predictions than the number of valence electrons, since the former is a better index for local electron distribution. In fact, this rule applies to excited states as well as ground states.

It should be noted, however, that the simple rule in Fig. 3-5 has certain limitations. (i) It is affected by the central-atom and central-symmetry effects, the

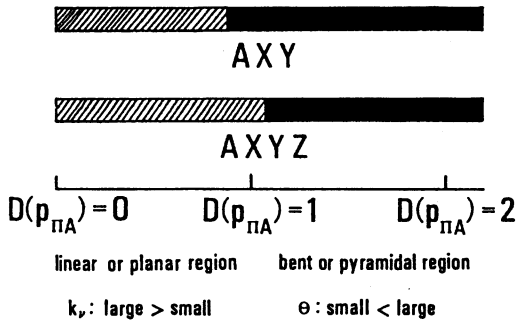

Fig. 3-5. A simple rule for the shapes of AXY and AXYZ molecules where A is the central atom and X, Y, Z are the substituents. $D(p_{\pi A})$, k_ν, and θ are, respectively, the electron density of the $p_{\pi A}$ AO in planar or linear structure, the out-of-plane bending force constant, and the out-of-plane angle. (Reproduced from Ref. 207, courtesy the American Chemical Society.)

former being especially important near the critical values of $D(p_{\pi A})$. (ii) It implicitly assumes near constancy in the nature of s_A AOs for various AX_n molecules. Since s_A electrons are more tightly bound than p_A ones, this assumption is usually justified, except when the number of valence electrons around A increases to fill the high-lying s_A-σ_X antibonding orbital (Fig. 3-6 below). Here, both s_A and $p_{\pi A}$ AOs are completely filled and, because of the central-symmetry effect, the molecule becomes linear or planar (e.g., XeF_2, ClF_3) even though $D(p_{\pi A}) \geqslant 2$.

3-3-7. Applications of the ESF Model to Molecular Shapes

3-3-7a. AH_2 and AH_3 Molecules. Based on the previous discussions, the reader will now be able to rationalize the shapes of those molecules in ground and excited states (Tables 3-3 and 3-4). $D(p_{\pi A})$ is the occupation number of the $n(\bar{\pi})$ orbital. Being symmetric about nucleus A, the electron densities in π and Rydberg orbitals do not exert force on A. When an electron jumps from the $n(\bar{\pi})$ to the π orbital, the apex angle increases substantially, e.g., $^*NH_2$ and $^*PH_2$ (Table 3-3). But when an electron jumps from π to Rydberg orbital, there is little change, e.g., $^‡H_2O$. The central-atom effect is observed for both ground and excited states; a sharp change occurs between first- and second-row elements. Limiting ourselves to the ground state, $D(n(\bar{\pi})) = 0, 1, 2$ corresponds to 4, 5, 6–8 valence electrons, respectively. Thus, the ESF model reproduces the Walsh rules (Table 3-1). This is also true for more complex molecules.

For the 2-valence-electron bent molecules H_3^+, Li_3^+, LiH_2^+ (*245, 249*), a direct application of the above model seems inadequate. For example, with LiH_2^+ it may be wrong to imagine a bond between Li and H, since the resulting EC force on Li will give a linear molecule. Rather, the electron cloud in these systems will

Table 3-3. Shapes of AH_2 Molecules.

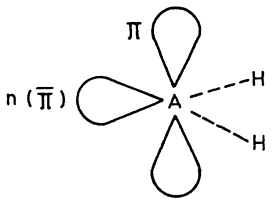

Shape	Occupation no. of orbital[a] $n(\bar{\pi})$	π	Rydberg	AH_2[b]
linear	0	0 or 1	0 or 1	BeH_2, BH_2^+, ‡BH_2, ‡AlH_2
bent	1	0	0	BH_2(131°), AlH_2(119°)
bent	1	1	0	$CH_2(^3B_1, 136°)$, $CH_2(^1B_1, \sim 140°)$, $NH_2^+[^3B_1, 143.2°]$[c]
bent	1	2	0	*NH_2(144°), *PH_2(123.1°)
bent	2	0	0	$CH_2(^1A_1, 102.4°)$, BH_2^-[102°], NH_2^+[110.5°][c], SiH_2(–)
bent	2	1	0 or 1	NH_2(103.4°), PH_2(91.5°), ‡OH_2(106.9°)
bent	2	2	0	OH_2(105.2°), SH_2(92.2°), SeH_2(91°), TeH_2(90.25°), NH_2^-(104°)

[a]See the diagram at the top of the table.
[b]Values in ( ) and [ ] mean the apex angles obtained experimentally or from ab initio calculations, respectively. The asterisk and double dagger mean, respectively, the $n \rightarrow \pi^*$ and Rydberg excited states.
[c]M. M. Heaton and R. Cowdry, *J. Chem. Phys.*, **62**, 3002 (1975).
SOURCE: Ref. 208. Reprinted courtesy the American Chemical Society.

Table 3-4. Shapes of AH_3 Molecules.

Shape	Occupation no. of π orbital	AH_3[a]
planar	0	HeH_3^+, LiH_3^+, BeH_3, BeH_3^-, BH_3, CH_3^+, ‡CH_3, SiH_3^+[b]
planar	1	CH_3, BH_3^-, NH_3^+, ‡NH_3, ‡PH_3
pyramidal	1	SiH_3(113.5°), GeH_3(115°), SnH_3(117°)
pyramidal	2	CH_3^-(–), NH_3(107.8°), PH_3(93.3°), AsH_3(92°), OH_3^+(117°), SiH_3^-[b]

[a]The double dagger means that the molecule is in the Rydberg excited state.
[b]B. Wirsam, *Chem. Phys. Lett.*, **18**, 578 (1973).
SOURCE: Ref. 208. Reprinted courtesy the American Chemical Society.

shield the three nuclei (or cores) more effectively if it accumulates within the nuclear triangle.

For AH_3 molecules (Table 3-4), almost all features have been discussed previously, including the sensitive problem of 7-valence-electron molecules. Since $D(p_{\pi A})$ is related to the number of valence electrons, the Walsh rules are again reproduced.

3-3-7b. Alkali Metal Derivatives of H_2O. The linear geometries of Li_2O (*42, 44, 128, 297*), LiOH (*44, 128*), KOH, RbOH and CsOH (*2, 172, 174, 186*) are quite interesting. Because of the highly ionic character of, e.g., Li_2O and LiOH, ab initio (*44*) and extended Hückel (*5*) angular correlation diagrams and the SOJT model (Section 3-2-3) were unsuccessful for these molecules.

The ESF model explains these linear shapes by noting that here all the substituent effects on the AD, EC, and EGC forces cooperate to increase the apex angle considerably. Since the highly electropositive alkali metal has vacant p valence AOs, it is a σ-donating and π-overlapping (like p_π-d_π overlap, Section 3-3-4) substituent and decreases the AD force on oxygen. Also, since the metal-oxygen bond electrons are highly polarized toward oxygen, the EC force on O increases considerably. The EGC force between terminal atoms is also repulsive. The linearity of Li_2O is also explained from the central-symmetry effect, since its electronic structure is almost $Li^+O^{2-}Li^+$(*4, 5*).

3-3-7c. XAY Molecules. The relevant MOs of these molecules (Fig. 3-6), in ascending energy order, are: $\bar{\pi}_u(0.37)$, $\sigma_u(0.0)$, $\bar{\pi}_g(0.0)$, $\bar{\pi}_u^*(0.77)$, $\sigma_s^*(0.0)$, the numbers indicating contribution to $D(p_{\bar{\pi}A})$ as calculated for the allyl radical, and the asterisk indicating antibonding orbitals. $\bar{\pi}_g$ is a nonbonding MO. Consider bending in the $\bar{\pi}$-plane. The π_u, π_g, and π_u^* MOs, perpendicular to the $\bar{\pi}$-plane, do not contribute to $D(p_{\bar{\pi}A})$ but contribute to the EC force through overlap effect (bond multiplicity). The σ_s^* MO is s_A-σ_X and s_A-σ_Y antibonding, and is closely related with central-symmetry effect.

From Fig. 3-5, we obtain the following predictions parallel to the Walsh rules:

1. When the $\bar{\pi}_u^*$ MO is empty ($<$16 valence electrons in ground state), $D(p_{\bar{\pi}A})<1$, at most $2 \times 0.37 = 0.74$. Hence, the molecule will be linear (Table 3-5).
2. When $\bar{\pi}_u^*$ is singly occupied (17 valence electrons in ground state), $D(p_{\bar{\pi}A})>1$, e.g., $0.74 + 0.77 = 1.51$, and the molecule is bent (experimentally, 122–136°; Table 3-5).
3. When $\bar{\pi}_u^*$ is doubly occupied (18–20 valence electrons in ground state), $D(p_{\bar{\pi}A})$ increases further, e.g., $0.74 + 2 \times 0.77 = 2.3$ and the molecule becomes more bent (experimentally, 100–126°).
4. When the σ_s^* MO is filled (22 valence electrons in ground state), the s_A, $p_{\bar{\pi}A}$ and $p_{\pi A}$ AOs are completely filled and the central-symmetry effect makes the molecule linear.

These conclusions are also applicable to excited states (Table 3-5).

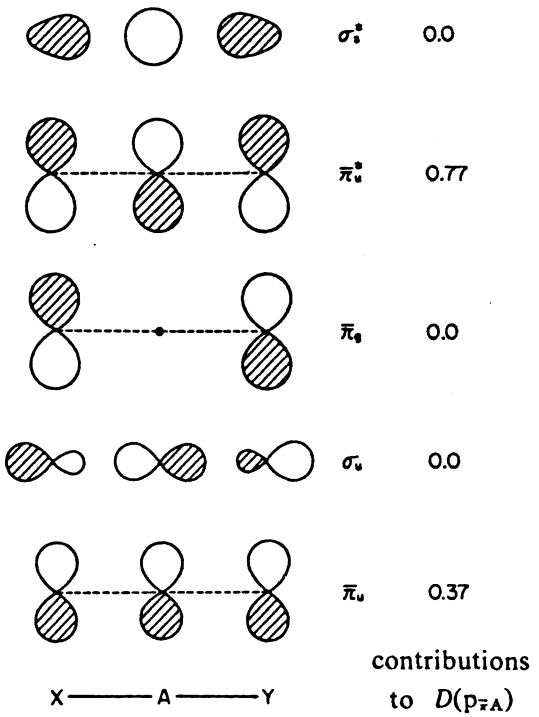

Fig. 3-6. Schematic MOs for XAY molecules. A hatch is made to show the bonding and antibonding character of the MOs. The right-hand number shows the contribution of each MO to $D(p_{\bar{\pi}A})$ calculated from the allyl system. (Adapted from Ref. 208, courtesy the American Chemical Society.)

3-3-7d. Alkaline Earth Dihalides. These 16-valence-electron XAY molecules are very interesting, since their shapes depend upon the metal–halogen combinations (Table 3-6), whereas according to Walsh rules they should all be linear. Actually, the light metal–heavy halogen combinations are linear, while the heavy metal–light halogen combinations are bent (*41*). If one modifies the Walsh diagram by considering the effect of normally unoccupied *d* AOs of the metal atom, then these trends can be explained (*64*, *126*, *131*).

The ESF model explains these trends as follows: Since the metal has vacant *p* valence AOs and low-lying vacant *d* AOs,[23] the halogen *p* electrons will flow into these vacant AOs by both overlap and π-donating inductive effects. Since these effects clearly increase from I to F and from Be to Ba, the AD force on metal increases in this order (the *p*–*d* mixing may also be important here[23]). Due to the increase in metal–halogen electronegativity difference the EC force increases in the same order (σ-inductive effect). Since both AD and EC forces are cooperative, this explains the trends in Table 3-6.

Table 3-5. Shapes of XAY Molecules.

Geometry and electronic configuration[a]	XAY[b]
linear $(\pi_u)^2(\sigma_u)^0$	OLi_2
linear $(\pi_u)^4(\sigma_u)^m(\pi_g)^n$ $m \leq 2$ $n \leq 4$	$C_3(2,0)$, $C_3^*(1,1)$; CCSi(2, 0), CCSi*(1, 1); CCN(2, 1), CCN*(1, 2); CNC(2, 1), CNC*(1, 2); NCN(2, 2), NCN*(1, 3); $BO_2(2,3)$, $BO_2^*(1,4)$; NCO(2, 3), NCO*(1, 4); $CO_2^+(2,3)$, $CO_2^{+*}(1,4)$; $OCS^+(2,3)$, $OCS^{+*}(1,4)$; $CS_2^+(2,3)$, $CS_2^{+*}(1,4)$; $N_3(2,3)$, $N_3^*(1,4)$; $NNO^+(2,3)$, $NNO^{+*}(1,4)$; NNO(2, 3)
linear $(\pi_g)^4(\pi_u^*)^0$	CO_2, CS_2, NCO^-, NCS^-, N_3^-, OCS, NNO, NO_2^+
bent $(\pi_g)^3(\pi_u^*)^1$; $(\pi_g)^4(\pi_u^*)^1$	$CO_2^*(122°)$, $CS_2^*(135.8°)$, $NCO^{-*}(-)$, $NCS^{-*}(-)$, $N_3^{-*}(-)$, $NO_2(4, 1, 134.1°)$
bent $(\pi_g)^m(\pi_u^*)^n$ $3 \leq m \leq 4$ $2 \leq n \leq 4$	$NO_2^*(3, 2, 121°)$[c]; $CF_2(4, 2, 104°)$, $CF_2^*(3, 3, -)$; $CCl_2(4, 2, -)$; $SiF_2(4, 2, 101°)$, $SiF_2^*(3, 3, -)$; $NO_2^-(4, 2, 115.4°)$, $NO_2^{-*}(3, 3, -)$; ONF(4, 2, 110°), ONF*(3, 3, –); $SO_2(4, 2, 119.5°)$, $SO_2^*(3, 3, 126.1°)$; SSO(4, 2, 118°), SSO*(3, 3, –); ONCl(4, 2, 116°), ONBr(4, 2, 117°), $O_3(4, 2, 116.8°)$, $NF_2(4, 3, 104.2°)$, $ClO_2(4, 3, 117.6°)$, $OF_2(4, 4, 103.8°)$, $OCl_2(4, 4, 110.8°)$, $SCl_2(4, 4, 101°)$, $TeBr_2(4, 4, \sim 98°)$, $ClO_2^-(4, 4, 110.5°)$
linear $(\pi_u^*)^4(\sigma_s^*)^2$	$IBrCl^-$, Br_3^-, ICl_2^-, $ClIBr^-$, IBr_2^-, I_3^-, XeF_2

[a]The MO density distributions are illustrated in Fig. 3-6. Both π and $\bar{\pi}$ MOs are written as π.

[b]Values in parentheses are m, n, and experimental apex angles. The asterisk means that the molecule is in the excited state.

[c]The structure of the Rydberg excited state of NO_2, $(\pi_g)^4(\pi_u^*)^0(3p\sigma)^1$ is linear.

SOURCE: Ref. 208. Reprinted courtesy the American Chemical Society.

3-3-8. Force along Internal Rotation and the Shapes of $X_m ABY_n$ Molecules

Since the shapes of $X_m AB$ and ABY_n fragments are readily understood from previous discussions, we are now concerned with a new problem, namely, internal rotation about the AB bond (single, double, or triple). By extension of these two treatments, the shapes of general $AX_k(BY_l)_m CZ_n$ molecules can be explained.

Table 3-6. Geometries of Alkaline Earth Dihalides.[a,b]

Central metal	Halogen F (4.0)	Cl (3.0)	Br (2.8)	I (2.5)
Be (1.5)	*l*	*l*	*l*	*l*
Mg (1.2)	*l*[c] or *b* (158°)[d]	*l*	*l*	*l*
Ca (1.0)	*b* (140°)[d]	*l*	*l*	*l*
Sr (1.0)	*b* (108°)[d]	*b* (120°)[e]	*l*	*l*
Ba (0.9)	*b* (~100°)[d]	*b* (~100°)[e]	*b*	*b*

[a] *l*, linear; *b*, bent. Values in parentheses are the Pauling electronegativities (*231*).
[b] L. Wharton, R. A. Berg, and W. Klemperer, *J. Chem. Phys.*, 39, 2023 (1963); Refs. 41, 42.
[c] M. Kaufman, J. Muenter, and W. Klemperer, *J. Chem. Phys.*, 47, 3365 (1967).
[d] V. Calder, D. E. Mann, K. S. Seshadri, M. Allavena, and D. White, *J. Chem. Phys.*, 51, 2093 (1969).
[e] D. W. White, G. V. Calder, S. Hemple, and D. E. Mann, *J. Chem. Phys.*, 59, 6645 (1973).

3-3-8a. Orbital Following and Preceding. In this section we shall see that the dominant origin of internal rotation barrier arises from an interesting behavior of electron density during rotation, namely, orbital following (*179*) and preceding. The ESF concept explained here is quite general and provides a new key to understanding nuclear rearrangement processes such as molecular structure, molecular vibration, and chemical reaction.

Consider the internal rotation barrier of ethylene (Fig. 3-7). Energetically, the

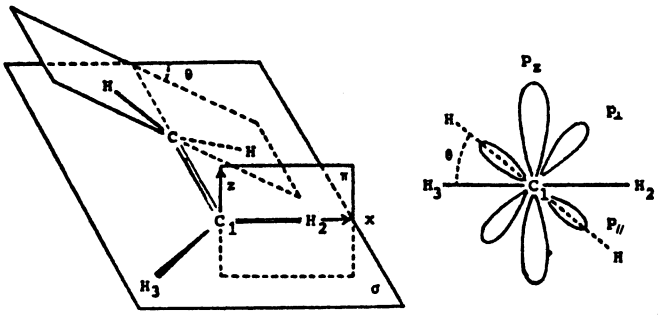

Fig. 3-7. The ethylene molecule twisted by the angle θ. The right-hand side shows the Newman-type diagram. Front-side and back-side CH_2 fragments are shown by solid and dashed lines, respectively. The p_z AO on the front-side CH_2 is decomposed into $p_\perp$ and $p_\parallel$ AOs, where the notations $\perp$ and $\parallel$ refer to the back-side CH_2 plane. (Reproduced from Ref. 209, courtesy the American Chemical Society.)

planar form is stable because the bonding interaction between two $p_{\pi C}$ AOs is maximum at planarity (*161, 201, 202, 204*). The ESF explanation considers the behavior of electron density in the C_1—H_2 bond region (Fig. 3-7): We switch off the interaction between two CH_2 fragments, rotate the back-side CH_2 by angle $-\theta$, and then resolve the p_z AO of the front-side CH_2 into $p_\perp$ and $p_\parallel$ components on the π-plane. When we switch on the interaction, electrons in $p_\perp$ AO flow into the C—C bond region owing to the bonding overlap with the p_π AO of back-side CH_2, but electrons in the $p_\parallel$ AO suffer little change, since it interacts with back-side C—H bond orbital which tightly binds the electrons (Section 3-3-4d). Consequently, the electron density along the C_1—H_2 bond changes (see Ref. 209 for detailed contour plot at $\theta = 45°$, using the extended Hückel method).[24] Indeed, the C—H bond electron cloud follows *incompletely* (*orbital following*) the rotation of the C—H axis in the θ direction (Fig. 3-8). This

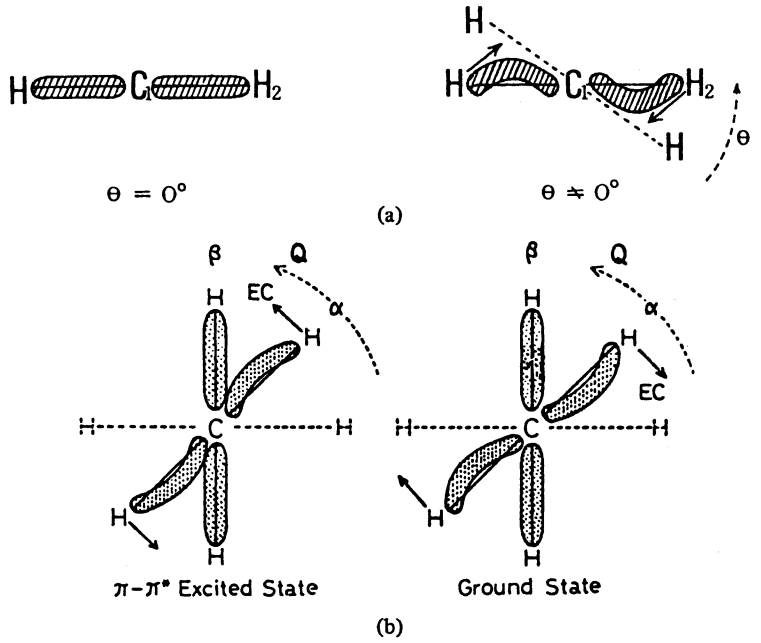

Fig. 3-8. General features of the C—H bond electrons during internal rotation of the ground and π-π^* excited states of ethylene. (a) Incomplete following of the C—H bond orbital in the ground state. In (b) the dashed C—H bonds belong to the back-side CH_2 group. Q is the coordinate of internal notation from planar to bisected configuration, α corresponds to the configuration of the intermediate rotational angle, and β to the bisected configuration. The arrows starting from protons at α show the EC forces acting on protons due to the preceding (π-π^* excited state) and incomplete following (ground state) of the C—H bond electron clouds. (Reproduced from Ref. 210, courtesy the American Chemical Society.)

causes an EC force (arrow in Fig. 3-8) which does not lie on the C—H axis and resists internal rotation. Extended Hückel calculations (*209*) for the $(\pi)^2(\pi^*)^0$ electronic configuration of ethylene reveal that the EC(H_2—C_1) force component (-0.0286 au) is the dominant contribution to $F_z(H_2)$, the total rotational force component (-0.0262 au).[25] Thus, ESF theory concludes that orbital following and the resulting resisting force are responsible for the planarity of ethylene (valid also for a wide range of double-bonded hydrocarbons).

On the other hand, there are situations where the C—H bond electron cloud *precedes* the rotation of C—H axis (*orbital preceding*). Consider the difference density map (Fig. 3-9) for the π-π^* excited state of ethylene, $(\pi)^1(\pi^*)^1$. The antibonding (π^*) overlap effect on the $p_\perp$ AO (Fig. 3-7) exceeds the bonding (π) overlap effect (Table 3-2) and causes orbital preceding. The resulting EC force on the proton further accelerates the rotational motion (Fig. 3-8) and makes the molecule stable in the bisected form, $\theta = 90°$. Extended Hückel calculations (*209*) again show that the EC(H—C) component is the major contribution

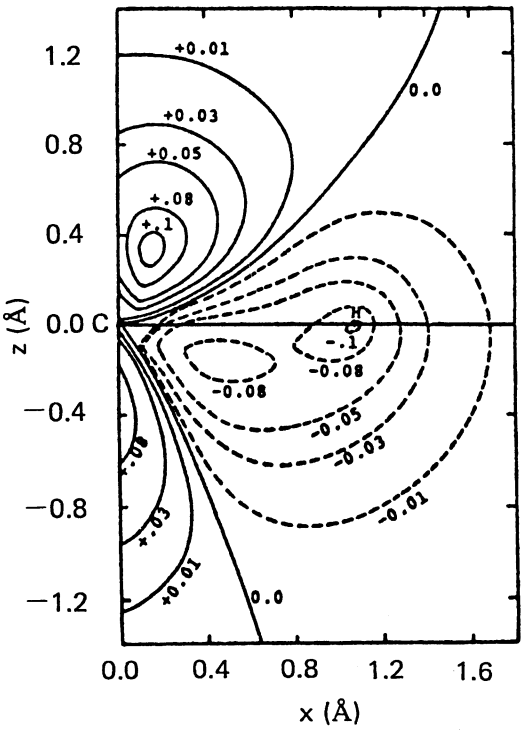

Fig. 3-9. The change in electron density along the C_1—H_2 bond on the π-plane induced by twisting the π-π^* excited state of ethylene through $\theta = 45°$. The electronic configuration is $(\pi)^1(\pi^*)^1$. (Reproduced from Ref. 209, courtesy the American Chemical Society.)

(0.0144 au) to the total accelerating force (0.0178 au). The same is true for the $(\pi)^0(\pi^*)^0$ configuration. Indeed, the π-π^* excited state of ethylene (*187, 298*), BH_2BH_2 (Frost, quoted in Ref. 233), and B_2F_4 (*114, 230*) all have the bisected form, $\theta = 90°$.

When both the p_π AOs of the two rotors are doubly occupied, $(\pi)^2(\pi^*)^2$, the overlap effect becomes similar to $(\pi)^1(\pi^*)^1$, although the extent of orbital preceding is now smaller (*209*). In the $(\pi)^2(\pi^*)^2$ case, both $D(p_{\pi A})$ and $D(p_{\pi B})$ are greater than 2 and both H_2AB and ABH_2 fragments become bent. Since the A—B bond here is regarded as a single bond, we shall discuss these structures in Section 3-3-8b.

It has been confirmed that for all ethylenic configurations depicted in Fig. 3-10, the $EC(H_2—C_1)$ force due to orbital following (negative region) and preceding (positive region) is the dominant factor in $F_z(H_2)$. Orbital following also occurs for the configuration $(\pi)^2(\pi^*)^1$. Interestingly, for the cation configuration $(\pi)^1(\pi^*)^0$ orbital preceding occurs when $0° \leqslant \theta \leqslant 45°$, but orbital

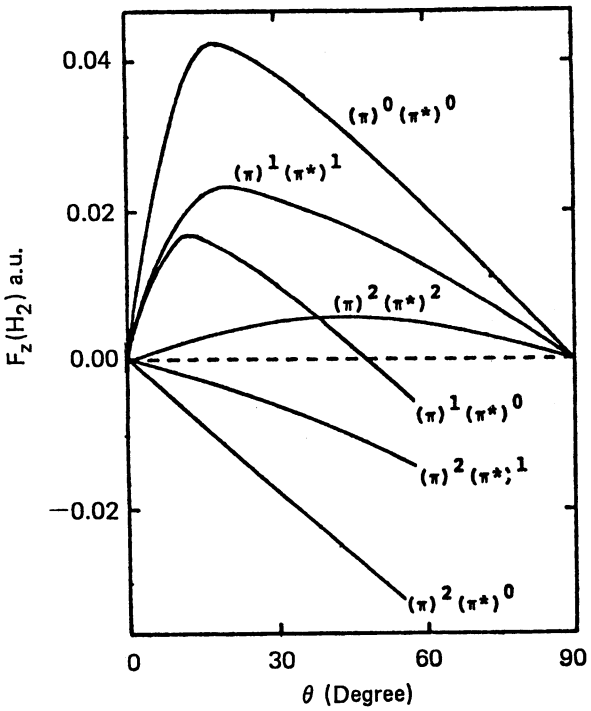

Fig. 3-10. Curves of the rotational force, $F_z(H_2)$ versus the twist angle θ, for various electronic configurations arising from ethylenic MOs calculated by the extended Hückel method. Since π and π^* MOs become degenerate at $\theta = 90°$, the plot is given only in the region $0° \leqslant \theta \leqslant 45°$ for the configurations $(\pi)^1(\pi^*)^0$, $(\pi)^2(\pi^*)^0$, and $(\pi)^2(\pi^*)^1$. (Reproduced from Ref. 209, courtesy the American Chemical Society.)

following occurs when $\theta > 45°$, suggesting the stable conformation to be near $\theta = 45°$. This agrees with other theoretical (*161, 206*) and experimental studies (*190–192*). The latter studies reported that for the first Rydberg excited state of ethylene $\theta \simeq 25°$, and suggested a similar possibility for the ethylene cation.

In summary, *orbital following and preceding are the origin of the rotational barrier and arise from the difference in interactions (overlap effects) of the $p_\perp$ and $p_\parallel$ AOs with the electron cloud of the rotor of another side.* If the bonding overlap effect on $p_\perp$ AO is larger than that on $p_\parallel$ AO, orbital following occurs; in the reverse case, orbital preceding occurs. The B—Y bond orbital of the other rotor does not affect the $p_\parallel$ AO significantly, since they are quite different in energy.

3-3-8b. Rotation about a Single Bond. The sensitive problem of the origin of the barrier to internal rotation about a single bond has been the subject of extensive theoretical studies (see Ref. 3 and Chapter 4). ESF theory gives a successful intuitive account of this problem.

Consider the following three factors for internal rotation about the A—B single bond in $H_m ABH_n$ molecules: (a) orbital following and preceding, (b) interaction of the concerned proton H_1 on one side with the B—H_2 bond on another side, and (c) interaction of the concerned proton H_1 on one side with the lone-pair electrons on another side. Factor a has already been discussed in Section 3-3-8a. For factor b, illustrated below, the electron cloud of the

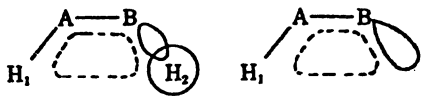

factor (b)

factor (c)

B—H_2 bond region and H_2 atomic region (enclosed by solid lines) attracts the H_1 proton, but this attraction is offset by the bare nuclear repulsion between H_1 and H_2. The force on H_1 due to the electron cloud shown by dotted lines will usually be repulsive, since the bond order between a nonbonded pair is usually negative (negative EC force). In the case of ethane (*216*) *the total effect of factor b seems repulsive.* For factor c, the interaction between the H_1 proton and the lone-pair electron cloud at B (shown by the solid ellipse) is attractive, but that due to the lone-pair electron cloud shown by dotted lines may be either attractive or repulsive. However, since the electron density in the solid ellipse is greater than that in the dotted region, the former attractive force will predominate and *the total effect of factor c will be attractive.* Note that in such arguments for factors b and c we have assumed complete following. From previous discussions, we expect that *for rotation about a single bond factor a will be most important, while factors b and c are of secondary importance.*

If the A—B bond has partial double-bond character, the molecule will be planar because of orbital following, e.g., butadiene (see Ref. 182 for numerous examples[26]). Molecules having no π bonds, e.g., BH_2BH_2 and BF_2BF_2, are also coplanar because of orbital following (Fig. 3-10). Factor a in fact includes the so-called hyperconjugation effect (*269*, *301*).

In contrast, when both A and B have lone pairs, orbital preceding becomes important. Since two lone pairs on either side lie in similar energy levels, they interact through the overlap effect (interaction between fully occupied AOs in Table 3-2). However, since $D(p_{\pi A})$ and $D(p_{\pi B})$ exceed 2 for these molecules, the bending of H_mAB and ABH_n fragments will also have to be considered. The top left-hand side of Fig. 3-11 shows the bisected form of NH_2NH_2 due to orbital preceding in the $(\pi)^2(\pi^*)^2$ configuration (factor a). Each NH_2 fragment bends from this form, since $D(p_{\pi N}) \simeq 2$, in agreement with experimental geometry. The same is true for NH_2OH (bottom left-hand side of Fig. 3-11), for which

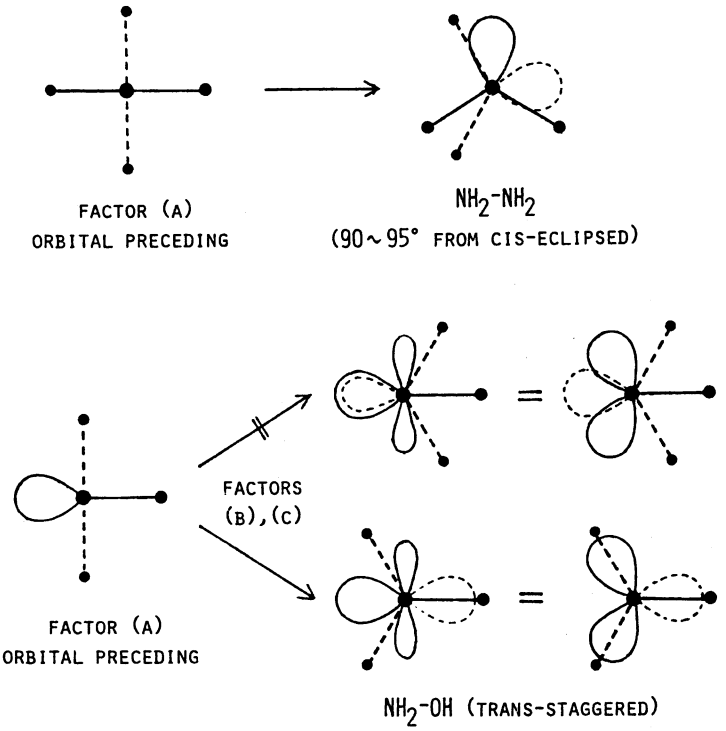

Fig. 3-11. Explanations for the structures of NH_2—NH_2 and NH_2—OH. The solid lines show the front-side NH_2 rotor (for NH_2—NH_2) or the OH rotor (for NH_2—OH) while the dotted lines show the back-side NH_2 rotors. The larger closed curves denote lone-pair orbitals; the equality sign implies equivalence.

one N—H bond is replaced by the σ lone pair of oxygen. For NH_2OH, the NH_2 fragment (dotted line) in the bisected form can bend in two different ways. But factors b and c favor the lower *trans* staggered form (in agreement with experiment) in which the O—H and N—H bonds are as far apart as possible (factor b) and eclipse with adjacent lone-pair orbitals (factor c). For HOOH and its derivatives the situation is simpler. Replacing one N—H bond of each rotor (see Fig. 3-7) with a σ lone-pair orbital, we predict from factor a that the relative orientation of the two rotors will be ~90°. The experimental data (*209*) are HOOH (111.5°, 119.8°), HSSH (90.6°), FOOF (87.6°), FSSF (87.9°), ClSSCl (82.5°), BrSSBr (83.5°). Note that factors b and c cooperate for such geometries, since two OH bonds repel each other (factor b) and they eclipse the adjacent π lone pair which is nearer than the σ lone pair. These factors lower the *trans* barrier (1.10 kcal/mole for H_2O_2) compared with the *cis* barrier (7.03 kcal/mole for H_2O_2). *In summary, when both A and B have lone pairs, we first write down the bisected form (factor a) and then bend each fragment considering factors b and c.*

When only one of A and B has a lone pair (or lone pairs), or neither A nor B has a lone pair, no significant orbital preceding occurs, since the A—H bond electrons are more tightly bound than lone-pair electrons. One may then use factors b and c. Lowe (*182*) summarized these molecules as ethanelike, $(X_1X_2X_3)A—B(Y_1Y_2Y_3)$ where Y_1 and/or Y_2 may be lone pairs, having staggered conformation; e.g., for ethane, factor b leads to a staggered form. Also, the staggered forms of molecules like CH_3NH_2, CH_3OH, having a lone pair (or lone pairs) on one side, may reflect factor b, since factor c will lead to the eclipsed form.

Actual force calculations (*216*) show that even in ethane factor a predominates for the staggered form. Throughout rotation, the EC(H—C) force arising from incomplete following of the C—H bond orbital predominates. The EC (other) force and EGC force, reflecting factor b, are minor repulsive forces. Both the EC(H—C) and EC (other) forces[27] may be interpreted as arising from the repulsive exclusion of the two approaching C—H bond orbitals,

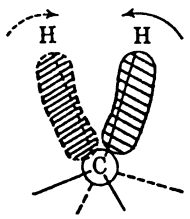

which is just the overlap effect between these orbitals. This is similar to the origin of the repulsive force between two He atoms at the overlap region.

3-3-8c. Geometries of H_2ABH Molecules. As another example of the previou discussions, consider the shapes of H_2AB and ABH fragments, and their relativ orientations:

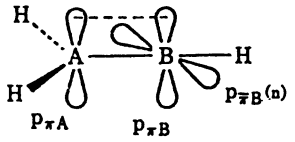

The $p_{\pi A}$ and $p_{\pi B}$ AOs form π and π^* MOs, and $p_{\bar{\pi} B}$ forms a nonbonding (n orbital, with the energy order $\pi < n < \pi^*$. The shape of the H_2AB fragmer can be predicted as follows (Fig. 3-5): When the π^* MO is (i) empty, $D(p_{\pi A}) \cdot$ 1, H_2AB is planar; (ii) singly occupied, $D(p_{\pi A}) > 1$, H_2AB is pyramidal;[28] (ii doubly occupied, H_2AB is more pyramidal. For the ABH fragment, if bendin occurs in the π-plane, the prediction is similar to H_2AB. If bending occurs i the $\bar{\pi}$-plane, then when (a) $p_{\bar{\pi} B}$ is empty, ABH is linear; (b) $p_{\bar{\pi} B}$ is singly c doubly occupied, $D(p_{\bar{\pi} B}) = 1$ or 2, ABH is bent.

Now consider the relative orientation of H_2AB and ABH fragments. Wit both π and π^* MOs empty, orbital preceding occurs, and the H_2A and ABl planes bisect each other. No experimental geometries are known for such e> cited states, $(\pi)^0(n)^{1\sim 2}(\pi^*)^0$. With π MO doubly occupied and π^* MO empt or singly occupied, orbital following occurs (Fig. 3-10) and the shape become planar [for $(\pi^*)^0$] or 90° from the *cis* staggered form [for $(\pi^*)^1$]. With bot π and π^* doubly occupied, orbital preceding occurs (factor a) and factors and c lead to a *trans* staggered form (Fig. 3-11). Rotational force calculation on vinyl (see Ref. 209) confirm these conclusions.

The above discussions can be combined to make predictions about the shape of H_2ABH molecules (Table 3-7), in agreement with known shapes. For H_2COH ESF theory predicts the relative orientation to be 90° from *cis* staggered form no experimental evidence is known as yet.

3-3-9. Comparison with the VSEPR Concept

A possible answer for the considerable success of the VSEPR model (Sectio 3-2-2) may be found by comparing the rule for the relative magnitude of Pau repulsions,

$$\text{lone pair} > \text{bond pair (triple} > \text{double} > \text{single)},$$

with the relative importance, as in (3-14), of AD and EC forces,

$$\text{AD force} > \text{EC force (triple} > \text{double} > \text{single)}.$$

Table 3-7. Shapes of H_2ABH Molecules.

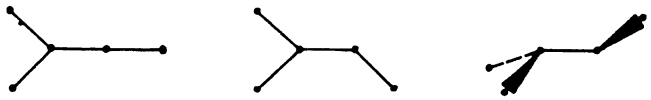

planar C_{2v} planar C_s nonplanar

Shape[a]	No. of valence electrons	Configuration π	Configuration $n_{\pi B}$	Configuration π^*	H_2ABH
planar C_{2v}	10	2	0	0	H_2CCH^+
planar C_s	11	2	1	0	H_2CCH
planar C_s	12	2	2	0	H_2CNH, H_2COH^+
nonplanar	13	2	2	1	H_2COH
nonplanar	14	2	2	2	H_2NOH[b]

[a]See representations above.
[b]*Trans* staggered configuration.
SOURCE: Ref. 209. Reprinted courtesy the American Chemical Society.

When applied to known molecules, e.g., NH_3, and isobutene (Section 3-3-3), they lead to same predictions in spite of essential differences in their basic ideas. The ESF concepts (e.g., AD, EC, and EGC forces) are well-defined and easily verifiable concepts (*221*), while the VSEPR concept is not clearly defined and justified (Section 3-2-2). Hence, it should be noted that this parallelism in predicted results, showing the success of VSEPR model, does not necessarily imply justification of its underlying concept.

3-3-10. Applications of ESF Theory

In comparison with other models of molecular structure, the ESF model has a remarkably wide applicability, e.g., to ground and excited states and the problem of the internal rotation barrier. It has been successfully applied so far to AH_2, AH_3, HAX, XHY, H_2AX, XAY, HAAH, HABX, H_2ABH, and H_2AAH_2 molecules and their various substituents (*207–209*). The underlying well-defined concepts, whose physical meanings are always very clear, have been verified by actually calculating AD, EC, and EGC forces from ab initio floating wavefunctions that satisfy the H-F theorem (*168*a, *220*, *221*, *221*a). Indeed, the ESF model has been very successful in explaining and predicting the regularity and variety in structural chemistry. It has recently been applied to predictions of geometries of molecules in strong electric fields (*221*b).

ESF theory is also applicable to various phenomena, e.g., chemical reactions (*16*, *168*a, *216*, *219*) and long-range forces (*215*; Section 7-2). Such versatility of the

theory, due essentially to the simplicity and exactness of the H-F theorem, would be quite useful for a unified understanding of these phenomena. For example, chemical reactions (molecular interactions) and molecular structure are closely related, since most chemical reactions proceed with changing the geometry of reactants, e.g., in a biological system. Sometimes a single EC force between reaction sites is a common origin of the driving force of the reaction and the change in the geometry of reactants (*207*). In some cases, such geometrical changes cause forces (e.g., the AD force) which play an essential role in driving the reaction. An example, the dimerization of two methyl radicals (*216*), is briefly described in Section 3-5-6 (see also Section 6-7).

3-4. A SIMPLE MECHANICAL FORCE MODEL FOR MOLECULAR GEOMETRY

3-4-1. Introduction

In this section we discuss a simple force model for molecular geometry proposed by Deb and co-workers (*76–79*, *82*). This model considers basically the MO *force* correlation diagram (fcd) in which the individual MO contributions to the H-F transverse force on the terminal nuclei are plotted against the bending angle (cf., the Walsh diagram, Section 3-2-1). The essential features of the fcd are depicted in a shape diagram which arranges the MOs according to their roles in planar (or linear)-bending correlation. The shape diagram was constructed intuitively by considering the qualitative MO densities and the model was greatly simplified by introducing the HOMO postulate (*76*) which assumes that the behavior of the HOMO mainly governs gross equilibrium geometry. The validity of the postulate was established by applying the model to many types of molecules, e.g., AH_2, AH_3, AH_4, AH_5, AB_2, HAB, ABC, AB_3, AB_4, AB_5, HAAH, BAAB, H_2AB, HAB_2, B_2AC, etc.

In order to provide the necessary background, we shall first discuss two earlier H-F force treatments of molecular geometry: (i) a reinterpretation study of the Walsh diagram (*66*) and (ii) the first-order Jahn-Teller distortion in VCl_4 (*65*).

3-4-2. Reinterpretation of the Walsh Diagram

Coulson and Deb (*66*) gave the following reasoning for the Walsh diagram. In the Hartree-Fock MO approximation, the H-F force on nucleus A is given by (3-18), where $f_{Ai} = \langle \phi_i | f_A | \phi_i \rangle$ is the MO contribution to the total electronic force which is a simple sum of all MO contributions. By integrating f_{Ai} over the displacement of nucleus A,[29] we obtain the change in electronic energy (relative to the lower limit of integration) as a simple sum of MO contributions. This quantity is identical with that calculated directly from the Hartree-Fock

method, if *exact* Hartree-Fock orbitals are used throughout displacement. Thus, in principle the electronic energy is expressible as a simple sum of MO contributions, although this is not true with the conventional Hartree-Fock energy formula (*252*) because of electron-electron repulsion terms. This summation provides a clue to the Walsh diagram, although this reasoning excludes the nuclear-nuclear repulsion energy of (3-18).

The above argument can be employed to construct Walsh-type diagrams. Consider an AH_2 molecule with apex angle α and A—H length λ. If the molecule is bent by symmetric transverse motions of the two hydrogens, with λ and the A atom fixed, then the total energy $E(\alpha)$, relative to the linear form ($\alpha_0 = 180°$), is

$$E(\alpha) = 2 \sum_{i}^{occ} w_e^i(\alpha) + \frac{1}{2}\left(\operatorname{cosec}\frac{\alpha}{2} - 1\right). \tag{3-26}$$

The two terms in (3-26) represent changes in electronic energy and nuclear repulsion energy, respectively, and

$$w_e^i(\alpha) = \lambda \int f_\perp^i \, d\alpha \tag{3-27}$$

represents the work done by ith MO contribution to the transverse force, $f_\perp^i$, acting on a proton during bending from 180° to α. Coulson and Deb (*66*; see also *64*) calculated $f_\perp^i$ for H_2O from the MOs of Ellison and Shull (*90*) and obtained $w_e^i(\alpha)$ by numerical integration. The resulting $w_e^i(\alpha)$ correlation diagram resembles very closely the Walsh-Allen (*240*) and the corrected Walsh diagrams[30,31] (Fig. 3-12). Note that the corrected Walsh diagram has a rising $2a_1$ curve, instead of a falling one as obtained earlier due to certain unrealistic assumptions of Walsh (Section 3-2-1; *136*, *165*, *263-265*). Thus, the above treatment gives a successful explanation of the Walsh and Walsh-Allen diagrams for H_2O, although it omits nuclear repulsion terms and $w_e^i(\alpha)$ is not always a good approximation to the difference in orbital ionization potentials between the bent (α) and linear molecules. Similar conclusions are also valid for NH_3.

Through a similar procedure, the internal rotation[32] in H_2O_2 was studied by calculating the transverse rotational force on a proton, using the wavefunctions of Kaldor and Shavitt (*160*). The resulting w_e^i correlation diagram (Fig. 3-13), relative to the *trans* planar form, resembles the corresponding Walsh-Allen diagram, even in slopes, although the unoccupied MO curves and the orders of the occupied MO curves do not match in the two diagrams. From zero net force, the equilibrium dihedral angle is ~65°, whereas the corresponding minimum-energy value is 120°. It is not surprising that both values are wrong (the experimental value is 111.5°), since the *trans* barrier of H_2O_2 is very difficult to reproduce (*102*, *226*, *238*).

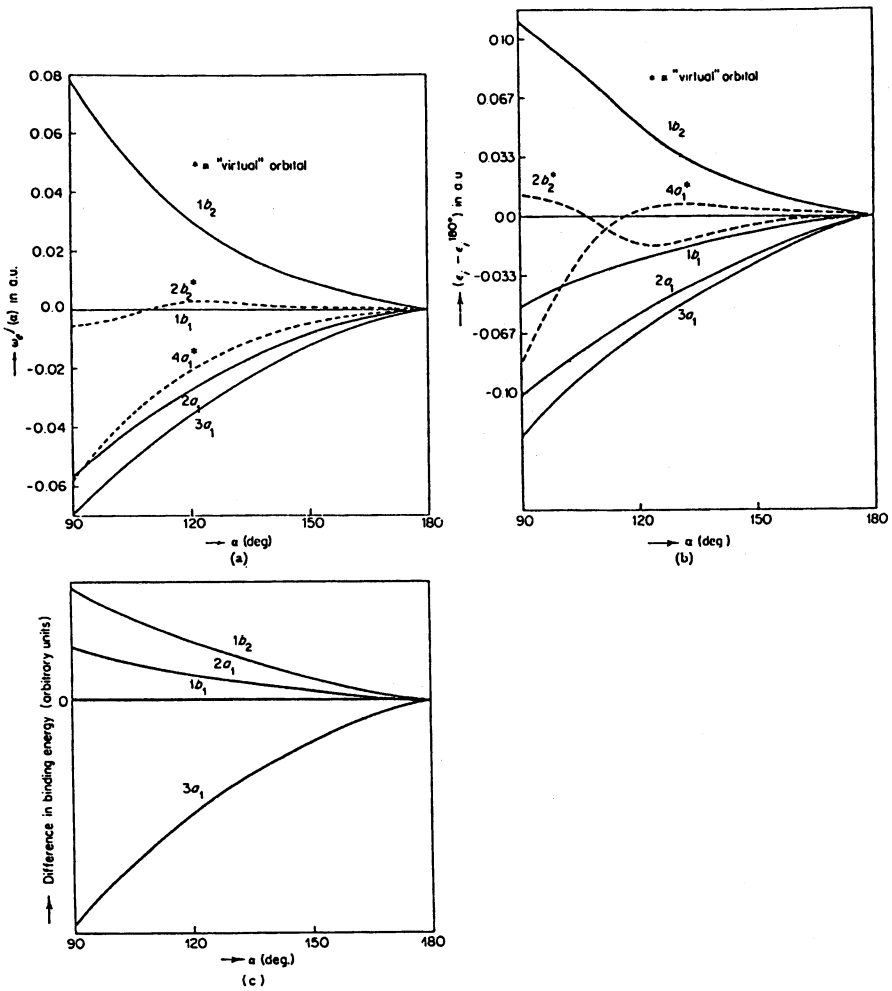

Fig. 3-12. Comparison of (a) Coulson-Deb, (b) "reduced" Walsh-Allen, and (c) original Walsh diagrams for H_2O. ϵ_i^{α} refers to the ith MO energy at the valence angle α. (Reproduced from Ref. 66, courtesy John Wiley & Sons, Inc.)

In Section 3-4-4 we shall consider the fcd's for these molecules which plot f_1^i against an angle and are just the derivatives of Coulson-Deb diagrams.

3-4-3. First-Order Jahn-Teller Effect

In Section 3-2-3 we have seen that (3-3) gives the energy of a molecule, under a small displacement Q_i, according to second-order perturbation theory. The

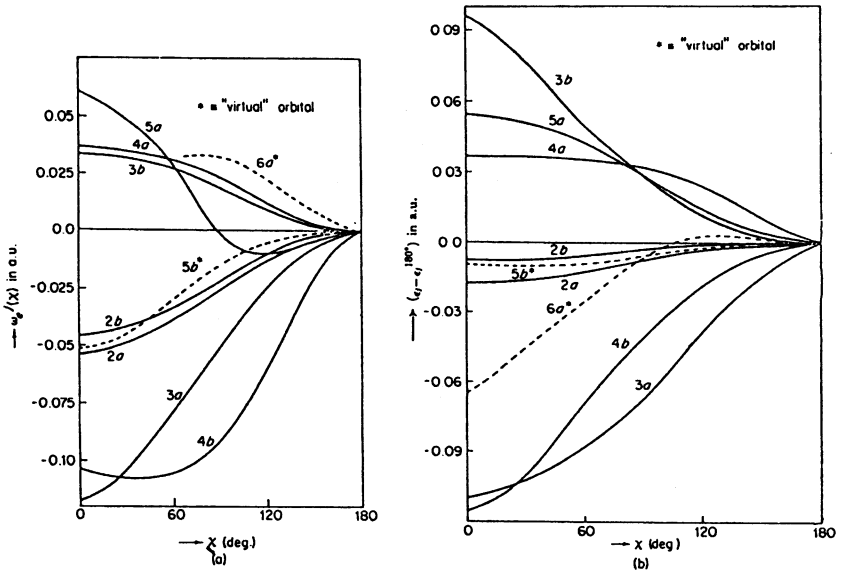

Fig. 3-13. Comparison of (a) Coulson-Deb and (b) "reduced" Walsh-Allen diagrams for H_2O_2. χ is the dihedral angle between two HOO planes (χ = 180°, *trans*-planar). (Reproduced from Ref. 66, courtesy John Wiley & Sons, Inc.)

significance of the second-order terms for molecular structure has already been discussed. We now discuss the role of the first-order term which survives only when the molecular wavefunction ψ_0 belongs to a degenerate energy level. The nonlinear[33] polyatomic molecule then tends to distort to a lower symmetry (first-order Jahn-Teller effect; Refs. 92, 153).

The H-F force formulation (*56*) of the static[34] JT effect is more advantageous than the energetic treatment in its conceptual simplicity and requires fewer assumptions for deriving the JT theorem. Only the Born-Oppenheimer approximation is assumed; there is no need to assume explicit Q_i dependence of the Hamiltonian, or invoke perturbation theory. The formulation has been applied to JT distortions in CH_4^+, CF_4^+, excited states of NH_3^+, NH_3 (*71*), and VCl_4 (*65*). We discuss the VCl_4 example below.

The electronic ground state (doubly degenerate) of tetrahedral VCl_4 may be written as $\ldots(a_1)^2(t_2)^6(t_1)^6(e)^1$, ^2E (*24*). One therefore expects that the static JT effect will distort the molecule from its idealized tetrahedral shape. We assume (i) that the electronic structure of VCl_4 differs from that of the hypothetical VCl_4^+, a closed-shell tetrahedral molecule, only in the presence of one electron in the nonbonding *e* MO (the frozen MO assumption; Refs. 55, 56); and (ii) that the doubly degenerate *e* MOs responsible for the distortion are composed of either the $3d_{z^2}$ or $3d_{x^2-y^2}$ AO of the central vanadium atom.[35] Then

the H-F force acting on a Cl nucleus in tetrahedral VCl_4 is given by

$$F_{Cl}(VCl_4) = F_{Cl}(VCl_4^+) + Z_{Cl}\int \phi^*\phi(r_{Cl}/r_{Cl}^3)\, d\tau, \qquad (3\text{-}28)$$

where Z_{Cl} is the effective nuclear charge of Cl (assumed to be unity) and ϕ is either $3d_{z^2}$ or $3d_{x^2-y^2}$ AO. Putting $F_{Cl}(VCl_4^+)$ as zero for tetrahedral VCl_4^+, we obtain the JT force tending to cause deformation as

$$F_{Cl}(VCl_4) = Z_{Cl}\int \phi^*\phi(r_{Cl}/r_{Cl}^3)\, d\tau. \qquad (3\text{-}29)$$

Using the Urey-Bradley (*293*) model, we rewrite (3-29) as

$$(K_1 + 4K_3)\,\Delta r = Z_{Cl}\int \phi^*\phi(z_{Cl}/r_{Cl}^3)\, d\tau \qquad (3\text{-}30a)$$

$$K_2 p = Z_{Cl}\int \phi^*\phi(x_{Cl}/r_{Cl}^3)\, d\tau, \qquad (3\text{-}30b)$$

where z_{Cl} and x_{Cl} are, respectively, along and perpendicular to a V—Cl bond; K_1, K_2, K_3 are Urey-Bradley force constants; Δr is the decrease in V—Cl bond length; and p is the transverse displacement of a Cl nucleus.

Interestingly, the following conclusions can be made (*75*) with the help of Fig. 3-14, even without any numerical calculations. (a) The attractive force on

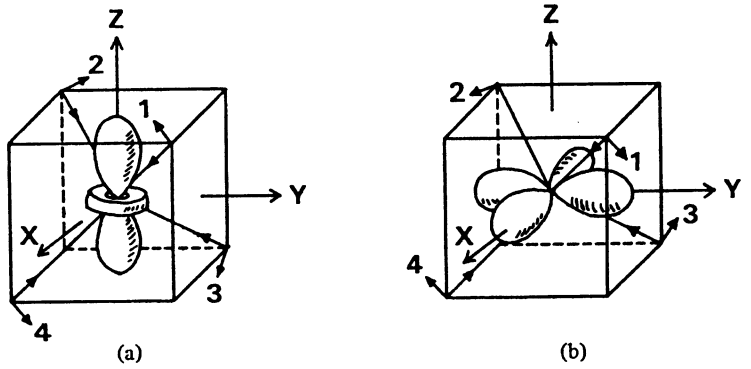

Fig. 3-14. The static Jahn-Teller effect in VCl_4, using (a) metal d_{z^2} and (b) metal $d_{x^2-y^2}$ AOs. The arrows on ligand atoms indicate the directions of distortion. Arrows 1,2 and 3,4 lie in the planes defined by the metal z-axis and the relevant V—Cl bonds. (Reproduced from Ref. 75, courtesy the American Institute of Physics.)

Cl due to d_{z^2} or $d_{x^2-y^2}$ density causes a totally symmetric decrease in V—Cl bond lengths; this does not reduce the tetrahedral symmetry. (b) Due to the symmetry of the d_{z^2} and $d_{x^2-y^2}$ AOs, the JT distortion [p in (3-30b)] occurs in the plane defined by the metal z-axis (S_4 or C_2) and the relevant V—Cl bond. (c) If the e electron occupies the d_{z^2} AO, the cube will be elongated along the metal z-axis (i.e., positive p), and if the $d_{x^2-y^2}$ AO is occupied, the cube will be flattened (i.e., negative p). These two distortions are distinguishable, resulting in the two distorted forms having different stabilities. There are three equivalent distortions of each type. (d) The two e orbitals lead to opposite and distinguishable distortions; the e electron is more likely to occupy (after deformation) either d_{z^2} or $d_{x^2-y^2}$ orbital rather than a linear combination of them, since this leads to greater bending distortion energy which is an upper bound for the barrier to interconversion among the three equivalent distorted forms via a tetrahedral form.

By using two sets of spectroscopic values for K_1, K_2, and K_3, and both Slater and SCF AOs for two vanadium configurations (*295*, *296*), Coulson and Deb (*65*) made detailed calculations for Δr, p, and the corresponding stabilization energies. The bending distortion energies for flattened and elongated tetrahedra were slightly different, implying that both forms are equally probable for VCl_4. This conclusion is consistent with low-temperature ESR results of Johannesen et al. (*156*), who reported a mixture of 58% flattened and 42% elongated forms.

3-4-4. A Simple Mechanical Model for Molecular Geometry

3-4-4a. Construction of the Model. According to the basic ideas outlined at the beginning of this section, we now explain the necessary steps in constructing the model. (1) qualitative construction of symmetry-adapted LCAO-MOs using valence s and p AOs as basis functions: the symmetry-group orbitals are combined in bonding, nonbonding, and antibonding ways; (2) arranging the MOs in energy order according to their bonding, nonbonding, and antibonding character, and by their symmetry properties; (3) assigning the role of each MO in, e.g., linear-bent correlation by using the qualitative picture of the H-F theorem to decide whether a given MO density causes a bending or linearizing force on a terminal nucleus [for example, in Fig. 3-15 if the MO accumulates more density inside the AB_2 triangle, it will cause a positive (bending) transverse force on nuclei B_1 and B_2, and vice versa; all these considerations are summarized in the shape diagram, which is a simplified version of calculated fcd[36]]; (4) Aufbau feeding of electrons into the MOs and then using the HOMO postulate to determine gross equilibrium molecular geometry. If the role of HOMO is to bend (or linearize) the molecule, the equilibrium shape will be bent (or linear). In case the HOMO is insensitive to a valence angle, the angular behavior of the

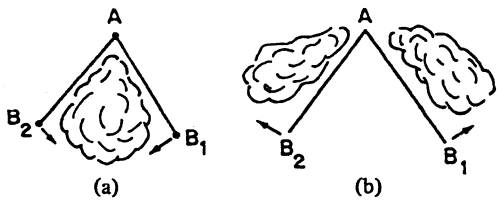

Fig. 3-15. Electron clouds, transverse forces, and terminal nuclear motions leading to bent or linear AB_2 molecules. The atom A and the A—B bond length are kept fixed during such motions. (Reproduced from Ref. 78, courtesy the American Chemical Society.)

next lower MO, if sensitive, will determine the shape. If this MO is insensitive too, then the next lower MO is to be examined, and so on. Cases where it is difficult to determine a unique HOMO occur when (a) the electronic states are orbitally degenerate (FOJT, Section 3-4-3), and (b) the HOMO and the MO next to it have opposite influences on a valence angle and cross each other in energy (accidental degeneracy; Ref. 76). In case b the next influence of these MOs is to be considered.[37] We shall now explain the stepwise applications of the model to AH_2, AH_3, AB_2, and HAAH molecules. The reader may compare these results with those from energetic models (Section 3-2) and the ESF model (Section 3-3).

3-4-4b. Illustrative Applications of the Model. *1.* AH_2 *Molecules.* From the three valence-group orbitals s_a, p_{za} (along the symmetry axis), and $h_1 + h_2$ belonging to the A_1 representation of C_{2v} (*76*) we can construct three a_1 MOs. The $1a_1$ MO is fully bonding (in-phase overlap) between all atom pairs (Fig. 3-16). The $2a_1$ MO is approximately nonbonding (lone pair), and is almost localized on the s_a and p_{za} AOs. If this MO is occupied, the variational principle will lead to a small bonding character for the p_{za}, $h_1 + h_2$ pair, since it is most effective to stabilize the MO. The $3a_1$ MO is strongly antibonding between A and H atoms. Similarly, from the two group orbitals p_{ya} (in the molecular plane) and $h_1 - h_2$ belonging to the B_2 representation, the bonding ($1b_2$) and antibonding ($2b_2$) MOs are constructed (Fig. 3-16). The nonbonding $1b_1$ MO is formed by p_{xa} AO alone (perpendicular to molecular plane).

The energy order of MOs is closely related to the number of nodes and the nature of AO interactions. Thus, Deb (*76*) summarized the order: bonding < feeble bonding (e.g., lone pair) < nonbonding < feeble antibonding < antibonding; and the suborders: more symmetric < less symmetric, π-antibonding < σ-antibonding. Using these orders, the AH_2 valence MOs may be arranged as $1a_1 < 1b_2 < 2a_1 < 1b_1 < 3a_1 < 2b_2$.

Consider now the transverse MO forces acting on terminal nuclei. Since each MO (assumed real) is given by, $\phi_i = \Sigma_p C_{ip} \chi_p$, where χ_p is an AO, the MO density becomes $\phi_i^2 = \Sigma_p C_{ip}^2 \chi_p^2 + \Sigma_{p \neq q} C_{ip} C_{iq} \chi_p \chi_q$, the first term giving rise to

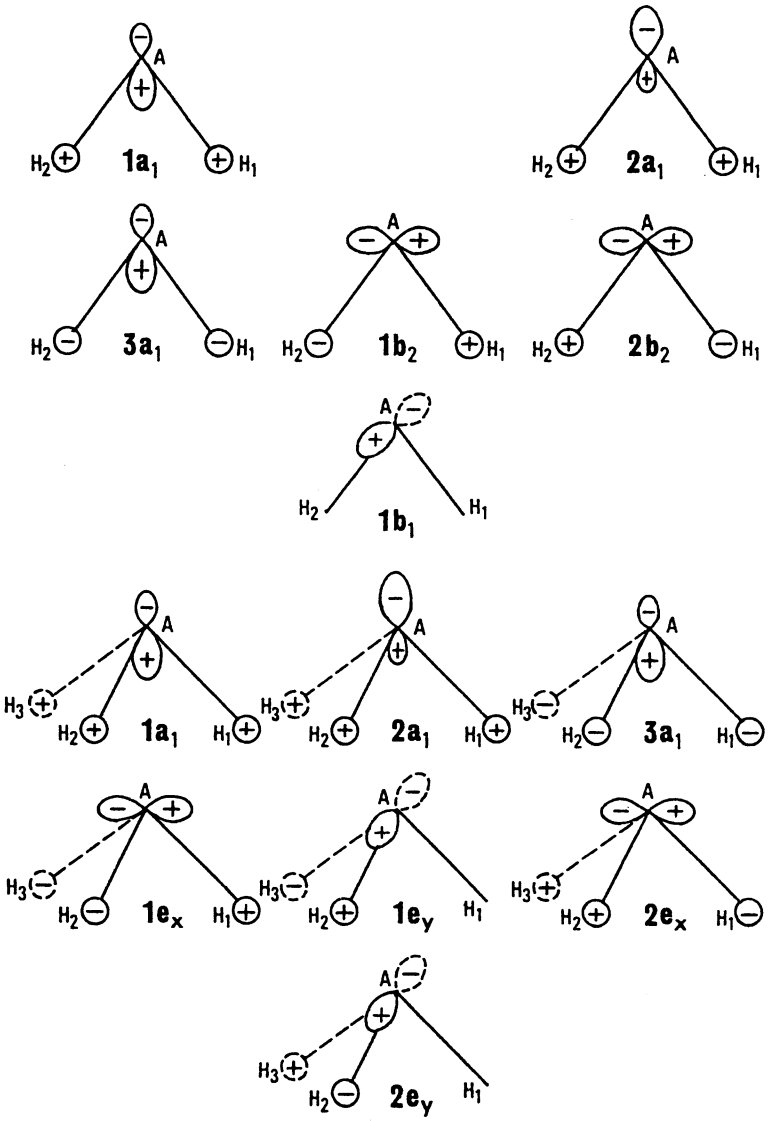

Fig. 3-16. Schematic MOs for AH_2 (top) and AH_3 (bottom) molecules. (Reproduced from Ref. 76, courtesy the American Chemical Society.)

atomic force and the second to overlap force. In case of the $1a_1$ MO (Fig. 3-16), both atomic and overlap densities are larger inside the triangle than outside and therefore this MO density exerts a positive transverse force on the terminal protons (see calculated fcd in Fig. 3-17). For the $2a_1$ MO, the atomic density on A

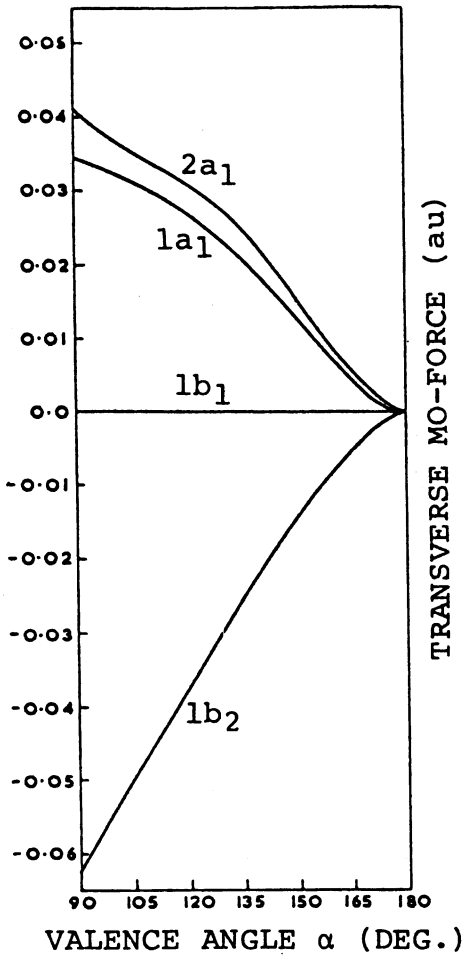

Fig. 3-17. Force correlation diagram for AH_2 molecules, constructed with the data for H_2O molecule. (Reproduced from Ref. 76, courtesy the American Chemical Society.)

pulls up the nucleus A (AD force in ESF theory, Section 3-3-2), but here we do not consider this effect because we are considering the transverse forces on terminal protons. This atomic density on A is larger outside the triangle than inside, and causes a negative transverse force on the protons. But the other atomic and overlap densities lead to positive forces and the net transverse force due to the $2a_1$ MO will be positive (Fig. 3-17). For the $1b_2$ MO, both atomic and overlap densities concentrate more charge outside, and therefore it gives a negative transverse force. The $1b_1$ MO does not exert any transverse force on the protons because of symmetry. These conclusions are summarized in the shape dia-

gram, Fig. 3-18. The electrons are filled in the circles, according to the given energy order, and then the HOMO postulate is applied.

For ground-state molecules having 1, 2 and 5, 6 valence electrons the HOMOs are $1a_1$ and $2a_1$. Therefore, such molecules will be bent. For molecules with 3, 4 valence electrons the HOMO is $1b_2$, and so the shape will be linear. For

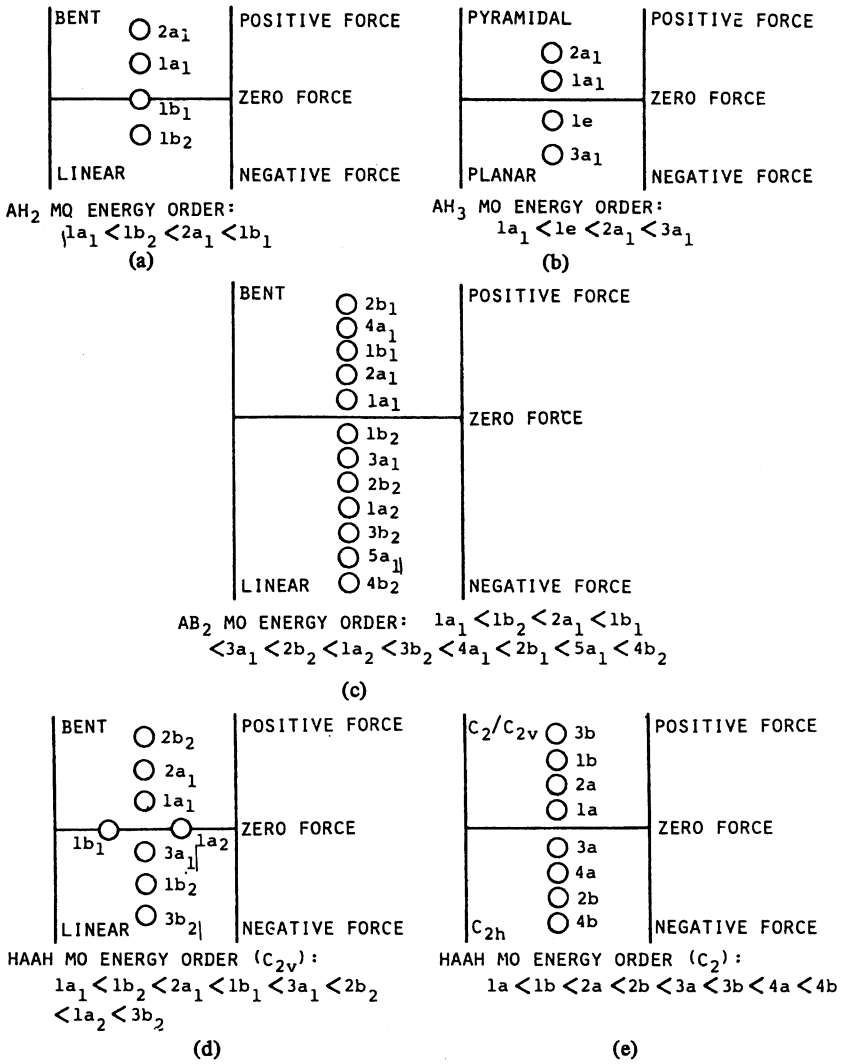

Fig. 3-18. Shape diagrams for (a) AH_2, (b) AH_3, (c) AB_2, (d) C_{2v} HAAH, and (e) C_2 HAAH molecules. (Reproduced from Refs. 76, 82, courtesy the American Chemical Society.)

Table 3-8. Geometry Predictions for Four Molecular Classes.

Molecule class	No. of valence electrons	Predicted ground-state geometry	Examples	Predicted excited-state geometry	Examples	Apparent exceptions
AH_2	1, 2	bent	H_3^+, LiH_2^+, HeH_2^{2+}	linear (HOMO $1b_2$)		
	3, 4	linear	BeH_2, HeH_2^+, BH_2^+	bent (HOMO $2a_1$)	BeH_2	BeH_2^+
	5–8	bent	CH_2, NH_2, OH_2, BH_2^-, BH_2, AlH_2, NH_2^+, NH_2^-	bent (HOMO $1b_1$) or linear (HOMO $1b_1$)	CH_2, NH_2 (both bent), BH_2 (linear)	
AH_3	1, 2	pyramidal		planar (HOMO $1e$)		
	3–6	planar	LiH_3^+, HeH_3^+, GaH_3, BeH_3, CH_3^+, BeH_3^-, BH_3	pyramidal (HOMO $2a_1$)		
	7, 8	pyramidal	CH_3 (?), NH_3, OH_3^+, CH_3^-, SbH_3, NH_3^+ (?), SiH_3	planar (HOMO $4a_1$)	NH_3	CH_3, NH_3^+
	9, 10	planar				
AB_2	1, 2	bent	Li_3^+	linear (HOMO $1b_2$)		Li_2H^+
	3, 4	linear	He_2H^+, $BeLi_2$, Li_2H^-, Be_2H^+	bent (HOMO $2a_1$)		
	5–8	bent		linear (HOMO $3a_1$)		He_3^+, Li_2O

	9–16	linear	HF_2^-, CO_2, CO_2^+, CS_2, N_3^-, BeF_2, $HgCl_2$, $CuCl_2^-$, $Ag(NH_3)_2^+$, UO_2^{2+}, UO_2^+, MoO_2^{2+}, PuO_2^{2+}, C_3, NC_2, CN_2, $C(CH_2)_2$, $C(CO)_2$, BO_2, NO_2^+	bent (HOMO $4a_1$ or $2b_1$)	NO_2^+, CO_2, CS_2	BaF_2, $BaCl_2$, $BaBr_2$, BaI_2, SrF_2, $SrCl_2$, CaF_2
	17–20	bent	NO_2^-, NO_2, ClO_2^-, ClO_2, SO_2, SCl_2, O_3, OCl_2, $SnCl_2$, PbI_2, $(CH_2)_3$, $InCl_2$, $Se(SCN)_2$, S_3^{2-}, $O(CH_3)_2$, CF_2, NF_2, ICl_2^+	linear (HOMO $5a_1$ or $4b_2$)		
	21–24	linear	XeF_2, I_3^-, ICl_2^-, F_3^{2-}, Cl_3			
HAAH	1, 2	bent (C_{2v}/C_2)				
	3, 4	linear				
	5, 6	bent (C_{2v}/C_2)				
	7, 8	bent (C_{2h})				
	9, 10	linear	C_2H_2, $N_2H_2^{2+}$	bent (HOMO $2b_2$)		
	11, 12	bent (C_{2v}/C_{2h})	N_2H_2, $(CH)_2H_2$			
	13, 14	bent (C_2)	H_2O_2	linear (HOMO $3b_2$)		
	15, 16	linear				

SOURCE: Refs. 76, 82. Reprinted courtesy the American Chemical Society.

molecules having 7, 8 valence electrons the HOMO ($1b_1$) is insensitive to valence angle, so the next lower MO ($2a_1$) determines the shape (bent). These predictions (Table 3-8) agree with known results except for BeH_2^+.[38] Apart from individual predictions, the model can also predict many trends. For example, since CH_2 ($^1A_1$, 104°), has one more electron in the $2a_1$ MO than BH_2 (131°), it should have a smaller bond angle. In the two series NH_2^+, NH_2 (103.3°), NH_2^- (104°), and BH_2^- (102°), CH_2 ($^1A_1$, 104°), NH_2 (103.3°), H_2O (105.2°), the apex angle should be more or less the same, since the molecules differ only in the occupancy of the indifferent $1b_1$ MO. The decrease in apex angle in the series H_2O (105.2°), H_2S (92.2°), H_2Se (91°), H_2Te (89.5°) may be explained as follows. From O to Te the valence *s* and *p* AOs become more diffuse (i.e., greater mean radii) and the tail of the lone-pair ($2a_1$ MO in Fig. 3-16) *sp* hybrid on A can overlap more effectively with the hydrogen AOs. Therefore, bending is facilitated more in, e.g., H_2S than in H_2O. For the excited states, the HOMO is the MO in which the excited electron enters. Thus, the first excited state of LiH_2^+ will be linear (HOMO $1b_2$). The bent BH_2 molecule becomes linear in the excited state (HOMO $1b_1$, next lower MO $1b_2$). The singlet excited state and triplet ground state of CH_2 will have larger and similar bond angles, since the transitions are from $2a_1$ to $1b_1$ MOs ($^1B_1$, 140°; $^3B_1$, ~136°; Refs. 134, 135).

When electrons fill a bonding or an antibonding MO, electron density will respectively increase or decrease in the binding region (see Section 3-3-4d); therefore the bond length will, respectively, decrease or increase. For the $2a_1$ and $1b_1$ MOs, the atomic density of A attracts the two protons and decreases the bond lengths, e.g., in the series BH_2 (1.18 Å), CH_2 (1.11 Å), NH_2 (1.02 Å), H_2O (0.958 Å). In the series H_2O (0.958 Å), H_2S (1.334 Å), H_2Se (1.47 Å), H_2Te (1.7 Å), the bond length increases because the valence *s* and *p* AOs become more diffuse from O to Te and the electron density in the binding region decreases from H_2O to H_2Te.

2. AH_3 *Molecules.* The approach here is very similar to that for AH_2 molecules. From seven symmetry-adapted (*76*) valence AO functions we obtain three a_1 and two sets of *e* MOs for a C_{3v} molecule. The $1a_1$ MO is fully bonding, the $2a_1$ MO is a lone-pair orbital almost localized on A, and the $3a_1$ MO is antibonding between the A and H atoms. The $1e_x$ (in-phase mixing of p_{xa} and $2h_1 - h_2 - h_3$) and $1e_y$ (in-phase mixing of p_{ya} and $h_2 - h_3$) are degenerate bonding MOs, while $2e_x$ and $2e_y$ are degenerate antibonding MOs (Fig. 3-16).[39] The energy order is given by the previous rules as $1a_1 < 1e < 2a_1 < 3a_1 < 2e$.

Figure 3-16 indicates that the $1a_1$ MO concentrates more charge inside the molecular pyramid and thus causes a positive transverse force on the terminal protons (see fcd in Fig. 3-19). The $2a_1$ lone-pair MO also exerts a bending force on the protons. The $1e_x$ MO concentrates more charge outside the pyramid and thus favors a planar structure, while the $1e_y$ charge density tends to open the

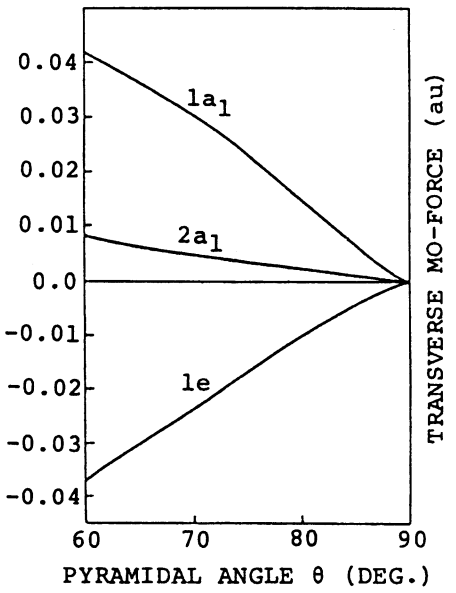

Fig. 3-19. Force correlation diagram for AH_3 molecules, constructed with the data for NH_3 molecule. (Reproduced from Ref. 76, courtesy the American Chemical Society.)

H_2AH_3 angle, favoring a T shape (planar). The overlap density in the $3a_1$ MO causes a negative transverse force (Fig. 3-18).

From the HOMO postulate, the ground states of AH_3 molecules with 1, 2, 7, or 8 valence electrons will be pyramidal, but those with 3-6, 9, or 10 valence electrons will be planar (Table 3-8). As in the Walsh rules, the model predicts 7-valence-electron CH_3, NH_3^+, BH_3^- (*285*, *286*) to be pyramidal, in disagreement with experimental and theoretical studies (Section 3-2-1). The planar Rydberg excited states of NH_3 (*134*) and PH_3 (*276*) will also constitute exceptions to the model (see Section 3-3-5).

The out-of-plane bending force constant increases in the planar series LiH_3^+, BeH_3, BH_3, because the $1e$ HOMOs are progressively filled. Because bonding and lone pair MOs are progressively filled, bond length should decrease in the series LiH_3^+, BeH_3, BH_3 (1.22 Å; Ref. 270), CH_3 (1.08 Å), NH_3 (1.02 Å). For the series NH_3 (1.02 Å, 106.6°), PH_3 (1.42 Å, 93.5°), AsH_3 (1.52 Å, 91.8°), the changes in bond lengths and angles have been attributed to the increasing diffuseness of the valence s and p AOs of the central atom.

For planar LiH_3^+ and BeH_3, the HOMO ($1e$) level is doubly degenerate, leading to an FOJT distortion. The $1e_x$ MO tends to shorten the A—H_1 bond relative to the other two (the hydrogen group orbital is $2h_1 - h_2 - h_3$), while the

$1e_y$ MO prefers a T shape and shortens the A—H_2 and A—H_3 bonds relative to the third. The resultant shapes are distinguishable, having different stabilities, but both belong to C_{2v} symmetry.

3. AB_2 *Molecules.* Using the same qualitative rules as for AH_2 and AH_3 molecules, one can pictorially construct the twelve valence MOs of C_{2v} AB_2 molecules (Fig. 3-20) and arrange them in the energy order $1a_1 < 1b_2 < 2a_1 < 1b_1 < 3a_1 < 2b_2 < 1a_2 < 3b_2 < 4a_1 < 2b_1 < 5a_1 < 4b_2$ (for details, see Ref. 76). For some AB_2 molecules, the $1a_2$, $3b_2$ and $5a_1$, $4b_2$ MOs may be reversed in energy, but this will not affect the predictions, since all these MOs prefer a linear form (see below).

The schematic MOs in Fig. 3-20 and the H-F force picture in Fig. 3-15 indicate the nature (positive or negative) of the transverse force exerted by each

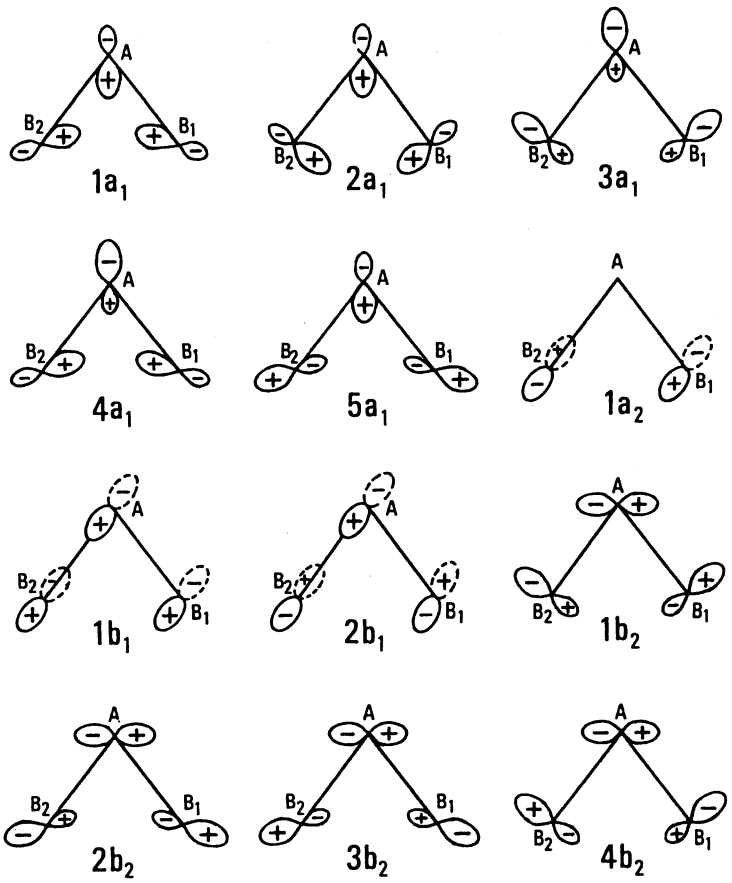

Fig. 3-20. Schematic MOs for AB_2 molecules. (Reproduced from Ref. 76, courtesy the American Chemical Society.)

MO on the terminal nuclei. The effects of the π MOs ($1a_2$, $1b_1$, $2b_1$) can be deduced from the signs of the π overlap densities between the terminal atoms. For the $5a_1$ MO, Deb explains that one atomic and one overlap term give strong negative forces that would surpass the two atomic and two overlap terms, which give smaller positive forces. Combining the resulting shape diagram with the MO energy order, the HOMO postulate leads to the following predictions for the shapes of ground-state AB_2 molecules: $1a_1$ (1,2;*b*), $1b_2$ (3,4;*l*), $2a_1$ (5,6;*b*), $1b_1$ (7,8;*b*), $3a_1$ (9,10;*l*), $2b_2$ (11,12;*l*), $1a_2$ (13,14;*l*), $3b_2$ (15,16;*l*), $4a_1$ (17,18;*b*), $2b_1$ (19,20;*b*), $5a_1$ (21,22;*l*), $4b_2$ (23,24;*l*), where the MO is the shape-determining HOMO, the numbers in parentheses refer to valence electrons, and *b* and *l* denote bent and linear forms, respectively (Table 3-8). Similar predictions can be made for excited states. These agree with known shapes. However, the 5-electron, linear He_3^+ (*245*) molecule seems to be an exception. Also, contrary to the predictions of Walsh, Deb, and Gillespie, the 16-valence-electron molecules BaF_2, $BaCl_2$, $BaBr_2$, BaI_2, SrF_2, $SrCl_2$, and CaF_2 are bent (Table 3-6). The 21-electron molecule ClF_2 might be another exception (*81*, *185*, *292*). Like Walsh's model, Deb's model does not accommodate predominantly ionic molecules such as Li_2H^+, Li_2O, and LiOH which are linear.[40]

The anchor shape of ClF_3 is explained as follows. The ClF_2 fragment in ClF_3 may be regarded as a 22-electron molecule and thus linear, giving rise to a T-shaped ClF_3. In this shape, the two ClF_2 fluorine nuclei "see" more electrons because of the remaining Cl—F bond; the resulting electron-nuclear attraction slightly bends the ClF_2 bonds (for the ESF explanation, see Section 3-3-4b).

Consider geometry changes due to ligand substitutions. The change from OF_2 (1.42 Å, 103.3°) to OCl_2 (1.70 Å, 111°) may be attributed to greater diffuseness of Cl valence AOs. Due to this the O—Cl bond will be longer than the O—F bond. Also, since the overlap between the terminal AOs is reduced for the HOMO ($2b_1$), the bond angle should be larger in OCl_2 (see the ESF account in Section 3-3-4d).

4. HAAH *Molecules.* The prediction of geometry of an HAAH molecule proceeds in two steps: (a) to decide on the linearity of the molecule by examining the in-plane transverse force on the protons in a planar *cis* (or *trans*) form, (b) to find the stable conformation for rotation about the A—A bond, by examining the transverse rotational force on the protons in a nonplanar (C_2) configuration. The present model cannot distinguish between C_2 and C_{2v} (planar *cis*) forms in geometry prediction.

Consider step a, starting from the *cis* form.[41] As before, the ten valence MOs of a C_{2v} HAAH molecule can be qualitatively constructed and arranged in energy order $1a_1 < 1b_2 < 2a_1 < 1b_1 < 3a_1 < 2b_2 < 1a_2 < 3b_2 < 4a_1 < 4b_2$ (*82*). In Fig. 3-21, the MOs which throw more electron density inside the molecular trapezeum favor a bent form, whereas those MOs which concentrate more charge outside will favor a linear form. Thus, the $1a_1$, $2a_1$, and $2b_2$ MOs

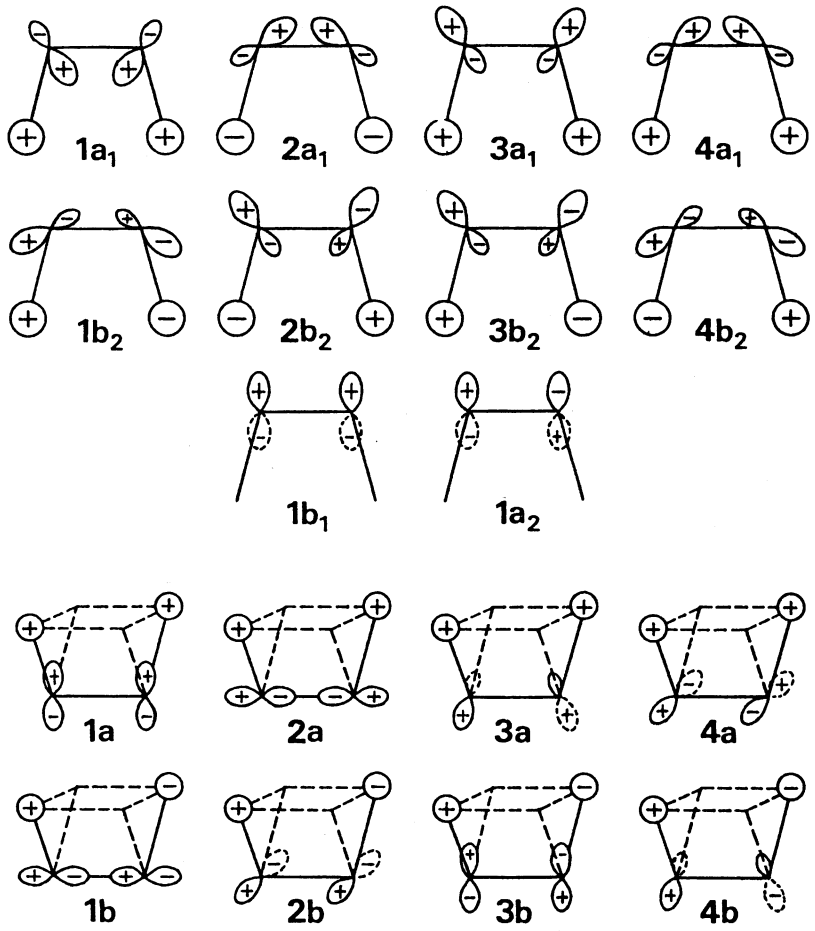

Fig. 3-21. Schematic MOs for C_{2v} HAAH (top) and C_2 HAAH (bottom) molecules. (Reproduced from Ref. 82, courtesy the American Chemical Society.)

favor a bent form, the $3a_1$, $1b_2$, and $3b_2$ MOs favor a linear form, and the $1b_1$ (π bonding) and $1a_2$ (π antibonding) MOs are almost insensitive to bending in the molecular plane. Using the shape diagram (Fig. 3-18) and the HOMO postulate, the predictions in Table 3-8 can be readily obtained. For the bent 11-14-valence-electron molecules the shape-determining MO ($2b_2$) is feebly A—A antibonding and feebly A—H bonding. This leads to an increase in the A—A bond length and a decrease in the A—H bond length in the series C_2H_2 (1.21, 1.06 Å), N_2H_2 (1.22, 1.08 Å), H_2O_2 (1.48, 0.97 Å) (*243*, *283*, *284*). The differences in the bond lengths and angles of H_2O_2 (0.97 Å, 105°), H_2S_2 (1.33 Å, 95°) may be attributed to greater diffuseness of sulfur valence AOs.

Consider now step b. The valence MOs of a C_2 HAAH molecule may be qualitatively constructed (*82*) and arranged in the energy order $1a < 1b < 2a < 2b < 3a < 3b < 4a < 4b$. From Fig. 3-21 we see that when an MO accumulates more electron density inside the molecular prism, it favors a C_2 or C_{2v} (*cis*) form, and when more electron density is accumulated outside the prism, a C_{2h} (*trans*) form is favored, if the MO maintains its role throughout the rotational fcd.[42] Thus, $1a$, $2a$, $1b$, and $3b$ MOs favor a C_2/C_{2v} form, while the $3a$, $4a$, $2b$, and $4b$ MOs favor a C_{2h} form. Therefore, one can readily predict rotational conformations of bent HAAH molecules (Table 3-8) using the shape diagram (Fig. 3-18) and the HOMO postulate. Since the $3b$ and $4a$ MOs cross each other at a dihedral angle of ~90°, both *cis* (or C_2) and *trans* forms are possible for 11, 12-electron molecules, whereas for 13, 14-electron molecules (e.g., H_2O_2, H_2S_2) the $3b$ MO seems to dominate over the $4a$ MO.

3-4-4c. Transferability of Geometry Predictions. The geometries of many large molecules can be predicted from the geometries of their fragments. For example, the AB_2 predictions may be employed for AB_3, AB_4, and AB_5 molecules (*76*, *78*). An example, ClF_3, has already been discussed in Section 3-4-4b. We consider here the shapes of AH_4 molecules. Since the two AH_2 planes are mutually perpendicular, each AH_2 fragment has little effect on the shape of the other. Therefore, if the $(n - 2)$-electron AH_2 fragment of a parent n-electron AH_4 is linear, the AH_4 molecule will be square planar; if the AH_2 fragment is bent, the AH_4 molecule will be tetrahedral (T_d) or D_{2d} (distorted tetrahedral). In cases of orbital degeneracy, one should also consider the FOJT effect. Using the AH_2 predictions in Table 3-8, we conclude that AH_4 molecules with 5, 6 valence electrons will be square planar and those with 3, 4, or 7-10 electrons will be T_d or D_{2d}. These predictions agree with known geometries and with predictions which are independently derived for AH_4 molecules *without* the help of AH_2 geometries. Deb (*76*, *78*, *79*) has thus noted that *shape is another property which is transferable, in quite a subtle way, from one molecule to another.*

3-4-4d. Why HOMO? The qualitative geometry predictions for many molecular classes made on the basis of the HOMO postulate are remarkably consistent with known geometries, although we occasionally come across minor exceptions as well as some difficulties in constructing the schematic MOs and shape diagrams for relatively large molecules and in the assignment of HOMO. Thus, the general validity of the HOMO postulate has been established.[43] The question therefore arises, why is only the HOMO, rather than other MOs, most important for molecular geometry? The reasoning might involve two steps. (1) In the model, the MOs are constructed at a configuration which is apart from symmetric and/or equilibrium geometry. At this geometry, the total electron

density *should* have the characteristics of incomplete following or preceding (Sections 3-5-2, 3-3-8a). If the MO contributes to electron-cloud preceding, it gives a positive (accelerating) transverse force (left-hand side of Fig. 3-8b), and if it contributes to electron-cloud following, it gives a negative (resisting) transverse force (right-hand side of Fig. 3-8b). However, we note that electron-cloud incomplete following and preceding are the behaviors of *total* electron density and not of the individual MO density. (2) Among the MOs, the HOMO is most loosely bound. Hence, the density due to the lower MOs tends to follow *more completely* the nuclear motion (Ref. 78; Section 3-5-4) and thus have less influence on molecular shape. While step 1 has a firm foundation (Section 3-5), step 2 does not have such a foundation at present and needs to be further examined using more reliable MOs.[44]

3-5. TWO COMMON TYPES OF BEHAVIOR OF AN ELECTRON CLOUD DURING THE NUCLEAR REARRANGEMENT PROCESSES

3-5-1. Introduction

Imagine a process in which the nuclear coordinates of a system change from one configuration to another. If the process is favorable (or unfavorable), the system receives an internal force which accelerates (or resists) the process. An important factor giving rise to such forces should be the dynamic behavior of electron cloud during the process. In this section we will study the characteristic features of such behavior in a fairly general way within the Born-Oppenheimer approximation (see also Section 3-3-8).

Linnett and Wheatley (*179*) considered the possibility that the bond-forming orbitals are distorted (i.e., bent bond) during molecular vibrations. Such distortions were confirmed by valence-bond calculations on the out-of-plane bending of CH_3 (*51*, *150*), and for more general hydrides (*158*). The important effects of such relaxations of molecular charge distributions (see Chapter 5) were pointed out for infrared intensities (*57*, *70*, *157*, *189*), temperature dependence of ESR hyperfine splitting constants (*98*, *267*, *268*), vibrational force constants (*7–11*, *15*, *17*, *259*), chemical reactions and long-range interactions (see, e.g., Refs. 216, 219–221). Interestingly, Feynman had conjectured in 1939 (*101*) that the van der Waals force might be due to the simultaneous polarization of the individual atomic densities toward each other, their magnitudes being proportional to $1/R^7$ This was confirmed much later (see Sections 2-3-1, 7-2; *105*, *140*).

In this section we will first deduce two common features of electron-cloud reorganizations in an ad hoc manner from the H–F theorem and the integral H–F theorem (*166*, *227*).[45] These lead to a guiding principle governing the nuclear rearrangement process, which will be illustrated in the case of molecular shapes.[46] Finally, we will discuss the changes in the geometries of reactants during chemical reactions and their role in driving the reaction (*216*).

3-5-2. Common Features in the Behavior of Electron Clouds

Let Q be the nuclear displacement coordinate of a system from initial (i) to final (f) states (Fig. 3-22), with α as an intermediate configuration and β as the final configuration. In general, Q is a linear combination of displacement coordinates (*300*), with that of nucleus A as an important element. Let us write the electrostatic H-F theorem (for α) and the integral H-F theorem (Chapters 1, 4) as

$$F_A^\alpha = Z_A \int r_A / r_A^3 \rho_\alpha(r)\, dr - Z_A \sum_{B \neq A} Z_B R_{AB} / R_{AB}^3, \qquad (3\text{-}31)$$

$$\Delta E(\alpha \to \beta) = \int \rho_{\alpha\beta}(r)\, \Delta H_{ne}(r)\, dr + \Delta V_{nn}, \qquad (3\text{-}32)$$

$$\Delta H_{ne}(r) = H_{ne}^\beta(r) - H_{ne}^\alpha(r), \qquad (3\text{-}33)$$

where $\Delta E(\alpha \to \beta)$ is the change in total energy for the isoelectronic process $\alpha \to \beta$; $\rho_{\alpha\beta}$ is the normalized transition density (Section 4-3) between α and β; ΔH_{ne} is the difference in nucleus-electron attraction operator between α and β, and ΔV_{nn} is the corresponding change in nuclear repulsion energy. The integrand in (3-31) is a 3-dimensional vector force density.

First, let the change $\alpha \to \beta$ satisfy the following two conditions. (a) It is a monotonous change from unstable (α) to more stable (β) configuration. (b) The displacement accompanies an increase in nuclear repulsion. Examples of these conditions are seen in (i) molecular structure and vibration, e.g., displacement from unstable linear (planar) to stable bent (pyramidal) forms of AX_n molecules; (ii) reactions forming stable molecules having no barrier between two points α and β; and (iii) approaches of two neutral atoms in the regions of dispersion forces. From condition a, the nuclei A of the system at α must receive the driving force F_A^α having components along Q (positive direction). From

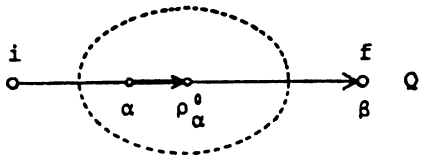

Fig. 3-22. Illustration of electron-cloud preceding in the H-F picture. The dashed ellipse denotes the electron cloud of the system in nuclear configuration α. ρ_α^0 shows the projection of the centroid of weighted density on the coordinate Q and the arrow from α to p_α^0 denotes the electronic part of the driving force acting at the configuration α. (Reproduced from Ref. 210, courtesy the American Chemical Society.)

condition b, the origin of the driving force must be the electronic part of (3-31), since the nuclear part is repulsive throughout. This is possible *if and only if* the center of gravity (ρ_α^0) of the weighted density $(1/r_A^3)\,\rho_\alpha(r)$ precedes the position(s) of A at α in the direction of Q. In Fig. 3-22 the arrow from α to ρ_α^0 is proportional to the electronic part of the driving force on A at α. The nuclear force is opposite to and smaller than this force (for a real system, see Ref. 219).

The preceding of the weighted density is generally expected to occur when the centroid of $\rho_\alpha(r)$ within some local region near A precedes the position of A in the Q direction (see dotted line in Fig. 3-22). The localness of such *electron-cloud preceding* comes from the $1/r_A^3$ factor in the weighted density; this is large near A but falls off rapidly with increasing distance. Note that although the preceding of weighted density is an exact consequence of a nucleus A receiving the electronic driving force in the Q direction, electron-cloud preceding is an approximate concept. However, the approximation is usually quite good, except possibly for very minute interactions, e.g., the long-range resonance force between the $1s$ and $2p$ states of two H atoms (*215*).

Similar conclusions are derived from (3-32). For conditions a and b, the destabilization energy due to ΔV_{nn} must be surpassed by the stabilization energy due to the electronic part. In (3-32) and (3-33), $H_{ne}^{\beta}(r)$ contributes to stabilization but $H_{ne}^{\alpha}(r)$ contributes to destabilization. Therefore, for the system to gain stabilization from the electronic part the transition density $\rho_{\alpha\beta}(r)$ should be denser (more positive) near the moving nuclei at β than at α (Fig. 3-23a). Such a situation will be realized if electron-cloud preceding occurs at α (Fig. 3-23b).

Now, let Q satisfy the following two conditions, which are opposite to the previous ones. (a) It is a monotonous change from stable (α) to unstable (β) configuration. (b) The displacement accompanies a decrease in nuclear repulsion. Such a displacement is realized by reversing the direction of Q in Fig. 3-22 (and Fig. 3-23). Therefore, during this process the opposite behavior, namely, incomplete following of the weighted density, $(1/r_A^3)\,\rho_\alpha(r)$, and *electron-cloud (incomplete) following* should occur.

To summarize, when electron-cloud preceding occurs during a process, the system receives a force that accelerates the process, but when electron-cloud following occurs the system receives a force that resists the process. This is the basis for the general guiding principle given below.

The primary importance of AD and EC forces in molecular shapes (Section 3-3) and chemical reactions (*16*, *216*, *219*) is closely related to the localness of electron-cloud preceding and following. The behavior of electron density in the atomic region of nucleus A manifests itself in the AD force on A and that in the A—B bond region manifests itself in the EC force on A. The electron density in the other regions (EGC force) should not greatly reflect the characteristics of electron-cloud preceding and following. Thus, these behaviors of electron density are reflected mainly in the AD and EC forces.[47] This is also supported

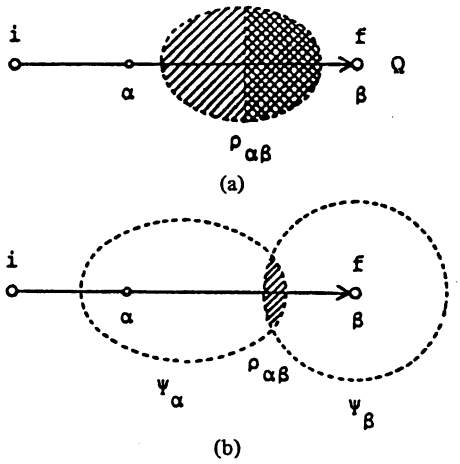

Fig. 3-23. Illustration of electron-cloud preceding in the integral H-F picture. (a) The ellipse illustrates the transition density $\rho_{\alpha\beta}(r_1)$ between the wavefunctions associated with configurations α and β. The density is higher in the cross-hatched region near β than in the singly hatched region near α. (b) The ellipse corresponds to the wavefunction associated with configuration α and is responsible for electron-cloud preceding. The circle centered on β corresonds to the wavefunction of the final state. Note that the hatched region, which shows the high-density region of $\rho_{\alpha\beta}$, is nearer to the position β than to α. (Reproduced from Ref. 210, courtesy the American Chemical Society.)

by the following relations for diatomic molecules, obtained by applying the interference partitioning of electron density (*255*) to the H-F force:

$$\left.\begin{array}{l}\text{AD force} = \text{intraatomic interference force} \\ \text{EC force} = \text{interatomic interference force} \\ \text{EGC force} = \text{quasi-classical force.}\end{array}\right\} \qquad (3\text{-}34)$$

We now remark on conditions a and b. Regarding condition a, even if the process has an energy barrier like the activation energy, electron-cloud preceding in some critical regions (e.g., those between reaction sites) and due to some mechanisms (e.g., charge transfer, Ref. 108) is quite important to reduce the barrier. Condition b is obviously too strong, since electron-cloud preceding and following should occur even if this condition is relaxed as follows: (b′) the electronic part is more important than the nuclear part.

We conclude this section with the density guiding rule for nuclear rearrangement processes: *Nuclei are pulled in the direction of electron-cloud reorganization. If the energy change is monotonous throughout the process $i \rightarrow f$, electron-*

cloud preceding (following) means that configuration f is more (less) stable than configuration i.

3-5-3. Perturbational Description

The perturbational treatment of electron-cloud following and preceding indicates a connection with the SOJT theory. Taking a small nuclear displacement δQ as a perturbation, the electron density correct to first order is (*13*, *14*) $\rho(Q) = \rho(Q_0) + \delta\rho$, with

$$\delta\rho = 2\delta Q \sum_{k \neq 0} \left[\int \rho_{0k}(Q_0) f(Q_0)\, dr / (E_k - E_0) \right] \rho_{0k}(Q_0), \qquad (3\text{-}35)$$

where $Q = Q_0 + \delta Q$, E_0 and E_k are ground- and excited-state energies at Q_0, ρ_{0k} is the transition density and $f(Q_0) = -(\partial H/\partial Q)_{Q_0}$ is the force operator; $\delta\rho$ represents the reorganization of electron density due to the perturbation.

It has been shown that if Q_0 is taken at the saddle point of the potential surface, $\rho(Q_0)$ and $\delta\rho$ represent, respectively, electron-cloud incomplete following and preceding. In order that preceding occur as a net effect, $\delta\rho$ should become appreciable and then the displacement along δQ will be further facilitated. If preceding does not occur, the electron cloud left behind at Q_0 (incomplete following) attracts the nuclei at Q in the $-Q$ direction and the system will revert to Q_0. Thus, the SOJT conditions (Section 3-2-3) are those under which electron-cloud preceding can occur appreciably.

When Q_0 is away from the saddle point (e.g., equilibrium geometry, geometry of highest symmetry, etc.) the unperturbed density $\rho(Q_0)$ itself would already have the characteristics of electron-cloud preceding and following. Thus, the SOJT model (employing both HOMO and LUMO) is based on $\delta\rho$ taking Q_0 at the saddle point, while Deb's model (employing only HOMO) considers basically electron-cloud following and preceding included in $\rho(Q_0)$ where Q_0 is away from the saddle point (see Section 3-4).

3-5-4. Electron-Cloud Reorganization and Molecular Shapes

3-5-4a. Examples and Roles. We shall now consider how electron-cloud following and preceding determine molecular shapes (see guiding principle in Section 3-5-2). Figure 3-8 reexpresses the ideas in Section 3-3-8 with, e.g., ethylene, from both H-F and integral H-F theorems (Figs. 3-22 and 3-23). In the H-F picture, the centroid of the C—H bond orbital precedes (π-π^* excited state) or incompletely follows (ground state) the rotational movement Q of the C—H axis. In the integral H-F picture, the overlap between the C—H bond orbitals

at α and β increases (decreases) due to the preceding (following) of the C—H bond orbital at α. The resulting dominant EC force (arrow in Fig. 3-8) operates to make the π-π^* excited state of ethylene a bisected form and the ground state a planar form, in agreement with experiment. This and other examples in Section 3-3-8 validate the above guiding principle.

For the out-of-plane bending displacement of AH_3 molecules (Fig. 3-24), with Q as a linear combination of Q_A and Q_H, the guiding principle is restated as follows. If electron-cloud preceding occurs when the molecule is bent from planar shape, the constituent nuclei receive forces that accelerate this bending; but when incomplete following occurs bending is resisted and the molecule is ex-

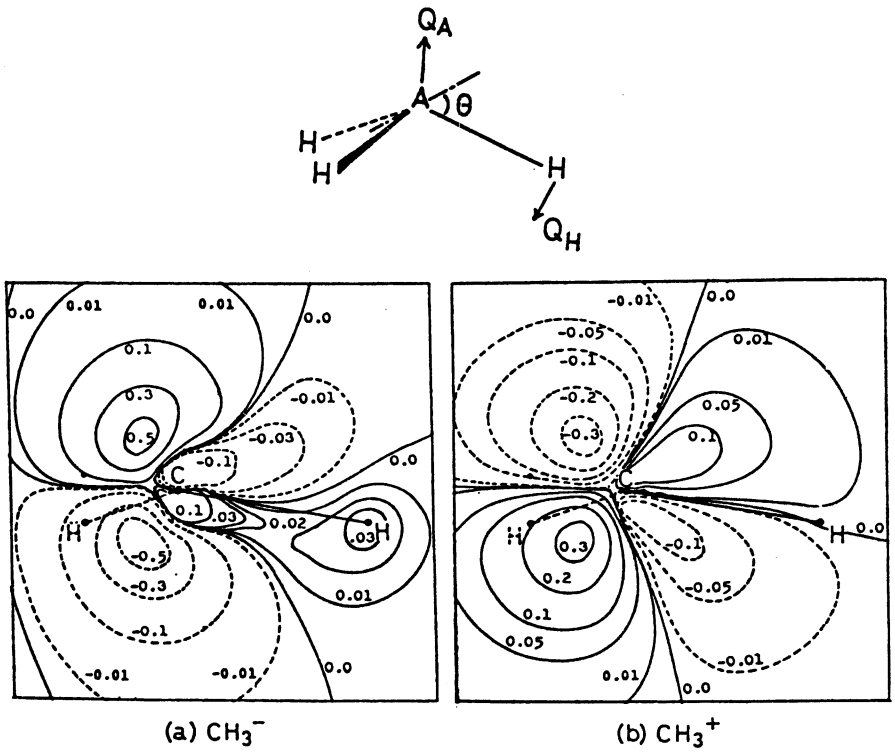

(a) CH_3^- (b) CH_3^+

Fig. 3-24. Out-of-plane bending displacement Q (top) of AH_3 molecules from planar to pyramidal configurations. The arrows Q_A and Q_H represent, respectively, the bending movements of the central atom A and of the protons, while θ is the out-of-plane angle. The contour maps (bottom) show the changes in electron densities of CH_3^- and CH_3^+ induced by the displacement $\theta = 30°$, using nonempirical SCF-MO wavefunctions based on the minimal set of Slater orbitals. The density at $\theta = 0°$ is subtracted from that at $\theta = 30°$. The solid and dashed lines show, respectively, an increase and a decrease in density. (Reproduced from Ref. 211, courtesy the American Chemical Society.)

pected to be planar. For example, when CH_3^- is bent from planar shape, the electron density increases immediately above the C nucleus and decreases in the region immediately below it, thus producing an upward atomic dipole on the C atom. The AD force due to this electron-cloud preceding in the atomic region facilitates the displacement of the C nucleus along Q_C (Fig. 3-24a). Along the C—H axis, electron density increases in the downward region but decreases in the upward region. This electron-cloud preceding in the C—H bond region causes a positive transverse EC force on the proton that accelerates bending along Q_H. Thus, both AD and EC forces induced by electron-cloud preceding make the molecule nonplanar (Fig. 3-25) as expected from the guiding principle and in accordance with experiment (*47*). Note that Q_C does not satisfy condition b of Section 3-5-2 but satisfies b′, while Q_H satisfies both b and b′.

The changes in electron density in CH_3^+ are just the reverse of those in CH_3^- (Figs. 3-24b, 3-25). Thus, a *downward* atomic dipole is generated on the C atom (electron-cloud incomplete following). The incomplete following in the C—H bond region causes a negative transverse EC force on the proton, which resists bending along Q_H. Thus both AD and EC forces, caused by incomplete following, operate to make the molecule planar in accordance with the guiding principle above.

Consider now the electron-cloud reorganization in CH_3 (*211*), calculated through unrestricted Hartree-Fock wavefunctions (*214*, *244*). The situation here is more complex than above, making a direct application of the guiding principle difficult. The electron density near the C atom seems to show the characteristics of electron-cloud preceding, although to a much smaller extent than in CH_3^-. However, in the C—H bond region, the electron cloud follows Q_H incompletely, the extent of following increasing with increase in the out-of-plane bending angle (*51*, *150*, *211*, *267*, *268*). More accurate calculations (*221*) have shown that the EC forces on C and H make the molecule planar, exceeding the AD force on C.[48]

Interestingly, the above differences in electron-cloud reorganization among

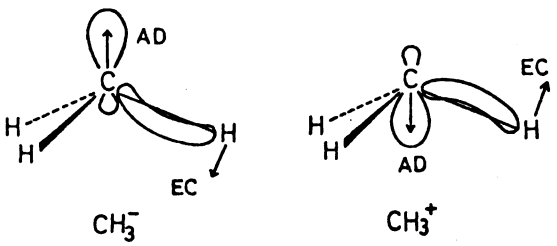

Fig. 3-25. Electron-cloud preceding in CH_3^- and incomplete following in CH_3^+ during out-of-plane bending movements. The arrows show the AD and EC forces induced by such preceding and following. (Reproduced from Ref. 211, courtesy the American Chemical Society.)

CH_3^-, CH_3^+, and CH_3 may be attributed chiefly to the singly occupied MO of CH_3. Also, electron-cloud reorganizations in isoelectronic molecules are similar (*211*, *221*). These facts support the validity of the ESF model and are also important in the force reasoning behind the Walsh diagram (*66*).

3-5-4b. Bent Bond in Equilibrium Geometry. Contour maps of the electron density in NH_3 (equilibrium configuration) indicate that the bond electron cloud is slightly distorted inwardly from the N—H axis (*20*, *21*, *159*, *223*, *253*, *254*). The occurrence of this "bent bond" can be explained as follows. Since the force on the protons vanishes at equilibrium geometry, the interproton repulsive force acting along $-Q_H$ (see Fig. 3-24) must exactly cancel the force of electronic origin. Considerations similar to those in Section 3-5-2 indicate that this is effectively achieved if the electron cloud near the proton and/or in the A—H bond region is distorted inwardly from the A—H axis. This is just a special ("frozen") case of electron-cloud preceding in the A—H bond region. See further Refs. 51a and 220.

3-5-4c. Localized Orbital Description. We have seen that the characteristics of electron-cloud following and preceding are expressed chiefly through the behavior of local electron clouds associated with bonds, lone pairs, etc. during nuclear rearrangement processes. One therefore expects that such characteristics would be reflected in localized MOs (*89*, *183*, *224*) obtained at nonequilibrium geometries.[49] For example, the general feature of the localized C—H bond orbital of nonplanar CH_3 may be illustrated as follows (*51*):

This clearly indicates incomplete following. In case of NH_3 (*159*), it is surprising that even in planar form the localized orbitals are *not* symmetrical with respect to the molecular plane, although the *total* electron density is symmetrical with respect to this plane. These examples show that the localized-orbital method would be a useful tool to describe intuitively electron-cloud following and preceding, and this would also hold for chemical reactions (*84*, *85*). Note, however, that the force calculated from a single localized orbital has little physical meaning. Electron-cloud following and preceding are types of behavior of *total* electron density (see the definition of bond paths and bond directions in Ref. 257).

3-5-5. Change in Molecular Geometry during Chemical Reactions

The ESF concepts applied in Section 3-3 to molecular geometry can be applied to chemical reactions without much modification. For a reaction to occur, the

interaction between reactants should increase electron density between the reaction sites, at the same time decreasing electron density in the region of the old breaking bond. This accumulation of electron density may occur in the overlap region common to both reaction sites, causing attractive EC forces, or in regions very close to reaction sites (e.g., the formation of *inward* atomic dipoles), causing attractive AD forces on the reaction sites. Although both of these types of electron-cloud preceding are important depending on the stages (initial, middle, final) and the classes (covalent, ionic) of reactions, the EC force seems to be more important in the significant middle stage of the reaction than the AD force, at least for homopolar reactions.

For instance, consider the dimerization of two planar CH_3 radicals to form ethane (*207*). When the two approach each other in the intermediate region (Fig. 3-26), the electrons in the $p_{\pi C}$ AO of each radical flow (precede) into the overlap region (see also Section 3-3-4d). The resultant EC force is the driving force of the reaction, since it pulls both carbons toward each other. At the same time, this EC force makes each CH_3 nonplanar as in ethane, the product, thus playing two important roles. In the final stage of the reaction, the EC(C—C) force nearly approaches the EC(C—H) force, resulting in an almost tetrahedral CH_3 fragment in ethane. Thus, in the ESF theory molecular geometry and chemical reaction are treated essentially on the same ground.

Consider also the formation of the coordinate bond in the NH_3—BH_3 system.

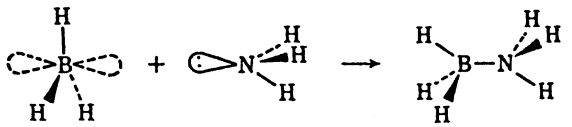

Here the p_π AO of planar BH_3 is vacant and the lone-pair orbital of NH_3 is doubly occupied. During reaction, the EC force is produced on B and the AD force on N in free NH_3 is partly transformed into the EC force. Consequently, during reaction BH_3 will gradually become pyramidal and the NH_3 valence angle will increase.[50] Deb (*76*, *78*) has also considered such changes in molecular geometry and reached similar conclusions on the basis of the model described in Section 3-4.

We now return to the dimerization of two CH_3 radicals for a more detailed

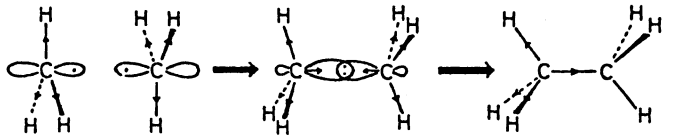

Fig. 3-26. Important forces in the reaction $CH_3 + CH_3 \rightarrow C_2H_6$. (Reproduced from Ref. 207, courtesy the American Chemical Society.)

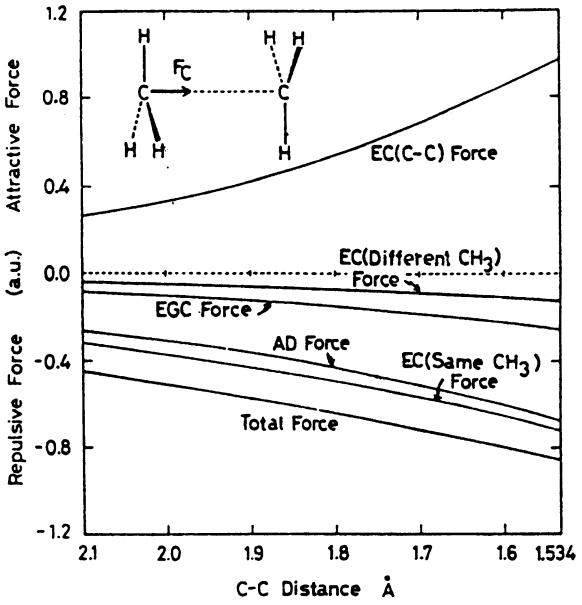

Fig. 3-27. Analysis of the force F_C acting on carbon when two *planar* methyl radicals approach each other. (Reproduced from Ref. 216, courtesy the American Chemical Society.)

study (*216*). We consider two reaction paths. (1) *planar approach*, in which the radicals are brought face to face with their configurations rigidly planar; (2) *gradually bending approach* in which the HCH angle of each radical is optimized along the path so that the bending transverse forces on protons vanish. The calculations employed extended Hückel wavefunctions (*141*) and optimized the orbital exponents in force integrals so that all forces vanish at the equilibrium geometry of ethane.

In the planar approach (Fig. 3-27), only the EC(C—C) force is attractive; all other forces, including the total force, are repulsive throughout.[51] This means that although electron density accumulates in the C—C region (see Fig. 3-28, near +0.95 Å, center of the forming C—C bond), the extent of accumulation is insufficient to drive the reaction. We also find an accumulation of electron density in the rear region along the C—H axis; this causes transverse EC(H—C) forces on protons which facilitate the *outward* bending of each radical. Clearly, this is also a kind of electron-cloud preceding, since the reaction coordinates should also include this out-of-plane bending displacement.

For the gradually bending approach (Figs. 3-29, 3-30), the AD, EC(C—C), and EGC forces are all attractive, and so the total force on carbon is attractive throughout the reaction. Comparing Figs. 3-27 and 3-30, we find that the largest effect of gradually bending each radical occurs in the AD force on car-

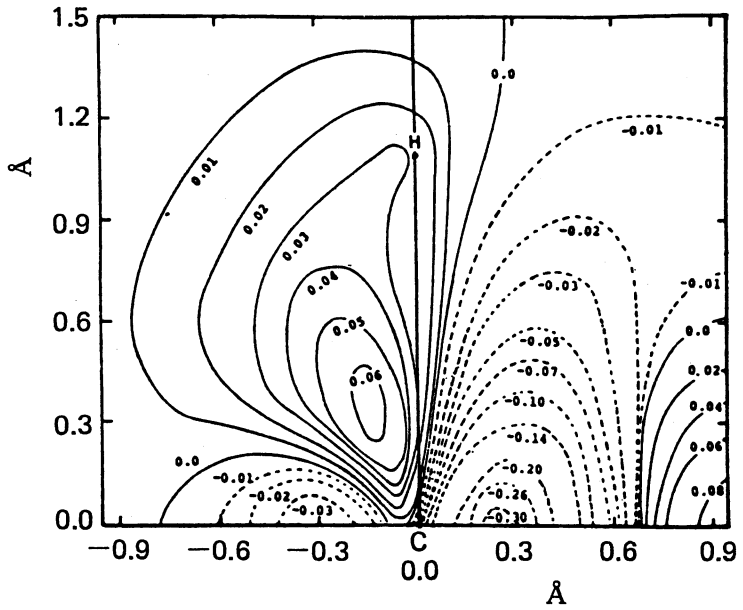

Fig. 3-28. Change in electron density induced by the interaction of two planar methyl radicals separated by 1.9 A, obtained by subtracting the density for two free methyl radicals from that for two interacting methyl radicals at the same separation. The map is on the HCC plane and corresponds to the left-hand methyl radical. (Reproduced from Ref. 216, courtesy the American Chemical Society.)

bon. This is understandable, since out-of-plane bending induces an atomic dipole on the C atom. Thus, a change in geometry of the reactants during reaction induces electron-cloud preceding in the atomic region of the reaction site. In order to attain sufficient electron-cloud preceding in the C—C region, this secondary mechanism of preceding is quite important, and it is also induced by electron-cloud preceding in the C—H bond region (Fig. 3-28). All three kinds of preceding, manifesting themselves in the EC(C—C) force on carbon,

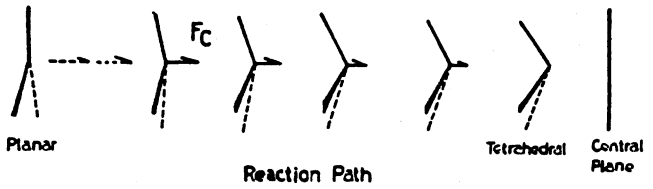

Fig. 3-29. Illustration of the gradually bending approach and the driving force F_C acting on the carbon nucleus. Another methyl radical is in the mirror-image position with respect to the central plane. (Reproduced from Ref. 216, courtesy the American Chemical Society.)

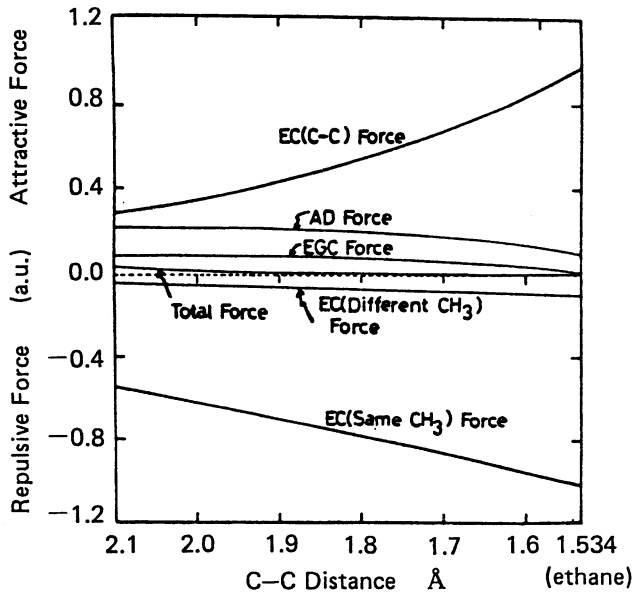

Fig. 3-30. Analysis of the driving force F_C acting on the carbon atom along the gradually bending approach of the two methyl radicals. (Reproduced from Ref. 216, courtesy the American Chemical Society.)

the EC(C—H) force on proton, and the AD force on carbon, *cooperate* to drive the reaction.

It is interesting to note (Fig. 3-30) the crossing of the curves of EC(C—C) force and AD force at C—C distance greater than 2.1 Å. This suggests that at the initial stage of the reaction the change in reactant geometry (inducing the attractive AD force) may be more important than the density accumulation in the overlap region of the two reactants. Although this is apparently similar to the dominant character of the AD force in the initial stages of H_2 formation (*16*, *140*, *215*), the mechanism is essentially different. In order to confirm this point, further study based on more accurate wavefunctions would seem to be necessary.

3-6. SUMMARY

In this chapter we have explained the force concepts applied to molecular geometry and compared them with energetic models. The two main force models, due to Nakatsuji and Deb, are quite successful for understanding and predicting the striking variety and regularity in structural chemistry. Although these two models are quite different, the force concepts used by them are very pictorial and attractive. In Section 3-5 using the force concept, we study the behavior of

electron density during the nuclear rearrangement processes and obtain a general density guiding principle for such processes. These concepts are equally applicable to molecular structure and chemical reactions, as well as to the interface between them.

These successes indicate that the force concept should become a quite general and useful approach for understanding wider areas of chemical phenomena. The wide applicability of the ESF theory due to Nakatsuji and co-workers to molecular structure, chemical reactions, and long-range interactions promise such developments of the force concept.

Acknowledgment

The authors would like to acknowledge Professor B. M. Deb for kindly editing throughout this chapter.

Notes

1. Correlation diagrams were first constructed by Hund (*145*, *146*) and Mulliken (*199*, *200*). Such diagrams have been very useful in explaining, e.g., spectra of diatomic molecules, molecular shapes, spectra of transition metal complexes, reactivity of organic molecules (*302*), etc.

2. Similar rules were suggested earlier by Cassie (*50*), Penney and Sutherland (*239*), and Sidgwick and Powell (*274*).

3. A sufficient condition for a general SCF wavefunction to satisfy the H–F theorem is that the basis set includes derivative $\partial\chi_r/\partial x_r$ for any basis χ_r. A procedure which includes 'parent' and first derivative AOs seems to be useful (*221*a).

4. This may be due to terminal atoms being usually more electronegative. Walsh (*294*) had noted this for AB_2 molecules.

5. This is a modification (*210*) of the partitioning procedure of Bader et al. (*18*, *19*) for diatomic molecules.

6. This assumes that the shielding of Z_B by the electrons in χ_{sB} is complete. Although it is an overestimate, it improves as the AB distance and/or the orbital exponent of χ_{sB} increases; e.g., for a C—C distance of 1.4 Å, the error is ~8%, but for a C—H distance of 1.09 Å, the error is ~30%.

6a. See note 6.

7. According to nonempirical calculations on NH_3 (*159*) the lone-pair orbital has s–p mixing [P_{sNpN} in (3-8)] 1.063, compared with 0.866 for sp^3 hybrid and 0.943 for sp^2 hybrid.

8. The AD force is small for H atom, since here the $1s$–$2p$ mixing is small.

9. This occurs because, although the integral part of the AD/EC ratio in, e.g., the series B, C, N, O increases, the extent of s–p mixing decreases [Fig. 3-4(b)].

10. See note 6.

11. Since the force on A along A—B is always the sum of EC and EGC forces, one can reduce the EC force by incorporating the EGC force into it ('bond' force in Ref. 221).

12. Unless otherwise mentioned, experimental values are from Herzberg (*134*) or Sutton (*283*, *284*).

13. Exceptions exist from Al to Ga and As to Sb.

14. This is why inner-shell electrons are not significant for molecular shapes.

15. Since the one-center coulomb repulsion integral is large (*305*), π-donating substituents are usually σ-attracting (e.g., halogens) and vice versa.

16. An important exception occurs when both s_A and p_A are completely filled (see Section 3-3-4b).

17. The overlap effect may also be called conjugative effect in structural theory in contrast with the inductive effect given in Section 3-3-4c.

18. For the role of *d* electrons in chemical bonding, see, e.g., Ref. 63. In speaking about the importance of *d* orbitals, experimental chemists usually assume a minimal basis set (i.e., only one basis for *s*-type AO, three for *p*, five for *d*, etc.). But in a refined calculation theoreticians employ many bases for *s*-, *p*-, and *d*-type orbitals (extended basis set; see, e.g., Ref. 281). When the addition of *d* orbitals is treated as a perturbation (*217*) the first-order correction raises the Hartree–Fock orbital energy but vanishes identically for the total energy, indicating the insignificance of *d* orbitals. This result applies to the second standpoint but may not apply to the first since the minimal *s*, *p* basis set does not satisfy the requirement for the zero-order MO in perturbation theory.

19. The transfer of electrons from the lone-pair orbital of N to N—Si and SiH_3 regions is supported by the fact that $N(SiH_3)_3$ is a weak base.

20. The repulsive EC and EGC forces are responsible for steric repulsion.

21. This applies to all planar (linear)–pyramidal (bent) correlations. In the planar (linear) form the bending force vanishes by symmetry.

22. The overlap effect and the inductive-substitutent effect may or may not be cooperative (Section 3-3-4d). In case of the former, a decrease in electron density in the atomic region (decrease in AD force) leads to an increase of electron density in the bond region (increase in EC force) and vice versa.

23. Hayes (*131*) noted that for both neutral atoms and cations, the *d* levels are lower than the *p* levels for Ca, Sr, and Ba, although both levels are lowered monotonously from Be to Ba.

24. When $\theta = 0$, the electron density of C—H bond is symmetric about the bond axis.

25. Minus sign means resisting force.

26. Experimental data cited in this subsection are from Ref. 182.

27. Their sum is a good approximation to the total force.

28. From Table 3-2, for $(\pi)^2(\pi^*)^1$,

$$D(p\pi_A) = \frac{1}{1+S} + \frac{1}{2}\frac{1}{1-S} \simeq 1.5, \text{ with } S \simeq 0.25.$$

29. See Refs. 93, 104, and 299 for integration over another variable, namely, nuclear charge.

30. Both the Walsh–Allen and original Walsh diagrams were "reduced" such that orbital energies are measured relative to the linear form (compare Figs. 3-1 and 3-12).

31. Such a resemblance does not hold for unoccupied MOs indicated by the dotted curves.

32. No Walsh diagram was proposed for internal rotation.

33. For linear molecules, the Renner effect occurs (*251*).

34. For an extension to the dynamic JT effect, see Ref. 54.

35. Consideration of overlap with chlorine AOs does not alter the nature of JT distortion.

36. Such simplification may cause problems when some MO curves in the fcd cross the zero-force line (Fig. 3-13). In the reduced Walsh–Allen diagram such sign changes occur only for unoccupied orbitals.

37. (a) When the number of valence electrons is such that only one of these two MOs are occupied, two different assignments of HOMO are possible, leading to a difficulty in prediction. (b) Since it is difficult to derive the HOMO postulate on an a priori quantum mechanical basis, its validity has been asserted by testing its predictions for a wide range of molecular classes. For other details regarding this model, see Refs. 76–79, 82.

38. For BeH_2^+ (bent ground state; Ref. 246), the interlacing of occupied MO curves makes the choice of HOMO difficult(*79*).

39. The z-axis is along C_3 axis, while the x axis lies in the plane defined by z-axis and the $A—H_1$ bond.

40. The ESF model can explain these trends for the alkaline earths and lithium (Section 3-3-7).

41. In principle, one can also start from the *trans* form. However, in this case, the $2b_u$ and $2a_g$ MOs cross each other in the Walsh–Allen diagram (*122*), making the choice of HOMO difficult for 5–10-valence-electron molecules (see note 37). Such MO crossing is fortunately not encountered if one starts from the *cis* form (*82*).

42. Note that the MO numberings here are different from Fig. 3-13 since the latter MOs incorporate inner-shell AOs. See note 36.

43. Deb and Mahajan (*80*) have further confirmed the validity of the HOMO postulate by studying the structures of 17 quixotic hypothetical molecules according to INDO and CNDO/2 MO methods: HCLi, HBBe, $HBLi^-$, HCB, HNBe, HNB^+, HBB^-, NaHLi$^+$, LiB_2^+, $MgBe_2$, LiB_2^-, MgB_2, LiH_3^{2+} (unstable), H_3O^-, CH_5^-, HBO_2^{2+} (unstable), HBF_2^{2+} (unstable). See also notes 36, 37.

44. Relaxation calculations (see Chapter 5) by Mahajan and Deb (*184*) on BeH_2, using INDO MO densities, indicates that step 2 may not be the real reason. For a link between the SOJT model and HOMO postulate, see Ref. 25.

45. The H–F and integral H–F theorems cannot be used (*218*) to determine a priori the electron density of a system (see, however, Refs. 20, 21). Attempts (*94*, *144*, *171*, *212*, *213*, *218*, *275*, *278*, *279*) to obtain a direct deterministic equation for the electron density without using the wavefunction are not yet completely satisfactory (see, e.g., Refs. 23 and 25a).

46. Koga et al. (*168*) have recently generalized the idea of the binding–antibinding diagram of Berlin (*32*), giving an unambiguous regional definition for the role of electron density.

47. For example, in both van der Waals and chemical reaction regions of the process $H + H \rightarrow H_2$, electron-cloud preceding occurs (*16*, *140*) and causes the

driving force of the reaction, namely, AD force at long range and EC force at shorter range. Note that in, e.g., ionic reactions, electron-cloud preceding also manifests itself in the EGC force, since electron transfer from one atom to another is also "preceding."

48. The behavior of electron densities calculated from floating wavefunctions for NH_3, CH_3^+, and NH_3^+ (*221*) were very similar to those given here for CH_3^-, CH_3^+, and CH_3, respectively.

49. Note that localization of MOs is a device for interpretative purposes. It utilizes the inherent unitary ambiguity of Hartree–Fock MOs and does not affect the total wavefunction (*138*, *139*, *252*).

50. No experimental data are known for this increase.

51. For experimental evidence, see Ref. 222.

References

1. Accad, Y., Pekeris, C. L., and Schiff, B., 1971, *Phys. Rev.*, A4, 516.
2. Acquista, N., Abramowitz, S., and Lide, D. R., Jr., 1968, *J. Chem. Phys.*, 49, 780.
3. Allen, L. C., 1969, *Ann. Rev. Phys. Chem.*, 20, 315.
4. ——, 1972, *Theoret. Chim. Acta* (Berlin), 24, 117.
5. —— and Russell, J. D., 1967, *J. Chem. Phys.*, 46, 1029.
6. Almenningen, A., Bastiansen, O., Ewing, V., Hedberg, K., and Traetterberg, M., 1963, *Acta Chim. Scand.*, 17, 2455.
7. Anderson, A. B., 1972, *J. Chem. Phys.*, 57, 4143.
8. ——, 1973, *J. Chem. Phys.*, 58, 381.
9. ——, Handy, N. C., and Parr, R. G., 1969, *J. Chem. Phys.*, 50, 3635.
10. —— and Parr, R. G., 1970, *J. Chem. Phys.*, 53, 3375.
11. —— and Parr, R. G., 1971, *J. Chem. Phys.*, 55, 5490.
12. Andrews, L. and Pimentel, G. C., 1967, *J. Chem. Phys.*, 47, 3637.
13. Bader, R. F. W., 1960, *Mol. Phys.*, 3, 137.
14. ——, 1962, *Can. J. Chem.*, 40, 1164.
15. —— and Bandrauk, A. D., 1968, *J. Chem. Phys.*, 49, 1666.
16. —— and Chandra, A. K., 1968, *Can. J. Chem.*, 46, 953; see also Chandra, A. K. and Sundar, R., 1971, *Mol. Phys.*, 22, 369.
17. —— and Ginsburg, J. L., 1969, *Can. J. Chem.*, 47, 3061.
18. ——, Henneker, W. H., and Cade, P. E., 1967, *J. Chem. Phys.*, 46, 3341.
19. —— and Jones, G. A., 1961, *Can. J. Chem.*, 39, 1253.
20. —— and Jones, G. A., 1963, *Can. J. Chem.*, 41, 586.
21. —— and Jones, G. A., 1963, *J. Chem. Phys.*, 38, 2791.
22. —— and Preston, H. J. T., 1966, *Can. J. Chem.*, 44, 1131.
23. ——, Srebrenik, S., and Nguyen-Dang, T. T., 1978, *J. Chem. Phys.*, 68, 3680.
24. Ballhausen, C. J., 1962, *Introduction to Ligand Field Theory* (McGraw-Hill, New York), pp. 193, 228.
25. Bamzai, A. S. and Deb, B. M., 1978, *Pramana*, 11, 191.

25a. —— and Deb, B. M., 1981, *The Role of Single-Particle Density in Chemistry*, *Rev. Mod. Phys.*, forthcoming.

26. Bartell, L. S., 1963, *J. Chem. Educ.*, **40**, 295.
27. ——, 1966, *Inorg. Chem.*, **5**, 1635.
28. ——, 1968, *J. Chem. Educ.*, **45**, 754.
29. Bent, H. A., 1960, *J. Chem. Educ.*, **37**, 616.
30. ——, 1961, *Chem. Rev.*, **61**, 275.
31. ——, 1966, *J. Chem. Educ.*, **43**, 170.
32. Berlin, T., 1951, *J. Chem. Phys.*, **19**, 208.
33. Bills, J. L. and Snow, R. L., 1975, *J. Am. Chem. Soc.*, **97**, 6340.
34. Bingel, W. A., 1959, *J. Chem. Phys.*, **30**, 1250, 1254.
35. ——, 1960, *J. Chem. Phys.*, **32**, 1522.
36. ——, 1961, *Z. Naturforsch.*, **A16**, 668.
37. ——, 1964, in *Molecular Orbitals in Chemistry, Physics, and Biology*, eds. P.-O. Löwdin and B. Pullman (Academic Press, New York), p. 191.
38. Blustin, P. H., 1977, *Chem. Phys. Lett.*, **46**, 386.
39. Born, M. and Oppenheimer, R., 1927, *Ann. Physik*, **84**, 457.
40. Britton, D., 1963, *Can. J. Chem.*, **41**, 1632.
41. Büchler, A., Stauffer, J., and Klemperer, W., 1964, *J. Chem. Phys.*, **40**, 3471; *J. Am. Chem. Soc.*, **86**, 4544.
42. ——, Stauffer, J., Klemperer, W., and Wharton, L., 1963, *J. Chem. Phys.*, **39**, 2299.
43. Bünau, G. V., Diercksen, G., and Preuss, H., 1967, *Int. J. Quantum Chem.*, **1**, 645.
44. Buenker, R. J. and Peyerimhoff, S. D., 1966, *J. Chem. Phys.*, **45**, 3682.
45. —— and Peyerimhoff, S. D., 1972, *Theoret. Chim. Acta* (Berlin), **24**, 132.
46. —— and Peyerimhoff, S. D., 1974, *Chem. Rev.*, **74**, 127.
47. Bugg, C., Desiderato, R., and Sass, R. L., 1964, *J. Am. Chem. Soc.*, **86**, 3157.
48. Byers Brown, W., 1958, *Proc. Cambridge Phil. Soc.*, **54**, 251.
49. Cade, P. E., Bader, R. F. W., and Pelletier, J., 1971, *J. Chem. Phys.*, **54**, 3517.
50. Cassie, J., 1933, *Nature* (London), **131**, 438.
51. Chang, S. Y., Davidson, E. R., and Vincow, G., 1970, *J. Chem. Phys.*, **52**, 5596.
51a. Chipman, D. M., Palke, W. E., and Kirtman, B., 1980, *J. Am. Chem. Soc.*, **102**, 3377.
52. Čížek, J., 1963, *Mol. Phys.*, **6**, 19.
53. Claxton, T. A. and Benson, G. C., 1966, *Can. J. Chem.*, **44**, 157.
54. Clinton, W. L., 1960, *J. Chem. Phys.*, **32**, 626.
55. —— and Hamilton, W. C., 1960, *Rev. Mod. Phys.*, **32**, 422.
56. —— and Rice, B., 1959, *J. Chem. Phys.*, **30**, 542.
57. Cohan, N. V. and Coulson, C. A., 1956, *Trans. Faraday Soc.*, **52**, 1163.
58. Cole, T., 1961, *J. Chem. Phys.*, **35**, 1169.
59. ——, Pritchard, H. O., Davidson, N. R., and McConnell, H. M., 1958, *Mol. Phys.*, **1**, 406.
60. Cooper, J., Hudson, A., and Jackson, R. A., 1972, *Mol. Phys.*, **23**, 209.

61. Corradini, P. and Allegra, G., 1959, *J. Am. Chem. Soc.*, **81**, 5511.
62. Coulson, C. A., 1962, *Valence*, 2nd ed. (Oxford University Press, New York), p. 111.
63. ——, 1972, *d-Electrons in Chemical Bonding* (Proceedings of the Robert A. Welch Foundation Conferences on Chemical Research. XVI. Theoretical Chemistry, Texas), p. 61.
64. ——, 1974, *Israel J. Chem.*, **11**, 683.
65. —— and Deb, B. M., 1969, *Mol. Phys.*, **16**, 545.
66. —— and Deb, B. M., 1971, *Int. J. Quantum Chem.*, 5, 411.
67. —— and Hurley, A. C., 1962, *J. Chem. Phys.*, **37**, 448.
68. —— and Luz, Z., 1968, *Trans. Faraday Soc.*, **64**, 2884.
69. —— and Nielson, A. H., 1963, *Disc. Faraday Soc.*, **35**, 71.
70. —— and Stephen, M. J., 1957, *Trans. Faraday Soc.*, 53, 272.
71. —— and Strauss, H. L., 1962, *Proc. Roy. Soc.* (London), **A269**, 443.
72. Davidson, E. R., 1964, *J. Chem. Phys.*, **41**, 656.
73. ——, 1965, *J. Chem. Phys.*, **42**, 4199.
74. Deb, B. M., 1971, *Proc. Indian Nat. Sci. Acad.*, 37A, 349.
75. ——, 1973, *Rev. Mod. Phys.*, **45**, 22.
76. ——, 1974, *J. Am. Chem. Soc.*, **96**, 2030.
77. ——, 1975, *J. Am. Chem. Soc.*, **97**, 1988.
78. ——, 1975, *J. Chem. Educ.*, **52**, 314.
79. ——, Bose, S. K., and Sen, P. N., 1976, *Indian J. Pure Appl. Phys.*, 14, 444.
80. —— and Mahajan, G. D., 1981, forthcoming.
81. ——, Mahajan, G. D., and Vasan, V. S., 1977, *Pramana*, **9**, 93.
82. ——, Sen. P. N., and Bose, S. K., 1974, *J. Am. Chem. Soc.*, **96**, 2044.
83. Devaquet, A., 1972, *J. Am. Chem. Soc.*, **94**, 5626, 9012.
84. Dixon, D. A. and Lipscomb, W. N., 1973, *J. Am. Chem. Soc.*, **95**, 2853.
85. ——, Pepperberg, I. M., and Lipscomb, W. N., 1974, *J. Am. Chem. Soc.*, **96**, 1325.
86. Drago, R. S., 1973, *J. Chem. Educ.*, **50**, 244.
87. Driessler, F., Ahlrichs, R., Staemmler, V., and Kutzelnigg, W., 1973, *Theoret. Chim. Acta* (Berlin), **30**, 315.
88. Dykstra, C. E., Hereld, M., Lucchese, R. R., Schaefer, H. F., III, and Meyer, W., 1977, *J. Chem. Phys.*, **67**, 4071.
89. Edmiston, C. and Ruedenberg, K., 1963, *Rev. Mod. Phys.*, 35, 457.
90. Ellison, F. O. and Shull, H., 1955, *J. Chem. Phys.*, **33**, 2348.
91. Ellison, G. B., Engelking, P. C., and Lineberger, W. C., 1978, *J. Am. Chem. Soc.*, **100**, 2556.
92. Englman, R., 1972, *The Jahn-Teller Effect in Molecules and Crystals* (John Wiley & Sons, New York).
93. Epstein, S. T., Hurley, A. C., Wyatt, R. E., and Parr, R. G., 1967, *J. Chem. Phys.*, **47**, 1275.
94. —— and Rosenthal, C. M., 1976, *J. Chem. Phys.*, **64**, 247.
95. Evans, J. C. and Lo, G. Y-S., 1966, *J. Phys. Chem.*, **70**, 11.
96. —— and Lo, G. Y-S., 1967, *J. Phys. Chem.*, **71**, 3697.

97. —— and Lo, G. Y-S., 1969, *J. Phys. Chem.*, **73**, 448.
98. Fessenden, R. W., 1967, *J. Phys. Chem.*, **71**, 74.
99. —— and Schuler, R. H., 1963, *J. Chem. Phys.*, **39**, 2147.
100. —— and Schuler, R. H., 1965, *J. Chem. Phys.*, **43**, 2704.
101. Feynman, R. P., 1939, *Phys. Rev.*, **56**, 340.
102. Fink, W. H. and Allen, L. C., 1967, *J. Chem. Phys.*, **46**, 2261.
103. Fletcher, R., 1970, *Mol. Phys.*, **19**, 55.
104. Frost, A. A., 1962, *J. Chem. Phys.*, **37**, 1147.
105. ——, 1966, University of Wisconsin Theoretical Chemistry Report, WIS-TCI-204, Dec.
106. ——, 1967, *J. Chem. Phys.*, **47**, 3707, 3714.
107. Fukui, K., 1966, *Bull. Chem. Soc. Jap.*, **39**, 498.
108. ——, 1970, *Theory of Orientation and Stereoselection* (Springer-Verlag, Heidelberg).
109. —— and Fujimoto, H., 1968, *Bull. Chem. Soc. Jap.*, **41**, 1989.
110. —— and Fujimoto, H., 1969, *Bull. Chem. Soc. Jap.*, **42**, 3399.
111. ——, Yonezawa, T., Nagata, C., and Shingu, H., 1954, *J. Chem. Phys.*, **22**, 1433.
112. ——, Yonezawa, T., and Shingu, H., 1952, *J. Chem. Phys.*, **20**, 722.
113. Gavin, R. M., Jr., 1969, *J. Chem. Educ.*, **46**, 413.
114. Gayles, J. N. and Self, J., 1964, *J. Chem. Phys.*, **40**, 3530.
115. Gerratt, J. and Mills, I. M., 1968, *J. Chem. Phys.*, **49**, 1719.
116. Gillespie, R. J., 1960, *J. Am. Chem. Soc.*, **82**, 5978.
117. ——, 1960, *Can. J. Chem.*, **38**, 818.
118. ——, 1963, *J. Chem. Educ.*, **40**, 295.
119. ——, 1967, *Angew. Chem. Intern. Ed.*, **6**, 819.
120. ——, 1972, *Molecular Geometry* (Van Nostrand Reinhold, New York).
121. —— and Nyholm, R. S., 1957, *Quart. Rev. Chem. Soc.*, **11**, 339.
122. Gimarc, B. M., 1970, *J. Am. Chem. Soc.*, **92**, 266.
123. ——, 1971, *J. Am. Chem. Soc.*, **93**, 593.
124. ——, 1971, *J. Am. Chem. Soc.*, **93**, 815.
125. Glidewell, C., Rankin, D. W. H., Robiette, A. G., and Sheldrick, G. M., 1970, *J. Chem. Soc.*, A318.
126. Gole, J. L., Siu, A. K. Q., and Hayes, E. F., 1973, *J. Chem. Phys.*, **58**, 857.
127. Goodisman, J., 1966, *J. Chem. Phys.*, **45**, 4689.
128. Grow, D. T. and Pitzer, R. M., 1977, *J. Chem. Phys.*, **67**, 4019.
129. Hall, G. G., 1961, *Phil. Mag.*, **6**, 249.
130. Harcourt, R. D. and Harcourt, A., 1973, *Chem. Phys.*, **1**, 238.
131. Hayes, E. F., 1966, *J. Phys. Chem.*, **70**, 3740.
132. Hedberg, K., 1955, *J. Am. Chem. Soc.*, **77**, 6491.
133. Hellmann, H., 1937, *Einführung in die Quantenchemie* (Franz Deuticke, Leipzig and Vienna), p. 285.
134. Herzberg, G., 1965, *Molecular Spectra and Molecular Structure. III. Electronic Spectra and Electronic Structure of Polyatomic Molecules* (D. Van Nostrand, Princeton, N.J.).

135. —— and Johns, J. W. C., 1971, *J. Chem. Phys.*, **54**, 2276.
136. Higuchi, J., 1956, *J. Chem. Phys.*, **24**, 535.
137. Hinze, J. and Jaffé, H. H., 1962, *J. Am. Chem. Soc.*, **84**, 540; *J. Phys. Chem.*, **67**, 1501.
138. Hirao, K., 1974, *J. Chem. Phys.*, **60**, 3215.
139. —— and Nakatsuji, H., 1973, *J. Chem. Phys.*, **59**, 1457.
140. Hirschfelder, J. O. and Eliason, M. A., 1967, *J. Chem. Phys.*, **47**, 1164.
141. Hoffmann, R., 1963, *J. Chem. Phys.*, **39**, 1397.
142. ——, 1974, *Chem. Eng. News*, **52**(30), 32.
143. ——, Gleiter, R., and Mallory, F. B., 1970, *J. Am. Chem. Soc.*, **92**, 1460.
144. Hohenberg, P. and Kohn, W., 1965, *Phys. Rev.*, **B136**, 864.
145. Hund, F., 1927, *Z. Phys.*, **40**, 742; **42**, 93.
146. ——, 1928, *Z. Phys.*, **51**, 759.
147. Hurley, A. C., 1954, *Proc. Roy. Soc.* (London), **A226**, 170, 179, 193.
148. ——, 1964, in *Molecular Orbitals in Chemistry, Physics, and Biology*, eds. P.-O. Löwdin and B. Pullman (Academic Press, New York), p. 161.
149. Ibers, J. A., 1964, *J. Chem. Phys.*, **40**, 402.
150. Itoh, T., Ohno, K., and Kotani, M., 1953, *J. Phys. Soc. Jap.*, **8**, 41.
151. Jackel, G. S., Christiansen, J. J., and Gordy, W., 1967, *J. Chem. Phys.*, **47**, 4274.
152. —— and Gordy, W., 1968, *Phys. Rev.*, **176**, 443.
153. Jahn, H. A. and Teller, E., 1937, *Proc. Roy. Soc.* (London), **A161**, 220.
154. Janoschek, R., Pruess, H., and Diercksen, G., 1968, *Int. J. Quantum Chem.*, **2**, 159.
155. Johansen, H. and Wahlgren, U., 1978, *Chem. Phys. Lett.*, **55**, 245.
156. Johannesen, R. B., Candela, G. A., and Tsang, T., 1968, *J. Chem. Phys.*, **48**, 5544.
157. Jones, W. D. and Simpson, W. T., 1960, *J. Chem. Phys.*, **32**, 1747.
158. Jordan, P. C. H. and Longuet-Higgins, H. C., 1962, *Mol. Phys.*, **5**, 121.
159. Kaldor, U., 1967, *J. Chem. Phys.*, **46**, 1981.
160. —— and Shavitt, I., 1966, *J. Chem. Phys.*, **44**, 1823.
161. —— and Shavitt, I., 1968, *J. Chem. Phys.*, **48**, 191.
162. Kari, R. E. and Csizmadia, I. G., 1969, *J. Chem. Phys.*, **50**, 1443.
163. Katriel, J., 1972, *Phys. Rev.*, **A5**, 1990.
164. ——, 1972, *Theoret. Chim. Acta* (Berlin), **23**, 309.
165. Kaufman, J. J., Sachs, L. M., and Geller, M., 1968, *J. Chem. Phys.*, **49**, 4369.
166. Kim, H. J. and Parr, R. G., 1964, *J. Chem. Phys.*, **41**, 2892.
167. Koga, T. and Nakatsuji, H., 1976, *Theoret. Chim. Acta* (Berlin), **41**, 119.
168. ——, Nakatsuji, H., and Yonezawa, T., 1978, *J. Am. Chem. Soc.*, **100**, 7522.
168a. ——, Nakatsuji, H., and Yonezawa, T., 1980, *Mol. Phys.*, **39**, 239.
169. Komornicki, A., Ishida, K., Morokuma, K., Ditchfield, R., and Conrad, M., 1977, *Chem. Phys. Lett.*, **45**, 595.
170. Kohl, D. A., 1972, *J. Chem. Phys.*, **56**, 4236.

171. Kohn, W. and Sham, L. J., 1965, *Phys. Rev.*, **A140**, 1133.
172. Kuczkowski, R. L., Lide, D. R., Jr., and Kriser, L. C., 1966, *J. Chem. Phys.*, **44**, 3131.
173. Lemberger, A. and Pauncz, R., 1969, *Acta Phys. Acad. Sci. Hung.*, **27**, 169.
174. Lide, D. R., Jr. and Kuczkowski, R. L., 1967, *J. Chem. Phys.*, **46**, 4768.
175. Liebman, J. F., 1971, *J. Chem. Educ.*, **48**, 188.
176. ——, 1974, *J. Am. Chem. Soc.*, **96**, 3053.
177. —— and Vincent, J. S., 1975, *J. Am. Chem. Soc.*, **97**, 1373.
178. ——, Politzer, P., and Sanders, W. A., 1976, *J. Am. Chem. Soc.*, **98**, 5115.
179. Linnett, J. W. and Wheatley, P. J., 1949, *Trans. Faraday Soc.*, **45**, 33, 39.
180. Löwdin, P.-O., 1955, *Phys. Rev.*, **97**, 1474.
181. ——, 1955, *Phys. Rev.*, **97**, 1490.
182. Lowe, J. P., 1968, *Progr. Phys. Org. Chem.*, **6**, 1.
183. Magnasco, V. and Perico, A., 1967, *J. Chem. Phys.*, **47**, 971.
184. Mahajan, G. D. and Deb, B. M., 1981, forthcoming.
185. Mamantov, G., Vasini, E. J., Moulton, M. C., Vickroy, D. G., and Maekawa, T., 1971, *J. Chem. Phys.*, **54**, 3419.
186. Matsumura, C. and Lide, D. R., Jr., 1969, *J. Chem. Phys.*, **50**, 71, 3080.
187. McDiarmid, R. and Charney, E., 1967, *J. Chem. Phys.*, **47**, 1517.
188. McIver, J. W., Jr. and Komornicki, A., 1971, *Chem. Phys. Lett.*, **10**, 303.
189. McKean, D. C. and Schatz, P. N., 1956, *J. Chem. Phys.*, **24**, 316.
190. Merer, A. J. and Mulliken, R. S., 1969, *Chem. Rev.*, **69**, 639.
191. —— and Schoonveld, L., 1968, *J. Chem. Phys.*, **48**, 522.
192. —— and Schoonveld, L., 1969, *Can. J. Phys.*, **47**, 1731.
193. Messmer, R. P. and Birss, F. W., 1969, *J. Phys. Chem.*, **73**, 2085.
194. Millie, P. and Berthier, G., 1968, *Int. J. Quantum Chem.*, **S2**, 67.
195. Milligan, D. E. and Jacox, M. E., 1967, *J. Chem. Phys.*, **47**, 5146.
196. Moccia, R., 1967, *Theoret. Chim. Acta* (Berlin), **8**, 8.
197. Morehouse, R. L., Christiansen, J. J., and Gordy, W., 1966, *J. Chem. Phys.*, **45**, 1751.
198. Morokuma, K., Pedersen, L., and Karplus, M., 1968, *J. Chem. Phys.*, **48**, 4801.
199. Mulliken, R. S., 1928, *Phys. Rev.*, **32**, 186.
200. ——, 1932, *Rev. Mod. Phys.*, **4**, 1.
201. ——, 1932, *Phys. Rev.*, **41**, 751.
202. ——, 1933, *Phys. Rev.*, **43**, 279.
203. ——, 1934, *J. Chem. Phys.*, **2**, 782.
204. ——, 1942, *Rev. Mod. Phys.*, **14**, 204.
205. ——, 1955, *J. Chem. Phys.*, **23**, 1833.
206. ——, 1959, *Tetrahedron*, **5**, 253.
207. Nakatsuji, H., 1973, *J. Am. Chem. Soc.*, **95**, 345.
208. ——, 1973, *J. Am. Chem. Soc.*, **95**, 354.
209. ——, 1973, *J. Am. Chem. Soc.*, **95**, 2084.
210. ——, 1974, *J. Am. Chem. Soc.*, **96**, 24.

211. ——, 1974, *J. Am. Chem. Soc.*, **96**, 30.
212. ——, 1976, *Phys. Rev.*, **A14**, 41.
213. ——, 1977, *J. Chem. Phys.*, **67**, 1312.
214. ——, Kato, H., and Yonezawa, T., 1969, *J. Chem. Phys.*, **51**, 3175.
215. —— and Koga, T., 1974, *J. Am. Chem. Soc.*, **96**, 6000.
216. ——, Kuwata, T., and Yoshida, A., 1973, *J. Am. Chem. Soc.*, **95**, 6894.
217. —— and Musher, J. I., 1974, *Chem. Phys. Lett.*, **24**, 77.
218. —— and Parr, R. G., 1975, *J. Chem. Phys.*, **63**, 1112.
219. ——, Koga, T., Kondo, K., and Yonezawa, T., 1978, *J. Am. Chem. Soc.*, **100**, 1029.
220. ——, Matsuda, K., and Yonezawa, T., 1978, *Chem. Phys. Lett.*, **54**, 347; *Bull. Chem. Soc. Jap.*, **51**, 1315.
221. ——, Kanayama, S., Harada, S., and Yonezawa, T., 1978, *J. Am. Chem. Soc.*, **100**, 7528.
221a. ——, Kanda, K., and Yonezawa, T., 1980, *Chem. Phys. Lett.*, **75**, 340.
221b. ——, Hayakawa, T., and Yonezawa, T., 1981, forthcoming.
222. Neunhoeffer, O. and Hasse, H., 1958, *Chem. Ber.*, **91**, 1801.
223. Newton, M. D., Switkes, E., and Lipscomb, W. N., 1970, *J. Chem. Phys.*, **53**, 2645.
224. Niessen, W. von, 1972, *J. Chem. Phys.*, **56**, 4290.
225. Orgel, L. E., 1960, *An Introduction to Transition-Metal Chemistry* (John Wiley & Sons, New York).
226. Palke, W. E. and Pitzer, R. M., 1967, *J. Chem. Phys.*, **46**, 3948.
227. Parr, R. G., 1964, *J. Chem. Phys.*, **40**, 3726.
228. ——, 1974, *CIT-JHU-UNC Quanta*, Third Issue (Dept. of Chemistry, University of North Carolina, Chapel Hill).
229. Parsons, A. E. and Searcy, A. W., 1959, *J. Chem. Phys.*, **30**, 1635.
230. Patton, J. W. and Hedberg, K., 1968, *Bull. Am. Phys. Soc.*, **13**, 831.
231. Pauling, L., 1960, *The Nature of the Chemical Bond*, 3rd ed. (Cornell University Press, Ithaca, New York).
232. Pearson, R. G., 1969, *J. Am. Chem. Soc.*, **91**, 1252, 4947.
233. ——, 1970, *J. Chem. Phys.*, **52**, 2167; **53**, 2986.
234. ——, 1970, *Theoret. Chim. Acta* (Berlin), **16**, 107.
235. ——, 1971, *Chem. Phys. Lett.*, **10**, 31.
236. ——, 1971, *Acc. Chem. Res.*, **4**, 152.
237. ——, 1976, *Symmetry Rules for Chemical Reactions* (John Wiley & Sons, New York).
238. Pedersen, L. and Morokuma, K., 1967, J. *Chem. Phys.*, **46**, 3941.
239. Penney, W. G. and Sutherland, G. B., 1936, *Proc. Roy. Soc.* (London), **A156**, 654.
240. Peyerimhoff, S. D., Buenker, R. J., and Allen, L. C., 1966, *J. Chem. Phys.*, **45**, 734.
241. Politzer, P., 1967, *J. Phys. Chem.*, **71**, 3068.
242. ——, 1976, *J. Chem. Phys.*, **64**, 4239.
243. Pople, J. A. and Beveridge, D. L., 1970, *Approximate Molecular Orbital Theory* (McGraw-Hill, New York).

244. —— and Nesbet, R. K., 1954, *J. Chem. Phys.*, 22, 571.
245. Poshusta, R. D., Haugen, J. A., and Zetik, D. F., 1969, *J. Chem. Phys.*, 51, 3343.
246. ——, Klint, D. W., and Liberles, A., 1971, *J. Chem. Phys.*, 55, 252.
247. Preuss, H. and Diercksen, G., 1967, *Int. J. Quantum Chem.*, 1, 641.
248. Pulay, P., 1969, *Mol. Phys.*, 17, 197.
249. Ray, N. K., 1970, *J. Chem. Phys.*, 52, 463.
250. Reichman, S. and Schreiner, F., 1969, *J. Chem. Phys.*, 51, 2355.
251. Renner, R., 1934, *Z. Phys.*, 92, 172.
252. Roothaan, C. C. J., 1951, *Rev. Mod. Phys.*, 23, 69.
253. Rothenberg, S., 1969, *J. Chem. Phys.*, 51, 3389.
254. ——, 1971, *J. Am. Chem. Soc.*, 93, 68.
255. Ruedenberg, K., 1962, *Rev. Mod. Phys.*, 34, 326.
256. ——, 1977, *J. Chem. Phys.*, 66, 375.
257. Runtz, G. R., Bader, R. F. W., and Messer, R. R., 1977, *Can. J. Chem.*, 55, 3040.
258. Salem, L., 1961, *Proc. Roy. Soc.* (London), A264, 379.
259. ——, 1963, *J. Chem. Phys.*, 38, 1227.
260. ——, 1968, *J. Am. Chem. Soc.*, 90, 543.
261. ——, 1969, *Chem. Phys. Lett.*, 3, 99.
262. —— and Wright, J. S., 1969, *J. Am. Chem. Soc.*, 91, 5947.
263. Schmidtke, H. H., 1962, *Z. Naturforsch*, 17a, 121.
264. ——, 1963, *Z. Naturforsch*, 18a, 496.
265. —— and Preuss, H., 1961, *Z. Naturforsch*, 16a, 790.
265a. Schmiedekamp, A., Cruickshank, D. W. J., Skaarup, S., Pulay, P., Hargittai, I., and Boggs, J. E., 1979, *J. Am. Chem. Soc.*, 101, 2002.
266. Schnuelle, G. W. and Parr, R. G., 1972, *J. Am. Chem. Soc.*, 94, 8974.
267. Schrader, D. M., 1965, *J. Chem. Phys.*, 46, 3895.
268. —— and Karplus, M., 1964, *J. Chem. Phys.*, 40, 1593.
269. Schwartz, M. S., 1969, *J. Chem. Phys.*, 51, 4182.
270. Schwartz, M. E. and Allen, L. C., 1970, *J. Am. Chem. Soc.*, 92, 1466.
271. Searcy, A. W., 1958, *J. Chem. Phys.*, 28, 1237.
272. ——, 1959, *J. Chem. Phys.*, 31, 1.
273. Shull, H. and Ebbing, D., 1958, *J. Chem. Phys.*, 28, 866.
274. Sidgwick, N. V. and Powell, H. M., 1940, *Proc. Roy. Soc.* (London), A176, 153.
275. Simons, J., 1973, *J. Chem. Phys.*, 59, 2436.
276. Smith, W. L. and Warsop, P. A., 1968, *Trans. Faraday Soc.*, 64, 1165.
277. Sovers, O. J., Kern, C. W., Pitzer, R. M., and Karplus, M., 1968, *J. Chem. Phys.*, 49, 2592.
278. Srebrenik, S. and Bader, R. F. W., 1975, *J. Chem. Phys.*, 63, 3945.
279. ——, Bader, R. F. W., and Nguyen-Dang, T. T., 1978, *J. Chem. Phys.*, 68, 3667.
280. Stenkamp, L. Z. and Davidson, E. R., 1973, *Theoret. Chim. Acta* (Berlin), 30, 283.
281. Stewart, R. F., 1970, *J. Chem. Phys.*, 52, 431.

282. Surratt, G. T. and Goddard, W. A., 1977, *Chem. Phys.*, 23, 39.
283. Sutton, L. E. (ed.), 1958, Chemical Society Special Publication No. 11.
284. —— (ed.), 1965, Chemical Society Special Publication No. 18.
285. Symons, M. C. R., 1969, *Nature* (London), 222, 1123.
286. —— and Wardale, H. W., 1967, *Chem. Commun.*, 758.
287. Takahata, Y., Schnuelle, G. W., and Parr, R. G., 1971, *J. Am. Chem. Soc.*, 93, 784.
288. Thompson, H. B., 1968, *Inorg. Chem.*, 7, 604.
289. ——, 1971, *J. Am. Chem. Soc.*, 93, 4609.
290. —— and Bartell, L. S., 1968, *Inorg. Chem.*, 7, 488.
291. Tsao, P., Cobb, C. C., and Classen, H. H., 1971, *J. Chem. Phys.*, 54, 5247.
292. Ungemach, S. R. and Schaefer, H. F., III, 1976, *J. Am. Chem. Soc.*, 98, 1658.
293. Urey, H. C. and Bradley, C. A., 1931, *Phys. Rev.*, 38, 1969.
294. Walsh, A. D., 1953, *J. Chem. Soc.*, 2260, 2266, 2288, 2296, 2301, 2306, 2321.
295. Watson, R. E., 1960, *Phys. Rev.*, 118, 1036.
296. ——, 1960, *Phys. Rev.*, 119, 1934.
297. White, D., Seshadri, K. S., Deves, D. F., Mann, D. E., and Leneusky, M. J., 1963, *J. Chem. Phys.*, 39, 2463.
298. Wilkinson, R. G. and Mulliken, R. S., 1955, *J. Chem. Phys.*, 23, 1895.
299. Wilson, E. B., Jr., 1962, *J. Chem. Phys.*, 36, 2232.
300. ——, Decius, J. C., and Cross, P. C., 1955, *Molecular Vibrations* (McGraw-Hill, New York).
301. Winnewisser, G., Winnewisser, M., and Gordy, W., 1968, *J. Chem. Phys.*, 49, 3465.
302. Woodward, R. B. and Hoffmann, R., 1970, *The Conservation of Orbital Symmetry* (Verlag Chemie GmbH, Weinheim, Germany, and Academic Press, New York).
303. Wulfman, C. E., 1959, *J. Chem. Phys.*, 31, 381.
304. ——, 1960, *J. Chem. Phys.*, 33, 1567.
305. Yonezawa, T., Nakatsuji, H., and Kato, H., 1968, *J. Am. Chem. Soc.*, 90, 1239.
306. ——, Nakatsuji, H., Kawamura, T., and Kato, H., 1969, *Bull. Chem. Soc. Jap.*, 42, 2437.